

Dissertation

Advanced Imaging in Head-Mounted Displays for Patients with Age-Related Macular Degeneration

Anabel Martín González



TECHNISCHE UNIVERSITÄT MÜNCHEN

Chair for Computer-Aided Medical Procedures & Augmented Reality

Advanced Imaging in Head-Mounted Displays for Patients with Age-Related Macular Degeneration

Anabel Martín González

Vollständiger Abdruck der von der Fakultät für Informatik der Technischen Universität München zur Erlangung des akademischen Grades eines
Doktors der Naturwissenschaften (Dr. rer. nat.)
genehmigten Dissertation.

Vorsitzender: Univ.-Prof. Dr. Helmut Krcmar

Prüfer der Dissertation:

1. Univ.-Prof. Dr. Nassir Navab
2. apl. Prof. Dr. Ines Lanzl

Die Dissertation wurde am 29.06.2011 bei der Technischen Universität München eingereicht und durch die Fakultät für Informatik am 05.09.2011 angenommen.

Abstract

According to the World Health Organization, age-related macular degeneration is one of the leading causes of blindness and low vision worldwide. It is a major cause of central vision loss for elderly people, which is increasing considerably without a suitable medical solution. Nevertheless, enhancement of people's vision by means of adaptive technology and modern techniques in the field of mediated reality is conceivable. This thesis proposes advanced imaging implemented on a head-mounted display based system for improving vision of patients with age-related macular degeneration. Central vision loss and distorted vision are the main symptoms of interest for the present research.

A head-mounted hybrid magnification system is developed, in order to enhance visual perception acquired with peripheral vision of low level visual resolution. A hybrid magnification technique is adjusted and implemented on a head-mounted display. The performance is evaluated by simulating central vision loss on normal sight volunteers.

Furthermore, a system for modeling and correcting distorted vision is proposed. The system obtains an inverted deformation model, termed correction model, of distorted vision in a patient by means of a deformable Amsler grid. The interactively deformable grid is based on cubic B-splines. To evaluate the modeling system, a method for simulating distorted vision is applied. By superimposing the model on Optical Coherence Tomography images of the macula, it is suitable to identify macular features, which could help on the development of an automatic method to model distorted vision.

This work presents a step toward implementing mediated-reality solutions in low vision rehabilitation to improve vision and quality of life of patients with age-related macular degeneration in the near future.

Keywords: Low vision rehabilitation, age-related macular degeneration, head-mounted magnification, metamorphopsia modeling.

Zusammenfassung

Die altersbedingte Makuladegeneration (AMD) ist eine der weltweit bedeutendsten Ursachen für Sehbehinderung ohne eine geeignete medizinische Lösung. Dennoch ist eine Verbesserung der Sehleistung durch Mediated-Reality denkbar. Diese Arbeit schlägt Advanced Imaging in einem Head-Mounted Display zur Verbesserung der Sehleistung von AMD-Patienten vor.

Ein Head-Mounted Vergrößerungssystem wurde entwickelt, um die visuelle Wahrnehmung peripheren Sehens mit niedriger visueller Auflösung zu verbessern. Ein hybride Technik zur Vergrößerung wurde an das Head-Mounted Display angepasst und entsprechend umgesetzt.

Darüber hinaus wurde ein System für die Modellierung und Korrektur von verzerrtem Sehen vorgeschlagen. Das System erhält ein Korrekturmodell mittels eines verformbaren Amsler-Gitters. Zur Beurteilung des Systems, wurde ein Verfahren zur Simulation verzerrte Sicht angewendet. Durch die Überlagerung des Modells auf Makula-OCT-Bildern, ist es möglich passende Makula-Features zu identifizieren, die für die Entwicklung einer automatischen Korrektur-Methode helfen könnten.

Die vorliegende Arbeit stellt Mediated-Reality Lösungen in Low Vision Rehabilitation vor, um die Lebensqualität von AMD Patienten in naher Zukunft zu verbessern.

Schlagwörter: Low Vision Rehabilitation, altersbedingte Makuladegeneration, Head-Mounted Vergrößerungssystem, Metamorphopsie Modellierung.

Acknowledgments

First of all, I want to thank God for giving me the life to complete an important step in my professional and personal development.

I would like to express my deepest gratitude to my supervisor, Prof. Nassir Navab, for his extraordinary guidance, valuable encouragement, and thoughtful supervision. I feel honored to work with such a great human being with an outstanding vision for novel technological ideas. I thank very much to my consulting supervisor, Prof. Dr. Ines Lanzl, for sharing with me her expert medical knowledge and valued time. I also want to thank my collaboration partners, Dr. Sandro Heining at Chirurgische Klinik und Poliklinik Innenstadt; Dr. Ing. Konstantin Kotliar, and Dr. Ramin Khoramnia at the Klinik und Poliklinik für Augenheilkunde, Klinikum rechts der Isar, Munich.

I am very grateful to all my colleagues at the chair of Computer Aided Medical Procedures for their great support and friendship over the last four years. My special thanks to my Latin-American colleagues Victor Castañeda, Diana Mateus, and José Gardiazabal for their warm hugs and affection. I wish to thank my best friend Asad Safi for his unconditional love, care, and moral support. I also want to thank Martin Horn and Martina Hilla for their kindness, friendship, and all the technical and administrative support. The group has been a source of friendships as well as good advice and collaboration.

I would like to thank my family for all their love and encouragement. For my parents, Guillermo and Rita, who raised me with love and supported me in all my pursuits. For my brothers, Carlos and Guillermo, who made me feel a loved sister. For Valentina, Karielita and Carlitos, who are lights in the family. For the constant love and support of my girlfriends at all time, Diana, Mercedes, Rosalucía, Cinthia, and Miriam. Thank you all.

I would like to express my sincere thankfulness to Dr. Carlos J. Castilla Centeno for his unconditional support, constant care, and kind love. His noble devotion to improve people's vision throughout his life has been the main source of inspiration for me to accomplish this work.

I gratefully acknowledge the generous support of my funding sources that made my Ph.D. work possible, the Bayerische Forschungsstiftung (three years), the Secretaría de Educación Pública de México (two years), the TUM Graduate School, and the TUM Gender Center.

Finally, I thank the Technische Universität München for the opportunity of becoming part of a great university.

Anabel Martín González

Contents

Abstract	iii
Zusammenfassung	v
Acknowledgements	vii
List of Figures	xiii
List of Tables	xvii
I. Introduction and Theory	1
1. Introduction	3
1.1. Motivation	3
1.1.1. Prevalence of Age-Related Macular Degeneration	3
1.1.2. Low Vision Rehabilitation: Assistive Technology	5
1.2. Head-Mounted Display Technology for Low Vision	7
1.3. Research Objectives	14
1.4. Contributions	17
1.5. Outline of the Thesis	18
2. Medical Background	21
2.1. Anatomy and Physiology of the Human Eye	21

2.2. Age-Related Macular Degeneration	27
2.2.1. Definition and Classification	27
2.2.2. Symptoms	29
2.2.3. Risk Factors	31
2.2.4. Medical Treatments	34
2.3. Visual Field Assessment	35
2.3.1. Perimetry	36
2.3.2. Noise Field Campimetry	37
2.3.3. Microperimetry	37

II. Methods 39

3. Head-Mounted Hybrid Magnification System 41	41
3.1. Related Work	41
3.2. Low Vision Rehabilitation System	43
3.2.1. Head-Mounted Display	43
3.2.2. Software Framework	44
3.3. Magnification Transformations	46
3.3.1. Linear Magnifications	46
3.3.2. Non-Linear Magnifications	47
3.3.3. Radial Magnification	47
3.3.4. Constrained Transformations	48
3.4. Hybrid Magnification Approach	48
3.5. Results	49
3.6. Discussion	50
3.7. Eye-Tracking based AMD Simulation System	52
3.7.1. Purpose	52
3.7.2. Methods and Materials	52
3.7.3. Experiments	53
3.7.4. Results	54
3.7.5. Discussion	57
3.8. Sight-based Magnification System for Surgical Applications	59
3.8.1. Hardware Setup	60
3.8.2. Magnification Sight-based Activation	63
3.8.3. Experiments	65

3.8.4. Results	66
3.8.5. Discussion	70
4. Metamorphopsia Modeling System	73
4.1. Related Work	73
4.2. Objective	77
4.3. Methods and Materials	77
4.3.1. Deformable Amsler Grid	78
4.3.2. Localizing Metamorphopsia in OCT Images	79
4.4. Results	81
4.5. Discussion	85
4.6. Eye-Tracking based Metamorphopsia Simulation System	85
4.6.1. Motivation	85
4.6.2. Method and Materials	85
4.6.3. Simulation of Distorted Vision	85
4.6.4. Experiments	86
4.6.5. Results	89
4.6.6. Discussion	93
 III. Final Conclusions	 95
 5. Conclusions	 97
5.1. Summary	97
5.2. Future Work	98
 Appendix	 103
 A. Eye Tracking	 103
A.1. Introduction	103
A.2. Technological Basics of Eye Tracking	104
A.2.1. Non-imaging Eye Tracking Approaches	104
A.2.2. Imaging-based Eye Tracking Approaches	105
 B. Glossary and Acronyms	 109
 Bibliography	 113

List of Figures

1.1. Low vision rehabilitation devices: (a) Hand magnifier, (b) Stand magnifier, (c) Spectacle-mounted magnifier, and (d) Electronic device. (<i>Images source: Vision Enhancers Ltd, www.visionenhancers.co.uk</i>).	6
1.2. Low vision imaging system (LVIS) [60].	9
1.3. Head-mounted mobility aid for low vision by Peli [113]: (a) User wearing the prototype device, (b) Binary image without 1-D enhancement, and (c) Binary image with 1D enhancement.	10
1.4. Head-mounted mobility aid for low vision by Everingham et al. [34].	11
1.5. Illustrations of the concept of augmented-vision head-mounted display systems by Peli [115]: (a) Wide-band enhancement for patients with central vision loss, and (b) Visual field expander for patients with tunnel vision (depicted with the elliptical area in the middle of the scene).	12
1.6. Simulation of the wide-band enhancement system for patients with central vision loss by Peli [117]: (a) Original scene view, and (b) Enhanced scene view through on-axis superimposed edges.	13
1.7. Simulation of the visual field expander system for patients with tunnel vision by Peli [117]. Restricted view of a street-crossing scene (upper image). Augmented view through superimposed minified edges of the wide field of view not covered by the patient vision (lower image).	15

List of Figures

1.8. ATDV system for patients with central vision loss [36]: (a) Original scene view, and (b) Scene view deformed by the ATDV system.	16
2.1. Human eye cross-sectional view (<i>Image source: Adaptation from National Eye Institute, National Institutes of Health; Ref: NEA09</i>).	22
2.2. Retinal layer (<i>Image source: Adaptation from Ramon y Cajal [165]</i>).	24
2.3. Distribution of rods and cones in the retina (<i>Image source: Gonzalez and Woods [50]</i>).	25
2.4. Reading acuity chart. All letters should be equally readable when the center of this chart is fixated, since each letter is ten times its threshold height (<i>Image source: Adaptation from Anstis [3]</i>).	26
2.5. AMD forms in retinal fundus images: (a) normal fundus, (b) dry form, and (c) wet form. (<i>Image source: National Eye Institute, National Institutes of Health; Ref: (a) EDA06, (b) EDA22, and (c) EDA24</i>).	29
2.6. Simulation of AMD Symptoms: (a) normal vision, (b) blurred vision, (c) central scotoma, and (d) distorted vision.	32
3.1. Programmable Remapper by Loshin and Juday [90]: (a) Face view occluded with a central scotoma, (b) Face view with zero effective scotoma remapping, and (c) Face view with partial effective scotoma remapping.	42
3.2. Example of image coordinate transformation by the PVA system [94].	43
3.3. Head-mounted magnification system for AMD patients.	44
3.4. Linear magnification functions.	46
3.5. Non-linear magnification functions.	47
3.6. Radial magnifications: (a) Linear magnification, and (b) Non-linear magnification.	48
3.7. Constrained magnifications: (a) Radial linear magnification, and (b) Radial non-linear magnification.	49
3.8. Hybrid magnification approach.	50
3.9. Illustration of magnification modes: (a) Original image, (b) Linear magnification, and (c) Hybrid magnification.	51
3.10. Patients with AMD assisted by the head-mounted hybrid magnification system.	52
3.11. Eye-tracking based simulation system.	53

3.12. Simulation of scotoma sizes for text reading. Left column: (a)–(c) Linear magnification. Right column: (d)–(e) Hybrid magnification.	55
3.13. Simulation of scotoma size for following routes on a map: (a) Linear mode, and (b) Hybrid mode.	56
3.14. Sight-based magnification head-mounted system.	61
3.15. Tracking system setup.	62
3.16. Setup for AR system. All transformations are depicted by annotated red arrows.	64
3.17. Illustration of the magnification sight-based activation.	65
3.18. Surgeons assisted by the magnification system.	67
3.19. Magnification modes displayed into the HMD: (a) Linear, and (b) Hybrid.	68
3.20. Suturing module, pointer and surgical tools.	69
3.21. Surgeon with surgical loupe attached to the glasses.	71
4.1. The Amsler grid.	74
4.2. Example of a chart drawn by a patient used to quantify metamorphopsia by Shinoda et al. [141].	75
4.3. Method of detecting metamorphopsia using M-CHARTS proposed by Matsumoto et al. [99].	75
4.4. Example of a stimulus used in the PHP. The subject should fixate the central dot during the test.	76
4.5. Cross-sectional view of a retinal volume from optical coherence tomography images of a patient with metamorphopsia.	77
4.6. Metamorphopsia modeling system.	78
4.7. Imaging components for alignment: (a) Fundus image, (b) OCT image, and (c) Metamorphopsia model grid.	82
4.8. Alignment of a macular OCT image and deformable Amsler grid on top of a fundus image.	83
4.9. Alignment examples of macular OCT images and deformable Amsler grid of four different patients: (a)–(d).	84
4.10. Metamorphopsia simulation and modeling system.	86
4.11. Deformation example on a non-squared grid.	87
4.12. Evaluated locations in: (a) Squared grid, and (b) Non-squared grid.	88
4.13. Volunteer and examiner performing an experiment.	89
4.14. Correction rate.	91

List of Figures

4.15. Minimum recognizable visual angles.	92
5.1. Wagon wheel pattern used in the Macular Mapping Test [92].	100
A.1. Scleral search coils: Coils embedded in contact lenses. (<i>Image source: www.chronos-vision.de/scleral-search-coils</i>).	105
A.2. Electro-oculography: Skin electrodes placed around the eyes to collect electrical potential variations. (<i>Image source: www.metrovision.fr</i>).	105
A.3. The corneal reflections produced by different eye-head positions. The corneal reflection appears as a bright white dot, just to the right of the pupil (A). The relative positions of the pupil and the corneal reflection change when the eye rotates around its horizontal (B) and vertical (C) axes. This relationship does not change, however, when the head moves and the eye is stable (D). (<i>Image source: Adaptation from Richardson and Spivey (2004) [128]</i>).	107

List of Tables

3.1. Augmented reality vision rehabilitation system specifications. . . .	45
3.2. Augmented reality system main PC workstation specifications. . .	45
3.3. Eye-tracking device technical specification.	53
3.4. Ratios of reading speed (hybrid mode over linear mode).	57
3.5. Reading speed (syllable/s).	57
3.6. Ratios of line return (hybrid mode over linear mode).	58
3.7. Route following speed (m/s).	58
3.8. Suturing task completion time.	66
3.9. First trial (linear mode: 3, hybrid mode: 2). Second trial (linear mode: 2, hybrid mode: 3).	69
4.1. SPECTRALIS SD-OCT specifications.	80
4.2. Deformable grid specifications.	83
4.3. Total correction rate (percent) on squared and non-squared grids. .	90
4.4. Correction rate (percent) for each evaluated location.	91
4.5. Minimum recognizable visual angles (in degrees) for each evalu- ated location.	92

Part I.

Introduction and Theory

CHAPTER 1

Introduction

MEDIATED and augmented reality have become major disciplines demonstrating their extraordinary potential in many application domains. In the field of ophthalmology and optometry, diverse methods and strategies for low vision rehabilitation are in constant progress aimed at improving residual visual functions of visually impaired people. Integration of mediated and augmented reality techniques into low vision rehabilitation enables the development of novel and improved technological solutions not possible or conceived before.

1.1. Motivation

The foundation of conducting this research is based on the growing number of people affected by age-related macular degeneration missing efficient low vision devices for rehabilitation, and the promising idea of integrating a head-mounted display with advanced imaging methods as a powerful mediated-reality interface into the field of low vision rehabilitation. A brief overview of the motivation facts directing this work is given in the following paragraphs.

1.1.1. Prevalence of Age-Related Macular Degeneration

Incidence of visual impairment worldwide is an imminent situation seriously increasing as populations grow and fast demographic fluctuations move in the di-

rection of the predominance of older age groups.

Age-related macular degeneration (AMD), is one of the major causes of legal blindness in Europe, North America, and Australia [143]. In accordance with the World Health Organization (WHO), age-related macular degeneration is the third leading cause of visual impairment in the world with a blindness tendency of 8.7%, which represents about three million people. It is also considered the principal source of visual deficiency in developed countries [127].

The largest proportion of blindness is necessarily related to ageing. Ranking third globally as a cause of severe vision loss after cataract and glaucoma, AMD affects mainly people over 50 years of age. Extensive studies during 1990 and 2002 expose that the size of the population aged 50 years and older in the world had increased by 30% [127]. In the United States, elder people are expected to increase by 54% between 2005 and 2025 [81]. As the percentage of the population being older than 50 continues to grow, AMD is becoming a major public health problem worldwide.

Although AMD almost never causes total blindness, the vision loss increasingly affects an individual's functional ability and interaction with the physical and social environment [158]. The ability of patients to function independently and to perform activities of daily living, such as reading, driving, distinguishing colors and facial expressions, is greatly impaired [15, 160]; and their quality of life is adversely affected [29, 88, 161].

Reading problems are part of the main concerns of patients with AMD, and reading performance is strongly linked to the quality of life dependent on vision [63, 125]. On the other hand, a visual impairment can decrease mobility through the environment, and increase the risk of injury caused by falls [72]. Moreover, people with AMD consider their face recognition disability to be of great significance [100], because this incapacity can affect social interactions.

In average, loss of independence and disability to enjoy leisure activities are predominant concerns of the older adult with a visual impairment [129]. Furthermore, visually impaired adults deal with preserving employment, productivity, and independence, in addition to maintaining a home and fulfilling family and social obligations [59, 129].

All this negative impact on a person's daily functioning can have serious mental health consequences. A number of studies shows that chronic vision impairment is associated with emotional distress, depression and the perception of diminished life quality [18, 74, 161].

1.1.2. Low Vision Rehabilitation: Assistive Technology

Low vision is defined as a state of visual impairment resulting in disability that cannot be corrected surgically, medically or with conventional eyeglasses.

Visual acuity is a measure describing the spatial resolution capacity of the visual system [1]. In other words, it is the ability of the eye to resolve fine detail. A person having a visual acuity of x/y will be able to resolve letters from a distance of x units, which a person with normal vision can resolve from a distance of y units. The numerator refers to the distance between the subject and the chart. The denominator is the distance at which the lines that make up those letters would be separated by a visual angle of 1 arc minute, which for the lowest line that is read by an eye with no refractive error (or the errors corrected) is usually 20 feet (6 meters). Thus, normal vision is generally considered 20/20 vision (i.e., 6/6 vision). Having 20/60 vision (6/18 vision) for example, means that this subject must be at 20 feet (6 meters) to see what a person with normal vision can see at 70 feet (18 meters).

In the 10th revision of the WHO *International statistical classification of diseases, injuries and causes of death* (ICD-10), the threshold criteria that define an individual as having *low vision* are an uncorrectable and irreversible visual acuity of less than 20/70¹ but equal to or better than 20/400, or a corresponding visual field loss to less than 20 degrees in the better eye [107].

Low vision rehabilitation is a contemporary subspecialty derived from the fields of ophthalmology, optometry, occupational therapy, and sociology [95]. According to the American Optometric Association (AOA), vision rehabilitation is the process of treatment and education that helps individuals who are visually disabled attain maximum function, a sense of well being, a personally satisfying level of independence, and optimum quality of life. Function is maximized by evaluation, diagnosis and treatment including, but not limited to, the prescription of optical, non-optical, electronic and/or other treatments [7].

People with low vision usually preserve residual visual functions. Attempting to exploit and maximize this available remaining vision, various low vision aids have been developed. A short description of several of the most commonly used devices for vision rehabilitation is presented next.

- **Hand Magnifiers.** A hand-held magnifier is the most basic vision aid (Fig-

¹A visual acuity 20/70 is the minimum acuity required to read standard newspaper print.

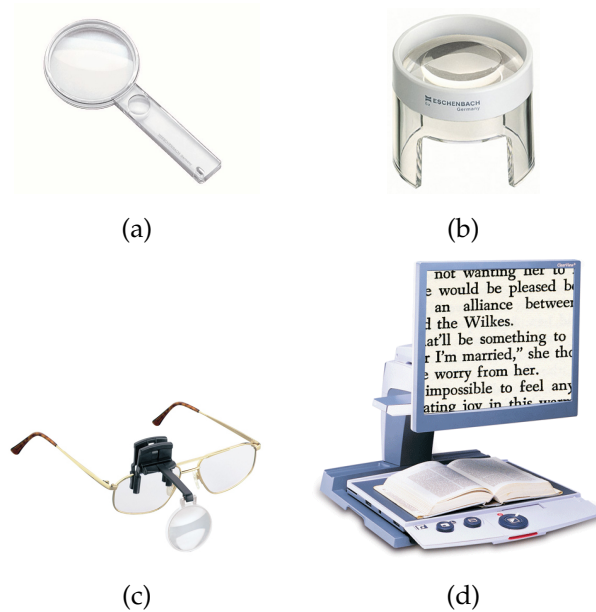


Figure 1.1.: Low vision rehabilitation devices: (a) Hand magnifier, (b) Stand magnifier, (c) Spectacle-mounted magnifier, and (d) Electronic device. (Images source: *Vision Enhancers Ltd, www.visionenhancers.co.uk*).

re 1.1 (a)). These devices allow magnification (up to $5\times$ and some up to $20\times$) at variable working distances, and are especially useful for viewing targets at arm's length or for short-term "spotting" activities. Hand-held magnifiers are used to assist with reading and viewing pictures. Their advantages are low cost and portability. The main disadvantage is that they require steady hands and good motor control, and so often work poorly when patients have tremor. Also, their narrow field of view (only a few letters at a time) requires movement of the device across text during reading, thus reducing speed.

- **Stand Magnifiers.** Stand magnifiers are magnifying lenses mounted on a stand that rest directly on the object or page being viewed (Figure 1.1 (b)). It is the simplest device for reading. When placed on the page, this type of magnifier is automatically in focus for reading. These magnifiers afford magnification (up to $20\times$) at a greater working distance with a smaller field of view than equivalent powered spectacles. Their main advantage over hand magnifiers is that they are hands-free. The drawback may appear with the book bindings since the magnifier may not remain in a stable or fixed

position. In addition, they are not as portable as smaller hand-held magnifiers.

- **Spectacle-Mounted Magnifiers.** Spectacle-mounted magnifiers are small extended lenses that are mounted on eyeglass frames (Figure 1.1 (c)). The magnifiers can be "microscopes" for near vision or "telescopes" for more distant vision. The microscope mode affords hands-free magnification, provide a wider field of view than other equivalent-powered systems, and are more "normal" looking than other reading devices [23]. Moreover, an individual can read for longer periods of time. The main disadvantage is adaptation to the close working distance required (e.g., 5 cm), which some people find difficult and which can interfere with adequate illumination of reading material. The telescope mode is designed for more distant viewing activities like watching television, painting, and looking at a computer monitor. Most telescopic devices provide between $2\times$ and $4\times$ magnification. Walking or moving about while looking through the telescope is not recommended because depth perception is distorted and balance is affected. With both modes, the field of vision is narrow.
- **Electronic Devices.** Commonly called closed-circuit television (CCTV), these devices use a video camera to project a magnified image onto a video monitor, a television screen, or a computer monitor (Figure 1.1 (d)). They permit variable magnification levels (up to $60\times$), manipulation of contrast and brightness, with color or reverse polarity (i.e., displaying printed materials as white letters on a black background), and binocular vision. A CCTV may enable the use of a more comfortable reading/writing posture, longer reading/writing duration, and faster reading speed than optical devices [51].

1.2. Head-Mounted Display Technology for Low Vision

Based on the concept of mediated reality introduced by Mann in 1994 [93], it is possible to enhance visual perception by means of hardware and/or software for filtering our vision of the real world. As a special case of mediated reality, augmented reality (AR) can be defined as a technology in which the user's view of the real world is enhanced or augmented by adding information generated with a computer [84].

In the last decades, various researchers have investigated the use of the head-mounted display in mediated-reality applications for visually impaired people. A short overview of these developments is presented next.

Electronic Head-Mounted Magnification Devices

In 1992, Massof and Rickman (from The Johns Hopkins Wilmer Eye Institute and the NASA Stennis Space Center) developed a low vision system aid known as the *Low Vision Enhancement System* (LVES) [97]. Thereafter, a commercial version of this technology, called *Low Vision Imaging System* (LVIS), was released. The LVIS combines monochrome video cameras mounted on a binocular head-mounted display, which provides variable magnification and contrast enhancement (Figure 1.2). Two video cameras (mounted approximately on axis with the line of sight) transfer an unmagnified binocular view of the world for orientation; and a third center-mounted video camera with zoom magnification optics (up to approx. $10.5\times$), provides the same image to both eyes. The maximum field of view supported is approx. 50° horizontally and 40° vertically. The head system is connected to a portable control box, which contains a battery, electronics, digital signal processor, video input-output jacks and user controls. This first generation of device does not provide any digital image enhancement.

Several generations of the LVIS device are made available in quick succession. Manufactured by Enhanced Vision Systems, the V-max², was developed in 1996. Analogous to the LVIS, the V-maxTM is also a battery powered head-mounted unit, with edge enhancement and contrast reversal features, but using a color video camera with zoom magnification (up to $19\times$) and liquid crystal displays. The maximum field of view is smaller than the LVIS (approximately 25° horizontally and 20° vertically). The V-maxTM is smaller and lighter (650 g) than the LVIS, and has a smaller and simpler control box.

In 1999, the V-maxTM was replaced by the JordyTM system (Enhanced Vision Systems). Along with a light weight of less than 285 grams, the JordyTM has a zoom magnification up to $30\times$. The JordyTM presents four viewing modes: full color, B&W, high contrast, positive & negative. It also provides enhanced and reverse contrast modalities.

Other electronic head-mounted devices, which are commercially available, include the MaxPortTM (by Enhanced Vision Systems in 2000) and the NuVisionTM (in

²Enhanced Vision Systems, Huntington Beach CA.



Figure 1.2.: Low vision imaging system (LVIS) [60].

2001 by Keeler Instruments, Inc.).

The main disadvantages in these devices are the reduced field of view, the complexity of operation (in the case of LVIS), difficulty for navigation, and safe mobility. The systems are unsuitable for patients with serious hand tremors or those patients physically unable to operate the controls.

Head-Mounted Vision Enhancement Devices

Based on the fact that high-contrast binary images (black and white) improve face recognition performance by the visually impaired people using static images [116], a binary head-mounted display device was adapted to present binary video images in real time as a testing platform for a low vision mobility aid [112, 113]. Since binarization of a video signal through a single threshold results in high-contrast but extremely poor image detail, application of bandpass filtering prior to thresholding was implemented to obtain a more detailed binary image. Such processing was enabled using an adaptive 2-D enhancement algorithm by a DigiVision™ device. To reduce the cost, weight, and power consumption of

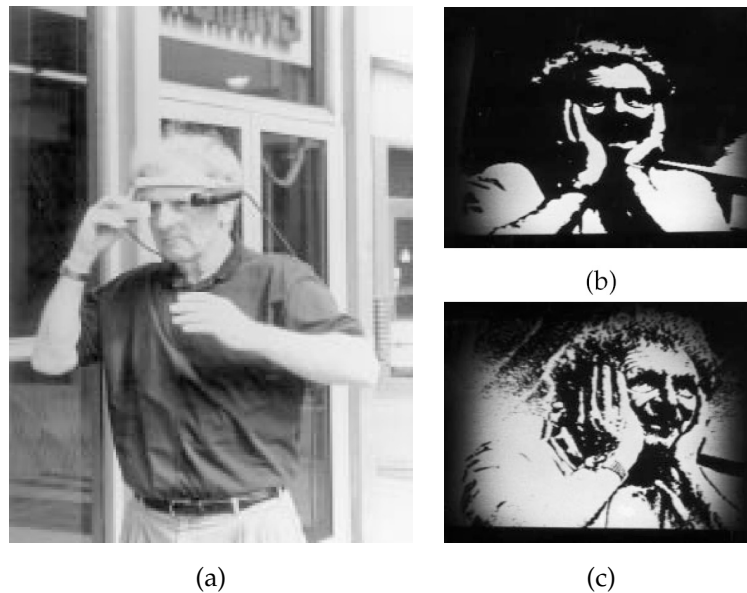


Figure 1.3.: Head-mounted mobility aid for low vision by Peli [113]: (a) User wearing the prototype device, (b) Binary image without 1-D enhancement, and (c) Binary image with 1D enhancement.

the portable aid, a one dimensional (1D) processing alternative was designed (Figure 1.3). The processing was applied only across the horizontal dimension, and it provided no enhancement of horizontal features in the image. However, in the head-mounted camera application the user could resolve such details by a slight tilt of the head.

Everingham et al. combined technology from the field of virtual reality with advanced computer vision techniques to achieve a new mobility aid for people with severe visual impairments [34, 35]. A neural network based head-mounted display system was developed to identify objects in images captured by a head-mounted camera, so that the scene content in the images specifically important for mobility may be made more visible. A high-saturation color scheme is used to enhance the images presented to the user by means of a head-mounted display. The scheme consists of assigning a different color to each type of object, resulting in images which are highly visible and easier to interpret (see Figure 1.4). The object classifier achieves a level of accuracy over 90%. Results from a pilot study conducted using people with a range of visual impairments are presented in which performance on a difficult mobility-related task was improved by over 100% using



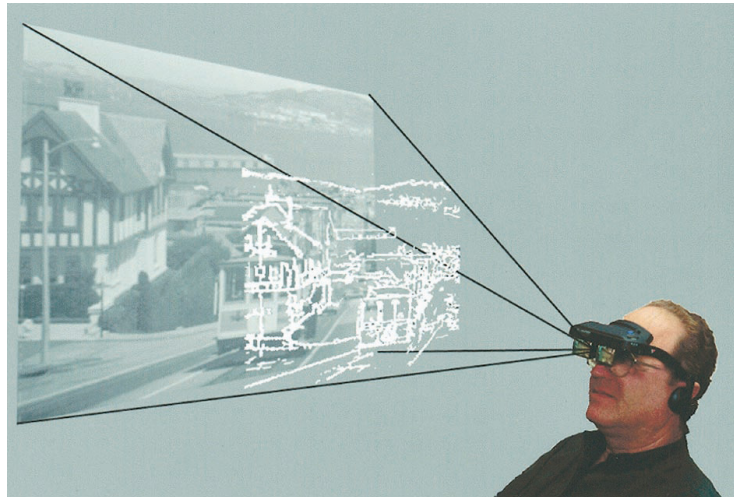
Figure 1.4.: Head-mounted mobility aid for low vision by Everingham et al. [34].

the system.

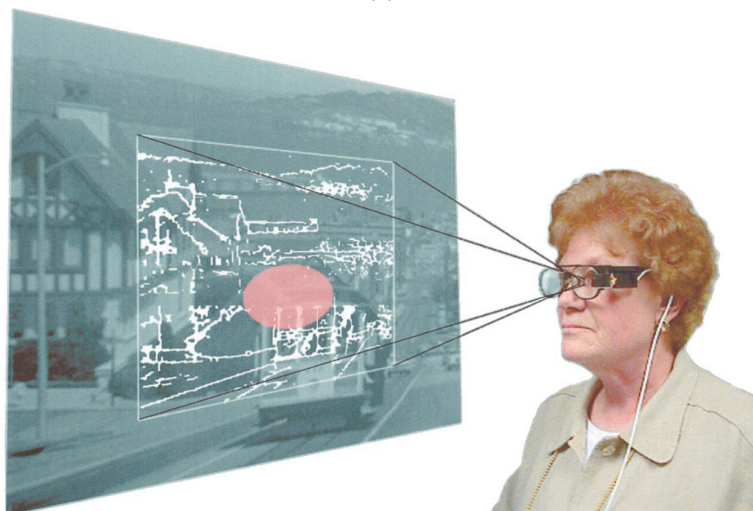
Peli et al. developed two applications using augmented-vision head-mounted display systems to address vision loss [114, 115] (see Figure 1.5).

The first application was designed to improve the visibility of the real world for patients with central field loss. Using an optical see-through head-mounted display and a miniature camera that is aligned with the user's pupil, central visibility is enhanced with 1:1 scale edge images of the real world superimposed over the patients' natural view, while still enabling the wide field of the unimpaired peripheral vision to be maintained (Figure 1.5 (a)). This method is called wide-band enhancement. In laboratory testing, the registration errors (i.e., the alignment of the virtual edges shown in the display and their real-world referent) were found to be low across a wide depth range [91]. Moreover, the major cause of registration error was the variability in the position of the HMD relative to the eye. Although the registration error of the on-axis HMD system was low, it was not ready for evaluations by patients with central vision loss. The edge images were not of sufficient quality, as the on-axis optics reduces the light reaching the camera. Also, the miniature camera used in the registration evaluation had limited light sensitivity [117]. A simulated view of the system through the head-mounted display is shown in Figure 1.6.

In the second application, minified edge images of a real-world scene captured by a head-mounted video camera are presented on a transparent see-through display to provide visual field expansion for people with peripheral vision loss (Figure 1.5 (b)), while maintaining the full resolution of the remaining central vision [114, 153]. The system uses a miniature monochrome video camera mounted on the HMD with a field of view substantially wider than that of the display (a



(a)



(b)

Figure 1.5.: Illustrations of the concept of augmented-vision head-mounted display systems by Peli [115]: (a) Wide-band enhancement for patients with central vision loss, and (b) Visual field expander for patients with tunnel vision (depicted with the elliptical area in the middle of the scene).



(a)



(b)

Figure 1.6.: Simulation of the wide-band enhancement system for patients with central vision loss by Peli [117]: (a) Original scene view, and (b) Enhanced scene view through on-axis superimposed edges.

factor of three to four times wider), enabling up to $4\times$ minification. A portable processor provides edge detection from the images captured by the camera. The minified contour map provides the patient with navigation information, which would otherwise be outside his view. The approach has been applied in daytime and nighttime devices [14]. A series of laboratory studies indicated that the system could help with visual search, obstacle avoidance, and nighttime mobility [118]. An augmented view of the visual field expander system through the display can be observed in Figure 1.7.

Although image visibility may be satisfactory in indoor environments and outdoors on cloudy days, head-mounted displays with optical see-through technology are not adequate neither in outdoors on sunny days nor indoors with high illumination. Moreover, in the case of superimposed edges, a tiny shift in the position of the display relative to the user's eye can produce a significant offset in registration of contours in the scene.

In 2005, Farago et al. developed an image transformation system denominated ATDV (Apoio Tecnológico aos Deficientes Visuais – Technological Support for Visual Impairments) [36]. Assuming only one defined area of the visual field with perception loss, denominated scotoma, the ATDV system uses the Convex Hull algorithm and Isoperimetric Mapping (by Haber et al. [58]) on data generated by the visual field exam to identify the scotoma limits. Scene information situated inside the scotoma is warped around the spot boundaries. A head-mounted display can be used to visualize the transformed images. Simulation of the final view obtained by the ATDV system is shown in Figure 1.8 (b).

In human vision science, there is no evidence about visual remapping of deformed information. As a matter of fact, severe distorted vision caused by specific eye diseases is significantly associated with reduced vision-related quality of life [43]. Therefore, the deformed information generated by the ADTV system may be very difficult to be interpreted by the observer, and hence not helpful for improving vision.

1.3. Research Objectives

The principal objective of this work is to investigate integration feasibility of advanced imaging methods into head-mounted displays to obtain a low vision enhancement system for patients with age-related macular degeneration. Individual



Figure 1.7.: Simulation of the visual field expander system for patients with tunnel vision by Peli [117]. Restricted view of a street-crossing scene (upper image). Augmented view through superimposed minified edges of the wide field of view not covered by the patient vision (lower image).



Figure 1.8.: ATDV system for patients with central vision loss [36]: (a) Original scene view, and (b) Scene view deformed by the ATDV system.

objectives are briefly highlighted next.

- One of the first specific goals is to determine and integrate the most efficient magnification technique into a head-mounted display as a plausible solution for the problem of improving residual visual functions of low vision patients.
- Since a modern Graphics Processing Unit (GPU) can perform faster numerical computations on high-resolution images visualized in HMDs compared with general purpose Central Processing Units (CPUs), and based on the concept of General Purpose computation on GPU (GPGPU) introduced in [62, 108], the goal is to implement the adopted magnification technique with GPU-accelerated algorithms for real-time computation in stereo vision images of head-mounted displays.
- Another leading goal is to examine the possibility of designing and implementing a novel approach for modeling and compensating distorted vision presented in some cases of visually impaired people, along with a system which permits the analysis of this indecipherable disorder for many experts in the ophthalmology field.
- A final and substantially important objective is the evaluation of the envisioned solutions with reliable and efficient approaches.

1.4. Contributions

The main contributions of this thesis consist in the development of a mediated-reality magnification system as a vision enhancement device for people with age-related macular degeneration, including the integration of a hybrid magnification approach into a head-mounted display combining efficient properties of linear and nonlinear transformations, and the adaptation of GPU-accelerated algorithms into the system for real-time performance.

Other significant contributions are the development of a practical and useful method to acquire a correction model for distorted vision; together with a novel system for alignment and analysis of the model with optical coherence tomography retinal images to find macular patterns which may lead to obtain an automatic modeling method. The correction model can be incorporated into an augmented-reality display device fulfilling certain requirements, discussed in this work, to compensate visual distortions of patients with maculopathies.

Finally, the design and creation of innovative simulation systems for evaluation of the mediated-reality solutions for low vision rehabilitation contribute as an efficient reference assessment framework for the scientific community to be applied in future developments.

The work presented in this thesis spawned a series of publications presented at major conferences in the field of ophthalmology and medical augmented reality. Below is an extract from this list:

- A. Martin-Gonzalez, I. Lanzl, R. Khoramnia, and N. Navab. Evaluation of Hybrid Magnification for AMD Patients with an Eye-Tracking based Simulation System. *The Association for Research in Vision and Ophthalmology, Inc. (ARVO) (Annual Meeting)*, Fort Lauderdale, Florida, USA, 2011.
- A. Martin-Gonzalez, I. Lanzl, R. Khoramnia, and N. Navab. Simulation and Modeling of Metamorphopsia with a Deformable Amsler Grid. In *Medicine Meets Virtual Reality 18 (MMVR18) conference proceedings*, Newport Beach, California, USA, pages 336-342, 2011.
- A. Martin-Gonzalez, I. Lanzl, R. Khoramnia, and N. Navab. System for Modeling and Localizing Metamorphopsia in OCT images. *The Association for Research in Vision and Ophthalmology, Inc. (ARVO) (Annual Meeting)*, at Fort Lauderdale, Florida, USA, 2010.

- A. Martin-Gonzalez, S. M. Heining, and N. Navab. Head-mounted virtual loupe with sight-based activation for surgical applications. *8th IEEE International Symposium on Mixed and Augmented Reality (ISMAR)*, Orlando, Florida, USA, pages 207-208, 2009.
- A. Martin-Gonzalez, I. Lanzl, K. Kotliar, and N. Navab. Real-Time Hybrid Magnification System for AMD Patients. *The Association for Research in Vision and Ophthalmology, Inc. (ARVO) (Annual Meeting)*, Fort Lauderdale, Florida, USA, 2009.

1.5. Outline of the Thesis

Each of the presently paragraphs provides the reader with a brief description of the individual chapters of the thesis.

PART I: INTRODUCTION AND THEORY

CHAPTER 1: INTRODUCTION

Chapter 1 serves as the introduction into this thesis. A brief summarize enclosing the reasons which motivated the work in this research is presented: the impact of age-related macular degeneration, the current low vision assistive technology, and an overview of head-mounted devices for low vision.

CHAPTER 2: MEDICAL BACKGROUND

In chapter 2 an anatomical and pathological background of the eye is provided. This chapter introduces the basic concepts of the visual human system used as a medical basis throughout this dissertation. It also provides a concise overview of age-related macular degeneration, which is the main pathology motivating this thesis.

PART II: METHODS

CHAPTER 3: HEAD-MOUNTED HYBRID MAGNIFICATION SYSTEM

Chapter 3 introduces a head-mounted system to enhance the use of peripheral visual perception due to central vision loss. Magnification techniques, materials, methods, and evaluation procedures are thoroughly described. In addition and as

part of the assesment process, an adaptation of the system for surgical procedures is demonstrated.

CHAPTER 4: METAMORPHOPSIA MODELING SYSTEM

Chapter 4 presents a comprehensive description of an innovative solution for modeling and correcting distorted vision (metamorphopsia), which is one of main symptoms affecting quality of life in patients with retinal maculopathies. A metamorphopsia simulation system is introduced in this chapter as an evaluation methodology of the proposed modeling system.

PART III: FINAL CONCLUSIONS

CHAPTER 5: CONCLUSIONS

This chapter concludes the thesis with a summary of the outcome and discusses the final remarks about feasible future research directions.

CHAPTER 2

Medical Background

ONE of the most sophisticated sensory capacities of the human being is the sense of sight, also known as vision. The fundamental organs of sight are the eyes. Through the eyes we are able to perceive the world surrounding us. Based on signals sent from the retina, the innermost layer of the eye, our brain is capable of producing 3D virtual images of the objects we are looking at, as well as analyzing their form, size, texture, color, depth, and movement. Vision allows to interpret information associated to the environment, providing not only humans, but also almost all animals with an indispensable skill to survive on the Earth.

Understanding the basic anatomy and function of the human eye is essential for expanding our knowledge of nature and to enhance the progress of technology of visualization which may enable people with visual disabilities to perceive the outside world once again.

2.1. Anatomy and Physiology of the Human Eye

The human eye is a complex organ responsible for detecting light, and converting it into electrical impulses. It involves a complicated optical system responsible for optimizing reception of light, and a neural system capable of transducing the light energy to electrical signals sent to the brain.

The eye is enclosed by three layers: the **outer layer**, which is formed by the

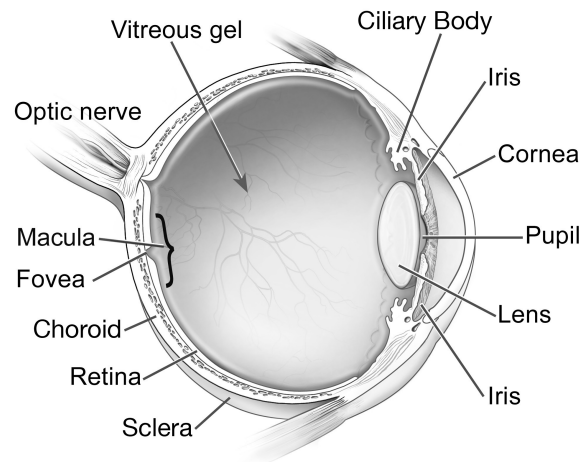


Figure 2.1.: Human eye cross-sectional view (Image source: Adaptation from National Eye Institute, National Institutes of Health; Ref: NEA09).

sclera and cornea; the **intermediate layer**, which is divided into the iris and ciliary body as anterior part, and the choroid as posterior part; and the **internal layer**, which comprises the retina (see Figure 2.1).

The eyeball also contains three chambers of fluid: **anterior chamber** (between the cornea and the iris); **posterior chamber** (between the iris and the lens); and **vitreous chamber** (between the lens and the retina). The first two chambers are filled with aqueous humor, a thick watery fluid that provides nourishment to the interior eye structures and keeps the globe of the eye inflated. The vitreous chamber is filled with a thicker fluid called the vitreous humor (vitreous gel).

The **cornea** is a tough, transparent fibrous tissue covering the anterior surface of the eye. In order to preserve transparency, the cornea is a non-vascular¹ structure. It obtains nutrients from tears on the outside, aqueous fluid on the inside, and small blood vessels located at the periphery. The human cornea is one of the most sensitive tissues in the body, as it is densely supplied with sensory nerve fibers. The cornea initiates the image-forming process by refracting light entering the eye.

Continuous with the cornea, the **sclera** is an opaque fibrous tissue enclosing and protecting the remainder of the eyeball. Known as the *white of the eye*, the sclera

¹Not supplied by blood vessels.

maintains the shape of the globe by providing resistance to internal and external forces, and supplies an attachment for the extraocular muscles.

The **choroid** is the posterior part of the intermediate membrane enclosing the eyeball located directly below the sclera. The choroid coat is highly pigmented in order to reduce the absorption of extraneous light entering the eye and to prevent scattering. The choroid receives the greatest blood supply that provides oxygen and nutrients to the retina [65]. At its anterior extreme, the choroid is divided into the ciliary body and the iris diaphragm.

The **iris** is a circular pigmented muscle, which primary function is to regulate the amount of light entering the eye [164]. The **pupil** is the central aperture of the iris. The size of the pupil varies in diameter from approximately 2 to 8 mm depending on the contraction of the muscle fibers in the iris.

The **ciliary body** consists of tissue that connects the iris with the choroid and includes a group of muscles, termed ciliary muscles, which act on the lens of the eye to change its shape.

The crystalline **lens** of the eye is a transparent, fibrous, flexible and elliptical structure located behind the iris. In conjunction with the cornea, the lens bends light to focus and form a clear image on the retina. By changing the curvature of the lens through the contraction or relaxation of the ciliary muscles, light coming from objects at different distances is focused on the retina.

The **optic nerve**, also called cranial nerve II, consists of the axons of neurons in the retina. Considered part of the central nervous system, the optic nerve carries all the visual information from cells in the retina to the brain for processing. The point where the optic nerve exits the eye produces a *blind spot* as a result of the absence of cells to detect light in that area of the retina. The blind spot is not normally perceived since the brain fills in with surrounding detail and with information from the other eye.

The innermost membrane of the eye is the **retina**. The retina is a layer of light sensitive tissue located in the inside surface of the back of the eyeball. The retina is a complex, layered structure with several layers of neurons interconnected by synapses. The main function of the retina is to convert light into electrical impulses and send them to the brain [69]. It contains special neurons sensitive to light called photoreceptors, as well as various types of neurons that are responsible for early stages of visual information processing.

The principal cell types in the retina are (Figure 2.2): the *photoreceptors*, which are the input layer; the *ganglion cells*, which are the only output from the eye,

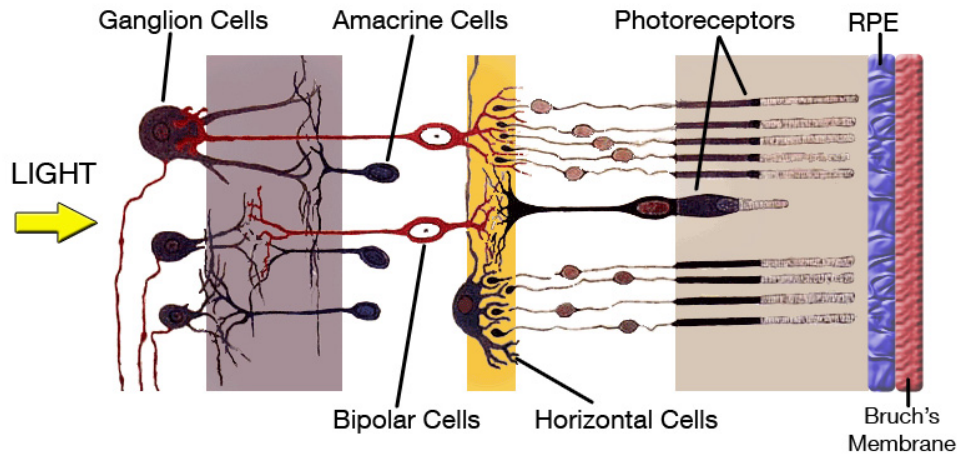


Figure 2.2.: Retinal layer (Image source: Adaptation from Ramon y Cajal [165]).

transmitting all processed information along the optic nerve to the brain [130]; the *bipolar cells*, which connect the photoreceptors to the ganglion cells; the *horizontal cells*, which converge signals from several rods and cones; and the *amacrine cells*, which converge signals from peripheral rods. The **retinal pigment epithelium** (RPE) is the pigmented cell layer, located just outside the neurosensory retina and firmly attached to the underlying choroid that nourishes the retinal cells.

The **photoreceptors** are responsible for converting the light they detect into neural impulses that are then sent onto the brain along the optic nerve. There are two fundamental types of photoreceptors: the cones and the rods. Figure 2.3 shows the density of photoreceptors along the retinal surface for a cross section of the right eye. With the exception of the blind spot region, the photoreceptors have a radially symmetric distribution about the fovea. Photoreceptor density is measured in degrees from the fovea.

The **cones** are sensitive to color and high-intensity light. Each human eye contains about 6 million cones. These cells are densely concentrated in the center of the retina and become sparser towards the periphery [123]. There are three kinds of cone cells in humans that are sensitive to a different range of the visual spectrum of light. Integration of impulses from different types of cone cells provides color vision [46]. Humans can resolve fine details with the cones cells largely because each one is connected to its own nerve end (one-to-one connectivity to ganglion cells) [123]. Furthermore, cones also have a much faster response to light than do rods, and hence they can perceive more rapid changes in stimuli.

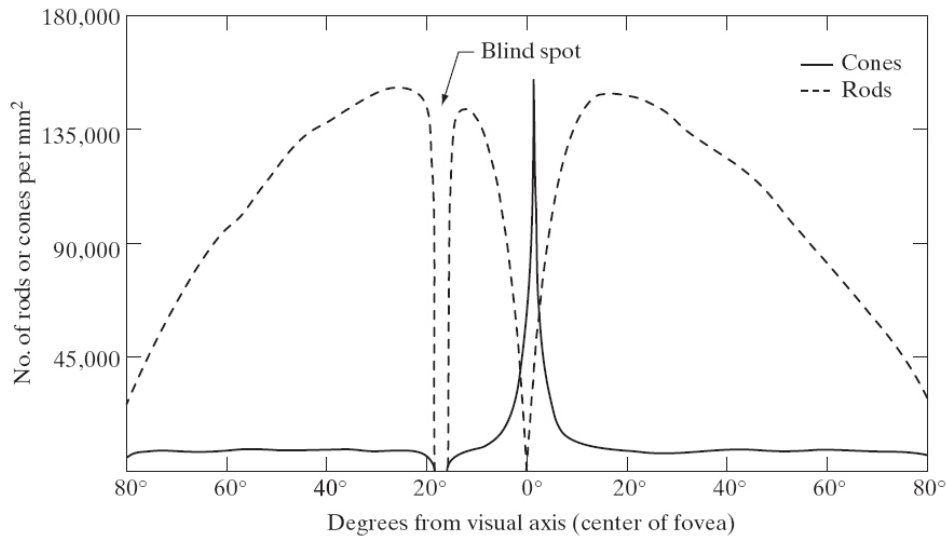


Figure 2.3.: Distribution of rods and cones in the retina (*Image source: Gonzalez and Woods [50]*).

The **rods** are sensitive to low light levels. Opposite to the cones, the rods cannot detect color. The human retina has between 75 to 150 million rods. They are distributed over the retinal surface. They are responsible for night vision and peripheral vision. The larger area of distribution and the fact that several rods are connected to a single nerve end reduce the amount of detail discernible by these receptors. Rods serve to give a general, overall picture of the field of view. While visual acuity or visual resolution is much higher with the cones, the rods are better motion sensors.

The **macula** is the central area of the retina of about 5 mm in diameter. The center of the macula is called the **fovea**, a small cavity of about 1.5 mm in diameter. The fovea is the region of highest visual acuity. As seen on the Figure 2.3, the fovea contains a high density of cones. Therefore, the fovea is responsible for sharp central vision, which is indispensable in humans for reading, watching television, driving, recognizing faces, and performing other activities that require fine, acute and straightforward vision. Consequently, the macula is responsible for central vision; and all the visual perception that occurs outside the macula of the retina is referred as peripheral vision. The visual acuity declines progressively from the fovea out to the periphery of the retina [3]. Figure 2.4 provides a feeling of peripheral visual acuity.

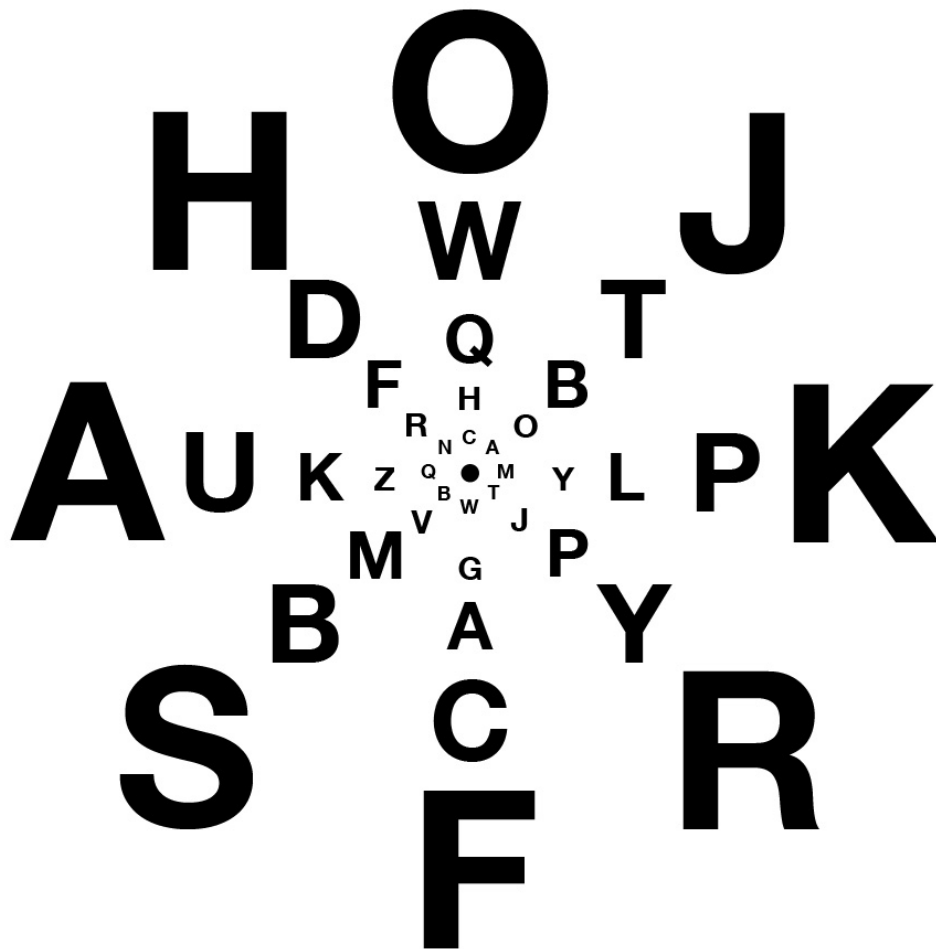


Figure 2.4.: Reading acuity chart. All letters should be equally readable when the center of this chart is fixated, since each letter is ten times its threshold height (*Image source: Adaptation from Anstis [3]*).

Outside the eye, there are small muscles, called the **extraocular muscles**, responsible to produce and control the horizontal, vertical and rotating movements of the eyeball. These muscles play an important role in the **vestibulo-ocular reflex (VOR)**, which main function is to stabilize an image on the retina during head motion by moving the eyes in the opposite direction to the head movement.

The entire area simultaneously visible to the steadily fixating eye is defined as the **visual field**. The human visual field in each eye normally covers 60 degrees nasally (toward the nose), 100 degrees temporally (away from the nose), and 60 degrees above and 75 below the horizontal meridian. The macula corresponds to the central 13 degrees of the visual field; and the fovea to the central three degrees.

2.2. Age-Related Macular Degeneration

Referred to as senile or age-related maculopathy, age-related macular degeneration (AMD) is a leading cause of irreversible visual impairment among the elderly population in the Western world [155]. Knowledge of a detailed AMD pathology may form the basis for understanding the conditions and mechanisms of the disease.

2.2.1. Definition and Classification

Age-related macular degeneration is a progressive eye disease associated with aging that deteriorates the macula. Degeneration of the photoreceptors in the macular area results in vision loss. The evolution of AMD can be slow in some people, causing no vision impairment for a long time; or can be faster, leading to a severe loss of vision in one or both eyes.

The clinical course of this medical condition is divided into two stages [30]. The **early stage** of age-related macular degeneration is characterized by the formation of yellow deposits, called *drusen*, in the central area of the macula. Generally, this early type is without significant vision loss, and visual symptoms are unnoticeable [67]. A large number of drusen increases the risk for the development of a late stage of AMD [83]. The **late stage** of age-related macular degeneration is identified by the growth of new choroidal vessels, termed choroidal neovascularization (CNV). In this late type, severe loss of vision is usual, and the two forms of AMD are present: dry (non-neovascular) and wet (neovascular).

Dry Macular Degeneration (non-neovascular)

Dry macular degeneration is the most common form of the disease, occurring in about 90 percent of people diagnosed with AMD. The dry form of AMD is characterized by the accumulation of drusen (deposits or debris from deteriorating tissue) in the macula, between the retina and the choroid (Figure 2.5 (b)). Degeneration of the photoreceptors in the macular area occurs when the retinal pigment epithelium cells with which they are associated deteriorate and die, gradually blurring central vision in the affected eye. This form may result from the aging and thinning of macular tissues. Nevertheless, the causes of dry macular degeneration remain so far unclear.

The dry form can be classified in three stages: early, intermediate, and advanced. In the **early dry AMD**, either small drusen or a few medium-sized drusen is visible; and may not have any symptoms or vision loss. The **intermediate dry AMD** has either many medium-sized drusen or one or more large drusen; and possibly without symptoms. In addition to drusen, **advanced dry AMD** provokes a breakdown of photoreceptors in the macula, causing a blurred spot in the center of vision.

Scientists are uncertain about the connection between drusen and AMD since drusen alone do not usually cause vision loss. However, an increase in the size or number of drusen raises the risk of developing either advanced dry AMD or wet AMD [83].

Dry AMD generally affects both eyes, but vision could also be disturbed in one eye while the other eye seems unaffected. The non-neovascular form can progress and cause vision loss without turning into the wet form; or can suddenly change into the wet form.

Wet Macular Degeneration (neovascular)

Wet macular degeneration, considered advanced AMD, occurs when abnormal blood vessels from the choroid grow and proliferate under the macula through breaks in the Bruch's membrane (a layer between the retina and choroid) to beneath the retinal pigment epithelium [15]. This process is called choroidal neovascularization (Figure 2.5 (c)). The new blood vessels tend to be very fragile, leaking blood and fluid. The abnormal leakage from these vessels can raise the macula from its normal place at the back of the eye. Along with scar formation from these blood vessels, wet macular degeneration can result in permanent vision loss.

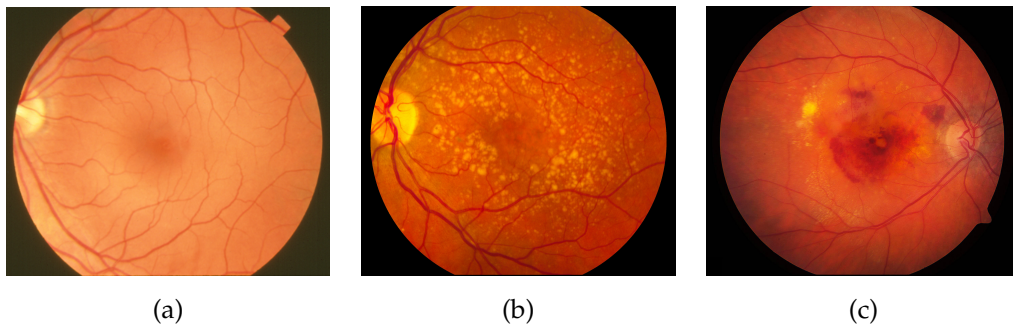


Figure 2.5.: AMD forms in retinal fundus images: (a) normal fundus, (b) dry form, and (c) wet form. (*Image source: National Eye Institute, National Institutes of Health; Ref: (a) EDA06, (b) EDA22, and (c) EDA24.*)

Estimates indicate that only about 10% to 20% of all patients with any sign of AMD have the neovascular form of the disease [37, 71]. However, this type is more severe than the early and intermediate stages of the dry form, being responsible for approximately 90% of cases with extreme vision loss [71].

A significant fact is that within five years of the development of choroidal neovascularization in the first eye, there is a high risk (>40%) of developing choroidal neovascularization in the second eye [55]. With wet AMD, deterioration of central vision can occur quickly.

2.2.2. Symptoms

Age-related macular degeneration usually causes a slow, painless loss of vision. Frequently, early stages of AMD initiate without symptoms, and only a comprehensive dilated eye exam can detect the presence of AMD. On the other hand, some patients might initially ignore symptoms of vision loss, considering them to be a normal part of the aging process or incorrectly attribute them to the development of cataracts [159].

Blurred vision, scotomas, and metamorphopsia are essentially the main symptoms in age-related maculopathy [38]. These symptoms are described next.

Central Vision Loss

The most common symptom of dry AMD is blurred vision, this is, a gradual loss of ability to see objects clearly (Figure 2.6 (b)). Since a reduced number of photore-

ceptors in the macula are able to function, details will be seen less clearly along with a progressive loss of color vision. As a result, the gradual central vision loss may cause difficulty for reading, recognising faces, and daily activities which depend on a good visual acuity. Frequently, brighter light improves blurred vision.

If the loss of photoreceptors becomes significant, light associated with those photoreceptors will not be sensed, generating a blind spot in the field of vision (Figure 2.6 (c)). Such a blind spot is termed **scotoma**, and can be defined as a retinal area of complete or partial absence of vision, surrounded by an area of vision.

Absolute scotomas are retinal areas that are insensitive to very bright objects, whereas *relative scotomas* are retinal areas that are insensitive to a light level relatively less than the very bright object. Scotomas are further defined by their retinal location in that *central scotomas* are in retinal areas involving the fovea, while *para-central scotomas* are in retinal areas within the central 20° of the visual field but not involving the fovea [137]. Scotomas appear usually in advanced stages of AMD.

Even though the complete visual field is almost never deteriorated by AMD, visual acuity of the remaining peripheral vision is usually low to perform satisfactorily day to day activities.

It has been demonstrated that the human visual system engages in a phenomenon known as *perceptual completion* or *filling-in* whereby the absence of visual input is not perceived [47]. In other words, it refers to seeing a figure as complete when part of it falls in a blind area of the visual field [140]. For many years, perceptual completion of the physiological blind spot at the optic nerve head has been known [17]. A similar filling-in phenomenon, responsible for completion of missing information across the physiological blind spot, can be observed in pathologic retinal scotomas [162, 167], in scotomas caused by cortical lesions [32, 140], in simulated scotomas [124], and in ordinary areas of the peripheral visual field [31]. According to studies, patients with macular scotomas due to AMD do not perceive black spots in the visual field where the scotomas are located. Rather, they describe objects as "vanishing", "having blurry parts" or "jumping out of nowhere", or a combination of features [135]. Crossland and Bex [27], have shown that different mechanisms for perceptual completion over the physiological blind spot and pathologic retinal scotomas are involved. Filling-in at the optic nerve head involves low-level visual system processes that may be hardwired, in which receptive fields span the blind spot and support fine orientation discriminations. Filling-in across pathologic scotomas appears to involve

higher level image processing-based mechanisms that operate even when their input is interrupted.

Furthermore, when the macular scotoma affects the fovea, the visual system develops one or more preferred retinal loci (PRLs) as a *pseudofovea* to perform visual tasks [136, 135]. The PRL becomes the new center of the visual field [148].

Metamorphopsia

The first symptom of wet macular degeneration is distorted vision, also termed *metamorphopsia*. This symptom is caused by the detachment of the retinal pigment epithelium or the neurosensory retina (which overlies the retinal pigment epithelium) from Bruch's membrane due to hemorrhagic fluid from the leaking blood vessels, disturbing the fine arrangement of photoreceptors [30]. Straight lines will not appear straight, but instead bent, wavy or crooked to people with metamorphopsia (Figure 2.6 (d)).

The severity of metamorphopsia is significantly associated with vision-related quality of life (VR-QOL) [43, 106].

2.2.3. Risk Factors

Although several studies regarding incidence and prevalence of AMD in large populations have enhanced the understanding of this eye disorder, the cause and development of the disease remain unclear.

Age is the principal risk factor to increase the probabilities of developing AMD. Nevertheless, a number of other risk factors associated with AMD have been identified, including genetic (e.g., complement factor H polymorphisms), demographic (e.g., ethnicity), nutritional (e.g., antioxidant vitamins, dietary fats), lifestyle (e.g., smoking), medical (e.g., cardiovascular risk factors, hypertension) and environmental factors (e.g., sun exposure), and ocular factors (e.g., cataract surgery) [20, 22, 39, 40, 120, 144, 152]. Some of these risk factors are briefly described as follows:

- **Smoking.** Smoking may increase the risk of AMD [146, 33]. Smoking has been postulated to cause AMD by depression of antioxidant levels and alteration of choroidal blood flow and detoxification of the retinal pigment epithelium. It has been hypothesized that decrease in luteal pigments in human retina due to cigarette smoking may cause light and oxidative damage



Figure 2.6.: Simulation of AMD Symptoms: (a) normal vision, (b) blurred vision, (c) central scotoma, and (d) distorted vision.

to the macula, thereby leading to an increased risk of developing AMD [76]. A positive association between smoking and neovascular AMD has been suggested in both men [53] and women [138].

- **Family history.** First-degree relatives of patients with AMD tend to have a higher risk of AMD [80, 147].
- **Gender.** Females appear to have a significantly higher risk of visual impairment than males in every region of the world. The number of women with visual impairment, as estimated from studies, is higher than that in men even after adjustment for age [127]. The high risk of AMD in females may be due to the loss of a protective effect of estrogens in postmenopausal women [154].
- **Race.** The incidence of AMD in blacks was found to be relatively lower compared with whites [82]. It has been demonstrated that drusen are common in both blacks and whites over the age of 40. However, more severe forms of AMD have a higher prevalence in older whites [41].
- **Nutrition.** Obesity appears to be related with a higher risk of early and advanced age-related macular degeneration, whereas an inverse association has also been found between dietary carotenoid² intake and AMD [70].

The evidence and strength of association of these factors and AMD remain variable in the literature. However, recent reviews and analysis in epidemiologic studies indicate that increasing age, current cigarette smoking, previous cataract surgery, and a family history of AMD have shown strong and consistent associations with advanced AMD [21, 25]. Risk factors with moderate and consistent associations were higher body mass index, history of cardiovascular disease, hypertension, and higher plasma fibrinogen. Risk factors with weaker and inconsistent associations were gender, ethnicity, diabetes, iris colour, history of cerebrovascular disease, and serum total and high-density lipoprotein (HDL) cholesterol and triglyceride levels [21]. In addition, genetic studies have recently implicated many genes in the pathogenesis of age-related maculopathy, demonstrating that environmental and genetic factors are important for the development of AMD [6, 16, 25].

²Natural food sources of carotenoids include fruits and vegetables.

2.2.4. Medical Treatments

Dry Macular Degeneration

Dry macular degeneration has unfortunately at the moment no treatment. Once dry AMD reaches the advanced stage, no form of therapy can prevent vision loss. The National Eye Institute's Age-Related Eye Disease Study (AREDS)³ found that high levels of antioxidants and zinc significantly reduce the risk of advanced AMD and its associated vision loss, slowing down the progression of the disease.

Wet Macular Degeneration

A number of therapeutic strategies are available for wet macular degeneration. In general, the main objective of these treatments is to stop the growth of new blood vessels. Usually, the treatment needs to be given as soon as the blood vessels start to grow in the eye since scarring produced by the copious growing of new blood vessels cannot be treated. None of these therapies is a cure for wet AMD. However, they can delay and possibly prevent the progression of the disease.

Treatment options for some people who progress to neovascular AMD include the following: laser photocoagulation surgery [54], photodynamic therapy with verteporfin [111], submacular surgery [57], and intravitreal injections of antiangiogenic drugs [52, 44]. Some of these neovascular AMD treatments are shortly described in the subsequent paragraphs.

Laser photocoagulation surgery. This therapy uses a laser to destroy abnormal blood vessels in the early course of the disease. A high energy beam of light is aimed directly onto the new blood vessels and destroys them, preventing further loss of vision. However, conventional laser power may also destroy some surrounding healthy tissue (including photoreceptors) and therefore some vision is instantly lost. In addition, the recurrence of new blood vessels developing after laser treatment is common. Repeated treatments may progress vision loss. Although peripheral vision is better preserved by laser surgery, the idea of treating an eye in the knowledge that central vision will be instantaneously destroyed has not been preferred for ophthalmologists and patients.

Intravitreal injections. One of the most recent treatments available for wet AMD is with an *anti-vascular endothelial growth factor* (anti-VEGF) drug, which is injected into the eye. People diagnosed with wet AMD have abnormal high lev-

³<http://www.nei.nih.gov/amd/>

els of a specific growth factor, promoting the growth of new blood vessels. An anti-VEGF drug blocks the effects of the growth factor and stops the vessels from growing. Thus, further damage to the sight is prevented.

The main complications of this treatment are the chance of a rise in pressure in your eye, retinal detachment, and eye infections. Current anti-VEGF agents in use are ranibizumab (Lucentis), pegaptanib (Macugen), and bevacizumab (Avastin). The treatment may normally require multiple injections.

Anti-VEGF therapy is usually the first treatment offered to people with wet AMD, having a high success rate and in most cases they stop sight getting worse.

Photodynamic therapy. Photodynamic therapy (PDT) consists of laser treatment, which uses a combination of a light-sensitive drug and a low energy (cold) laser to stop new blood vessels growing.

A photosensitive drug called verteporfin (Visudyne) is injected in the patient's arm. Once this drug has made its way to the new blood vessels which grow in wet AMD, a very bright light (a cold laser) can be targeted onto these blood vessels. The light activates the drug, which destroys the new blood vessels. Since the drug is activated by light, the patient must avoid sunlight exposure or bright indoor light for five days after treatment.

The major advantage is that, unlike laser surgery, PDT can be used to treat cases where the blood vessels have already reached the fovea, without destroying surrounding healthy tissue (including overlying photoreceptors) and worsening vision. Although it cannot stop vision loss, photodynamic therapy minimizes visual loss in patients with choroidal neovascularization due to AMD.

2.3. Visual Field Assessment

Visual acuity is a standard clinical testing which measures the capacity to discriminate the fine details of objects. It consists on determining the smallest letters a person can read on a standardized chart (Snellen chart) held 20 feet (6 meters) away. Color vision testing, flicker sensitivity, contrast sensitivity, pupillary responses and motion testing are some of the other methods of evaluating vision. Even when the visual acuity test is still the gold standard in clinical practice, it does not entirely reflect functional vision (which describes the impact of sight on quality of life activities).

2.3.1. Perimetry

Perimetry or campimetry is a visual field assessment technique which measures a patient's capability to perceive light originated at different positions across the field of view. In other words, it is the measurement of sensitivity to light across the retina. It consists of the detection of sequential dots of light presented at different locations and with certain intensity on a defined background. The purpose of perimetry is to identify and follow up defects in the visual field, for instance, scotomas, loss of peripheral vision, or more subtle vision loss. The two most commonly used schemes are kinetic and static perimetry.

In *kinetic perimetry* a stimulus (dot of light) is presented and moved manually throughout the visual field (gradually from the periphery toward the center of the visual field) to determine the region in which it is visible for the patient. The Goldmann perimetry, introduced in 1945 [48], is a common example of kinetic perimetry. It is typically used for patients with visual field defects outside the central 30°, with severely decreased vision, or who benefit from interaction with the examiner. One of the main advantages of kinetic perimetry is that the examiner can move rather quickly over areas of minor interest and spend relatively more time inspecting critical regions [61]. Nevertheless, limitations of kinetic perimetry include the need for a skilled perimetrist [150], as well as the examiner bias, lack of reproducibility and standardization, and manual examination variability [121].

In *static perimetry* a location of the visual field to present the target is chosen and the stimulus intensity or size changed until it is large enough and bright enough for the patient to see it, thus measuring essentially the same locality, so the stimulus is stationary, or static [61]. The Octopus (Interzeag International, Bern-Koniz, Switzerland) and the Humphrey Field Analyzer (Zeiss Humphrey Systems, Dublin, CA) are common examples of static perimeter. Static perimetry was found to be superior to kinetic perimetry in detecting visual field loss in the central 30° earlier [75], with more standardization, and without the need for skilled perimetrists. Limitations of static perimetry included the need for greater patient concentration and initiative, and decreased efficacy in delineating complex lesions that extend into the peripheral field [78].

Perimeters can also be classified as *manual* or *automated*, depending on whether the stimulus is moved by hand as in the Goldmann perimeter, or if the stimulus location is changed by a computer, as in the Humphrey Field Analyzer.

2.3.2. Noise Field Campimetry

Since the filling-in phenomena normally prevents the subjective perception of scotomas, mapping of the affected retinal areas may be a difficult task. Aulhorn and Köst exposed that these phenomena can, in some situations, be overcome by gazing at random visual noise, such as video static [8].

Noise field campimetry (also called entoptic perimetry) is a visual field assessment technique which makes scotomas visible that are not normally perceived by patients because of perceptual filling in [8, 122]. The technique consists of having the patient looking at a video display that is filled with small black and white spots flickering randomly at high frequency. A normally sighted subject will perceive that the field is completely filled with random visual noise patterns, often described as "snow" or "static". Patients with visual field defects may perceive their affected area as a region that can variously appear motionless, dark, grey, or otherwise different from the noise pattern. Mapping the vision defect may be possible once the scotoma is recognized.

In order to enhance scotoma perception during entoptic perimetry, Crossland et al. employed the *twinkle after-effect* (TwAE), which is an illusion that can be induced following adaptation to a random noise stimulus [28]. When the noise pattern is suddenly replaced with a uniform field, the affected region within the visual field (i.e. a scotoma) will appear to "twinkle" if the noise pattern did not stimulate that area [124].

Noise-field campimetry is a promising tool for self-assessment of macular function in patients with macular degeneration. However, the subjective appreciation of scotomas is completely foreign to most people, making it potentially difficult for some patients to understand and perform the test without supervision. Moreover, not all patients are capable of perceiving their scotomas using currently available noise-field campimetry techniques [149].

2.3.3. Microperimetry

Standard visual field examination is insufficient for the accurate functional evaluation of macular diseases, especially if the patient has unsteady or extrafoveal fixation. Moreover, in low vision patients, conventional perimetry is insensitive to small scotomas ($< 5^\circ$); does not allow a precise identification of size, shape and depth of scotomas; and is unable to identify preferred retinal locus [101]. These limitations have been overcome by the introduction of microperimetry.

2. Medical Background

Microperimetry (also known as fundus perimetry) assesses the visual function by exactly correlating retinal sensitivity to retinal morphology [102]. In microperimetry a dot of light is projected onto the retina through the pupil at a certain retinal point and with certain intensity. The patient is asked to confirm perception of some brightness at some point in the visual field. Therefore, by changing the stimulus intensity, microperimetry determines differential light sensitivity or threshold at a certain retinal point. As a main difference to perimetry, microperimetry associates retinal sensitivity to retinal structures since the obtained sensitivity map can be registered precisely to the corresponding fundus or OCT retinal image of the patient taken during the test. Furthermore, microperimetry compensates for the eye movements during examination due to eye tracking, which eliminates fixation stability as an error factor in visual field assessment.

Part II.

Methods

CHAPTER 3

Head-Mounted Hybrid Magnification System

DUE to the deterioration of the macula, which is responsible for central vision, patients with age-related macular degeneration use remaining peripheral vision. However, peripheral retinal regions comprise less photoreceptors to perceive light than the macular area, causing inability to perform common daily activities that require visual precision such as reading, driving or recognizing faces (see Chapter 2).

In order to compensate the lack of light sensors in the periphery it is necessary to magnify the information perceived by the eye. On that account, a head-mounted hybrid magnification system is proposed and developed; providing the user real-time magnified stereo vision enclosing a global context of the scene for enhancing visual resolution in the peripheral vision.

The following sections present the complete developed system, its methodology, and the different evaluation procedures performed.

3.1. Related Work

Linear magnification techniques, similar to the effect produced by magnifying glasses, have been the most common approach for many low vision rehabilitation aids, from optical to electronic head-mounted devices (see Chapter 1). The main disadvantages of a linear magnification are the reduced field of view, the loss of

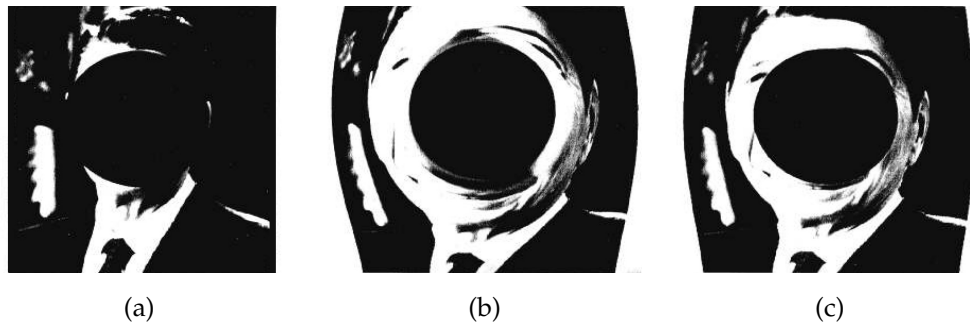


Figure 3.1.: Programmable Remapper by Loshin and Juday [90]: (a) Face view occluded with a central scotoma, (b) Face view with zero effective scotoma remapping, and (c) Face view with partial effective scotoma remapping.

information not covered but occluded by the magnified area, and the abrupt transition of spatial levels (i.e., changing the perception from the normal resolution view to the higher resolution view).

In the last decades, scientists have proposed head-mounted magnification systems as a low vision device for people with retinal diseases. For instance, Loshin and Juday proposed a low vision aid, called the *Programmable Remapper*, for subjects with visual field defects [90]. In the case of people with central vision loss, the system provided a spatial coordinate transformation consisting of “stretching” out the visual information falling within the field defect and wrapping this information around the edges of the scotoma with an unconstrained non-linear magnification function. Two types of remapping algorithms were shown: the *zero effective scotoma* remaps the entire occluded information, and the *partial effective scotoma* remaps only half of the occluded information, losing the remaining hidden portion. Figure 3.1 presents a simulation of the final view after applying these remapping algorithms.

Steve Mann proposed a mediated-reality system, denominated the “Personal Visual Assistant” (PVA), as a prosthetic device for the partially sighted [94]. The PVA system permitted transformation of spatial coordinates for magnifying the view similar to the work presented by Loshin and Juday, but without “stretching” out the information occluded by the scotoma (see Figure 3.2).

The main disadvantage in these remapping approaches is the effect of distorted central magnification displayed in the remaining vision of the user, since central

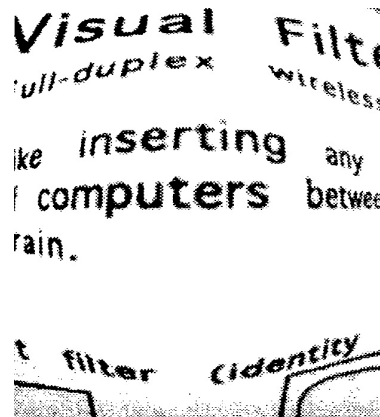


Figure 3.2.: Example of image coordinate transformation by the PVA system [94].

deformations may inhibit image recognition and hence vision enhancement.

In order to overcome limitations presented in the state of the art, a head-mounted display using a hybrid magnification approach is proposed as a low vision rehabilitation system for subjects with central vision loss.

A complete description of the system is presented in the following sections.

3.2. Low Vision Rehabilitation System

The low vision rehabilitation system used throughout this work consists of a video see-through HMD, a high performance PC workstation with high end GPU, and a software framework (CAMPAR [142]) to combine input data from all hardware systems and drive the visualization on the HMD.

3.2.1. Head-Mounted Display

A head-mounted display (HMD) is a display device, worn on the head, which has a small display optic in front of one (monocular HMD) or each eye (binocular HMD) of the user.

The binocular HMD used in this work is a video-see through HMD with resolution of 1280×1024 pixels (px) at 60 frames per second (fps) with 60° of monocular field of view (FOV). A video-see through HMD displays only a computer-generated image (CGI), in contrast to an optical-see through HMD which displays a CGI superimposed on a real-world view.



Figure 3.3.: Head-mounted magnification system for AMD patients.

A set of two color cameras are rigidly attached to the HMD and have resolution of 1024×768 pixels at 30 fps, playing the role of the user's artificial eyes by capturing live images of the scene. An illustration of the overall system can be observed in Figure 3.3, and its corresponding technical specifications are shown in table 3.1.

The main workstation for computing the magnification approach is a personal computer (PC) with an Intel Core 2 Quad Q9550 processor at 2.83 GHz with 3.25 GB RAM and Nvidia GeForce GTX 280 graphics card (see table 3.2).

3.2.2. Software Framework

The AR software framework CAMPAR [142] was used for combining all dynamic input data (i.e. video streams). CAMPAR is a modular, multiple layer, component based framework, with a small core library for the most common functionality in medical AR. It features an easy to extend API for access to various input and output devices. Input devices are grouped in categories, e.g. video input devices or tracking input devices. A set of input device classes wrapping access to the most common tracking and camera devices is included within the core library. Instances of output device classes are in general used for displaying the augmented reality scene on the HMD, single or multiple monitors, or write data to a file stream. Additional input/output devices can be created by deriving from

	Low Vision Rehabilitation System
HMD	nVisor SX (nVis, Inc.)
HMD resolution	SXGA: 1280×1024 px
HMD monocular FOV	60°
HMD overlap	100°
HMD color format	True-Color, 24 bit
HMD update rate	60 Hz
HMD arc minute per pixel	<2.2
HMD eye relief	23mm to 30mm
Color cam.	Flea IEEE-I394, Point Grey Research®
Color cam. resolution	1024×768 px
Color cam. update rate	30 Hz
Imaging sensor	1/3" Sony®CCD sensor
HMD + Camera Weight	~1 Kg
Max. system frame rate	30 Hz
Min. system latency	~1.3 ms

Table 3.1.: Augmented reality vision rehabilitation system specifications.

	PC Workstation
CPU	Intel Core 2 Quad Q9550, 2.83 GHz
Memory	3.25 GB
GPU	Nvidia GeForce GTX 280
Number Shaders	240
Memory	1 GB

Table 3.2.: Augmented reality system main PC workstation specifications.

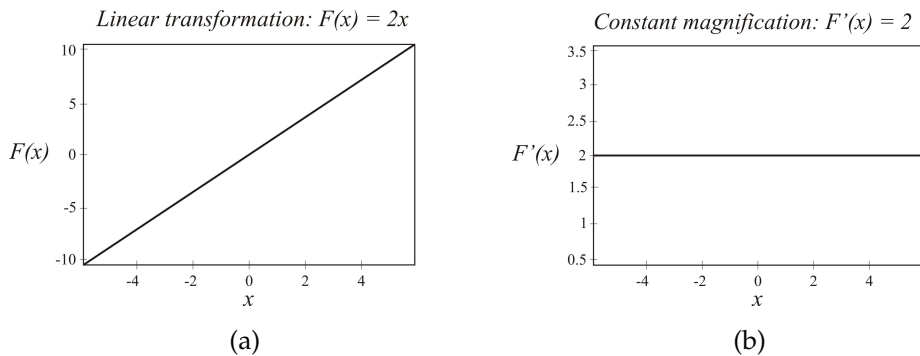


Figure 3.4.: Linear magnification functions.

generic base classes, adding new functionality, and creating a plugin dynamic-link library (DLL) that will be loaded by the driver application. To synchronize input and output, CAMPAR employs a synchronizer that implements a set of temporal synchronization policies. In the default case the synchronizer will wait for the slowest system component prior to updating the displayed AR scene.

The software is implemented with C++ programming language and the novel OpenGL Shading Language¹ (GLSL) [131] in order to get direct access to graphics hardware and therefore, a real-time performance.

3.3. Magnification Transformations

There are different methods for implementing general non-linear magnification transformations presented by Keahey and Robertson [77]. We have adapted and applied these concepts into a head-mounted display for augmented reality.

3.3.1. Linear Magnifications

A linear magnification is the most ordinary magnification technique. It involves the application of a linear transformation function (Figure 3.4), which produces a constant level of magnification across the domain (a similar effect perceived through a typical optical magnifying glass). Nevertheless, linear magnifications have limitations, such as, occlusion of information and a disjoint level of resolution in the image.

¹OpenGL Shading Language - www.OpenGL.org

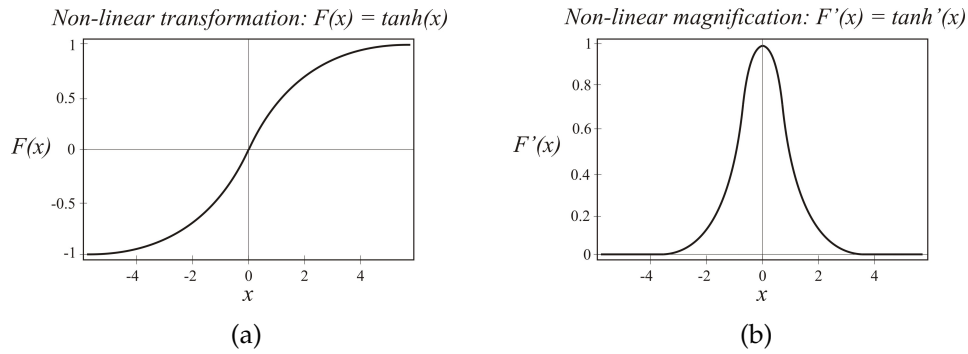


Figure 3.5.: Non-linear magnification functions.

3.3.2. Non-Linear Magnifications

Non-linear magnifications overcome some of the problems with linear magnification, providing an enhanced local resolution with global context preservation.

Hyperbolic Tangent Function

The hyperbolic tangent function $h(x) = \tanh(x)$ is one example of a non-linear transformation function to produce a non-linear magnification. The parameter β can be added to control the degree of magnification, so that $h(x, \beta) = \tanh(\beta x)$. This function is well-behaved across all domains. Figure 3.5 shows the $\tanh(x)$ transformation function and its associated magnification function.

A function that is computationally less expensive and produces a similar effect to that of $\tanh(x)$ is the modified logistic function: $h(x, \beta) = \frac{2}{1+e^{-2\beta x}} - 1$.

For moving the center of magnification across the domain it is necessary to replace $h(x)$ with $(h(x - x_0) + x_0)$, where x_0 is the new center of maximal magnification.

3.3.3. Radial Magnification

The radial magnification is a two-dimensional magnification that can be produced by transforming each point in the domain as follows:

1. Given a center point of magnification $C = (C_x, C_y)$ and a point to transform $P = (P_x, P_y)$, let $\hat{P} = P - C$.
2. Find the radius component of the polar coordinates of \hat{P} : $r = \sqrt{\hat{P}_x^2 + \hat{P}_y^2}$.

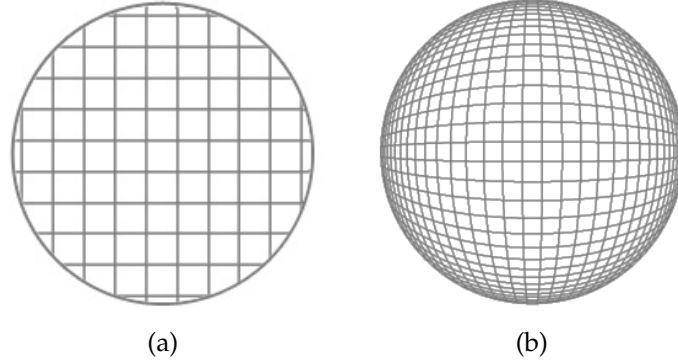


Figure 3.6.: Radial magnifications: (a) Linear magnification, and (b) Non-linear magnification.

3. The new coordinates are then $C + \frac{h(r)}{r} * \hat{P}$, where $h(r)$ is a one-dimensional transformation function.

Radial transformations preserve angles relative to the magnification center (see Figure 3.6).

3.3.4. Constrained Transformations

In a constrained magnification, transformations are performed inside a sub-area of the domain, and all points outside the domain remain untransformed (Figure 3.7). This produces a non-occluding magnification which can be moved over the source domain. In addition, the boundaries of the global context remain fixed even as the center of the magnification is changed.

3.4. Hybrid Magnification Approach

The hybrid magnification approach proposed consists of a radial linear magnification surrounded by a radial non-linear magnification, containing a smooth interpolation of hidden non-magnified information lying below the linearly magnified area, with constrained domain. Figure 3.8 shows the final result of applying such combined transformations to a regular grid of two dimensional points.

In order to avoid occlusion of information produced by the linear magnification, the use of a non-linear magnification is combined, where:

$$h(x, \beta) = \frac{2}{1 + e^{-2\beta x}} - 1 \quad (3.1)$$

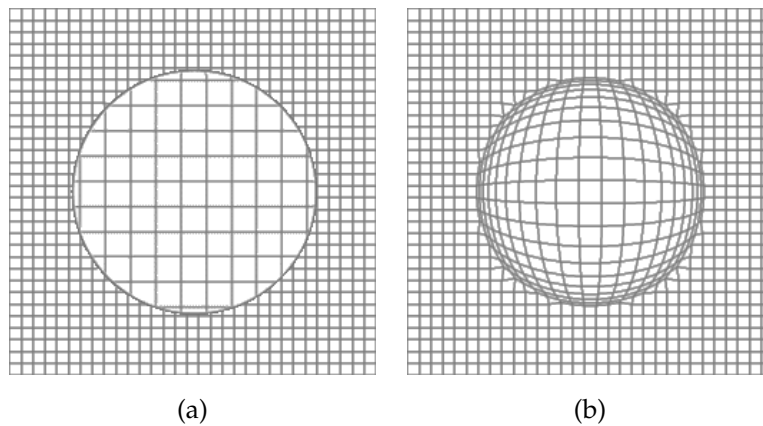


Figure 3.7.: Constrained magnifications: (a) Radial linear magnification, and (b) Radial non-linear magnification.

The distortion-free magnification produced by a linear transformation permits the user to visualize the image data at the area of maximal magnification without the distortions presented by non-linear transformations. By constraining the transformed points of a sub-area to the same sub-area, preservation of global context in the scene is achieved.

3.5. Results

The magnification approach was successfully implemented and integrated on the head-mounted display through GPU-accelerated algorithms that provide direct access of graphics hardware for a real-time computation.

Examples of the simulated view of the hybrid magnification versus the linear magnification are shown in Figure 3.9.

The magnification system computational time with stereo cameras is 8.98 ms. This time is still less than the time for the arrival of the next video frame (33.33 ms) provided by the camera rate (30 fps); therefore the program can execute the video image processing in real-time without losing any video frame, providing the user with a more natural feeling of visual continuity.

The magnifying approach combines desirable properties from linear, non-linear and constrained magnifications with a single transformation. For instance, the visual information after being magnified presents an undistorted central zooming (due to linear magnification), continuity between magnified and non-magnified

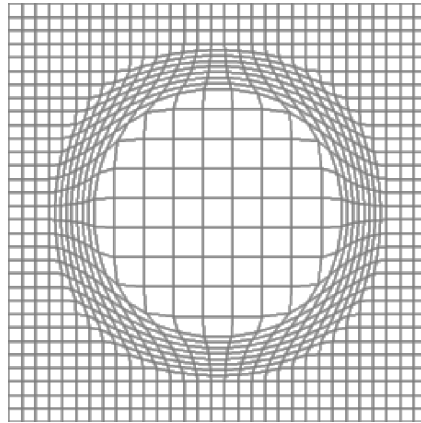


Figure 3.8.: Hybrid magnification approach.

areas plus no-hidden information (due to non-linear magnification), and global context (due to constrained domain).

The system was used by two patients with dry AMD for reading short texts and following routes on a map (see Figure 3.10). Even when the forced head movement for performing the tasks was a substantial disadvantage for the users, the qualitative feedback obtained from this initial examination was positive.

3.6. Discussion

The proposed head-mounted magnification device for patients with age-related macular degeneration will only be completed with an integrated eye-tracking system, which follows the gaze of the user to allocate the magnification in a preferred retinal area; for instance, outside the affected macular area. Unfortunately, the existing technology of eye trackers mounted inside a head-mounted display is not still suitable enough to be used by patients with AMD, considering that patients with a central scotoma cannot perform the calibration procedure enclosed in the current eye tracker systems, which requires central vision fixation of points on the monitor for adjusting internal parameters of the device.

Under this assumption, a novel system to provide a more extensive and quantitative evaluation of the introduced magnification system is presented next.

which in turn regulates the elect
 a. These include the bipolar neu
 n along the light-path and the ho
 at transmit information sideways
 lar to the light-path. The last neu
 glion cells, the retina's output neu
 erves connecting the eye to the br

(a)

which in turn regulates the elect
 a. These include the bipolar neu
 n along the light-path and the ho
 at transmit information sideways
 lar to the light-path. The last neu
 glion cells, the retina's output neu
 erves connecting the eye to the br

(b)

which in turn regulates the elect
 a. These include the bipolar neu
 n along the light-path and the ho
 at transmit information sideways
 lar to the light-path. The last neu
 glion cells, the retina's output neu
 erves connecting the eye to the br

(c)

Figure 3.9.: Illustration of magnification modes: (a) Original image, (b) Linear magnification, and (c) Hybrid magnification.

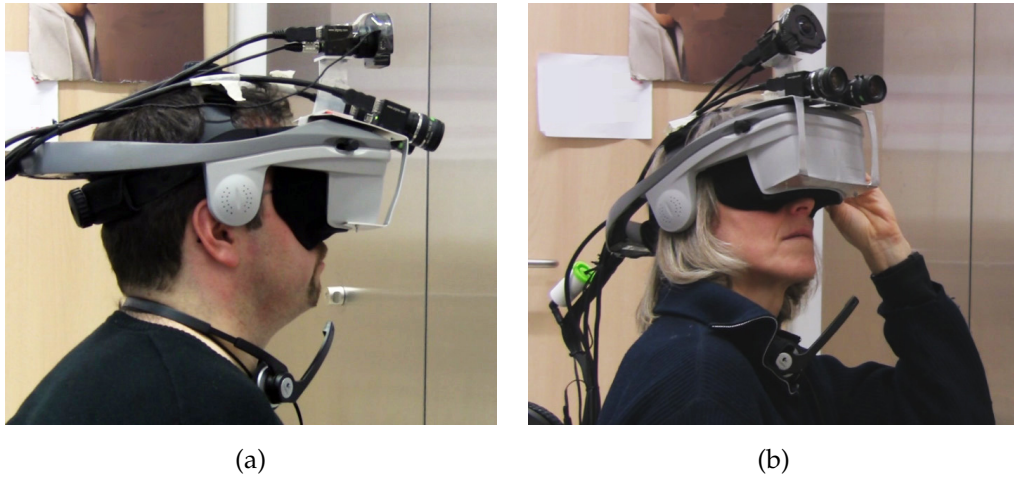


Figure 3.10.: Patients with AMD assisted by the head-mounted hybrid magnification system.

3.7. Eye-Tracking based AMD Simulation System

3.7.1. Purpose

With the objective to evaluate the performance of the hybrid magnification approach implemented on the head-mounted display as a vision enhancement device for patients with age-related macular degeneration, an eye-tracking based AMD simulation system is developed for being tested on people with normal vision.

3.7.2. Methods and Materials

The simulation system setup combines an eye tracker of binocular tracking with 0.5 degrees of accuracy at 60 Hz data rate (for details see table 3.3), a 17" external monitor (1600×1200 pixels of resolution), and a workstation with Intel Core Duo CPU at 2.40 GHz, 2GB of RAM (see Figure 3.11).

For the work presented in this section, a CAMPAR output device plugin, combining the techniques presented in section 3.4 and the current hardware setup, was developed.

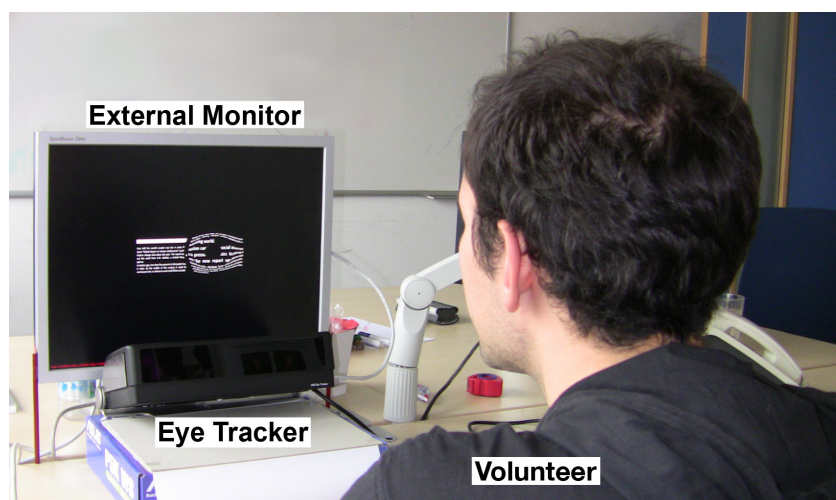


Figure 3.11.: Eye-tracking based simulation system.

	Eye-Tracking Device
Model	Tobii X60, Tobii Eye Tracking Research
Accuracy	0.5 degrees
Drift	<0.3 degrees
Data rate	60 Hz
Freedom of head movement	44×22×30 cm
Binocular tracking	yes

Table 3.3.: Eye-tracking device technical specification.

3.7.3. Experiments

The experiment consists of simulating central vision loss (central scotoma) on a subject with healthy vision while reading a short text or following a route on a map assisted by a magnification mode: hybrid magnification versus linear magnification. Three scotoma sizes are simulated for reading and only one for following routes. In the experimentation, three texts and two routes per mode are examined.

The visual angle V corresponding to an object in the visual field (e.g. scotoma) can be computed by the following equation:

$$V = 2 \arctan(S/2D) \quad (3.2)$$

where S is the object length in the real world and D is the distance from the eye to

the object location (i.e., monitor distance).

In order to avoid a learning curve while reading, a total of six different texts are created. Each text is composed of 84 syllables (64 ± 3 words, 329 ± 6 characters with spaces). The text length criteria are not only equal number of words, but mainly equal number of syllables. This is because a word that consists of a single syllable (monosyllable), for example *dog*, will take shorter time to be read than a word with three syllables (trisyllable), for instance *amusement*. Under this assumption, the reading speed unit used is syllables per second (syllable/s) instead of words per minute (wpm).

For measuring speed in following routes on a map, two different routes on a subway map are selected for testing one magnification mode and the same two routes on the inverted image of the subway map are used for the remaining magnification mode. Thus, the length of the routes is equivalent for the evaluation. The route following speed unit used is meters per second (m/s).

The eye tracker employed obtains the subject's gaze position on the monitor where the scotoma and the magnification center should be displayed.

Each experiment performed is recorded (gaze movements on the monitor) in order to measure and analyze task completion time.

3.7.4. Results

In total, 25 volunteers with healthy vision (20/20 best corrected visual acuity) were able to fulfill the experiment consisting of reading texts and following routes on a map assisted by a magnification mode with a simulated central scotoma.

The scotoma sizes generated for reading were 0.5° , 1.3° and 2.1° visual angles, seen at a distance of 75 cm away from the monitor. The scotoma size of 0.5° was selected for following routes on a map with a wider linear magnification area. The scotoma dimension was determined experimentally, taking into account that a larger scotoma size causes higher difficulty for the normal sighted subject to perform the tasks with peripheral vision. On the other hand, the magnification size was also established experimentally, trying to have a magnification area larger than the scotoma size and covering a sufficient region for a subject to read comfortably. The linear magnification factor was two ($2\times$). Once all parameters were determined, they were fixed and applied to all the participants. Figures 3.12 and 3.13 present examples of the simulated scotomas and the magnification modalities. The median value, obtained from the overall results in the experiments, shows



Figure 3.12.: Simulation of scotoma sizes for text reading. Left column: (a)–(c) Linear magnification. Right column: (d)–(e) Hybrid magnification.

3. Head-Mounted Hybrid Magnification System

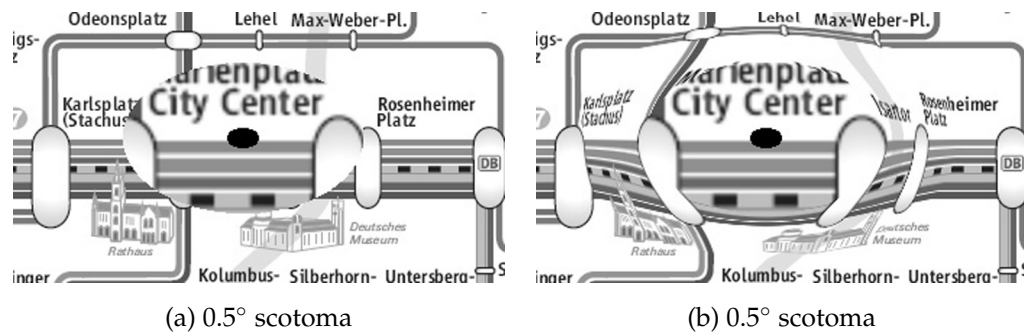


Figure 3.13.: Simulation of scotoma size for following routes on a map: (a) Linear mode, and (b) Hybrid mode.

that a subject reads 1.2 times faster with hybrid magnification mode than with linear mode, with a minimum value of 1.0 and a maximum value of 2.4; and follows routes 1.5 times faster with hybrid mode than with linear mode, with a minimum value of 1.1 and a maximum value of 2.6.

In Table 3.4, the reading speed improvement according to each scotoma size is shown. The ratios of reading speed with hybrid mode to those with linear mode are calculated for every experiment and a median value is obtained. The minimum value of 1.0 shows that the hybrid mode permits the user to have the same reading speed as the linear mode in the worst case; and it will improve the user reading speed up to 2.4 times than the linear mode in the best case. Out of these results it can be said that the larger the scotoma size the larger the difference between magnification modes.

Table 3.5 shows reading speed median values (per magnification mode) based on the unit syllables per second. It is interesting to remark that the ratio of the reading speed with hybrid mode and a 1.3° scotoma to that with linear mode and a 0.5° scotoma is approximately 1.0; a nearly similar result is achieved in the case of 2.1° scotoma and 1.3° reading speeds. This indicates that with hybrid mode it is possible to reach the same reading speed as with linear mode and a smaller scotoma problem.

During the experiments, measurements of a line return (i.e. the time taken by the eyes to move the focus from the end of one text line to the beginning of the next text line) were made. Observations of the ratio of the line return with hybrid mode to that with linear mode are presented in Table 3.6. As seen in the results, there is time improvement on performing a line return by using hybrid mode. The

	Scotoma 0.5°	Scotoma 1.3°	Scotoma 2.1°
Median	1.2	1.2	1.4
Min	1.0	1.0	1.0
Max	1.8	2.2	2.4

Table 3.4.: Ratios of reading speed (hybrid mode over linear mode).

	Scotoma 0.5°		Scotoma 1.3°		Scotoma 2.1°	
	Linear	Hybrid	Linear	Hybrid	Linear	Hybrid
Median	2.11	2.39	1.69	2.12	0.91	1.62
Min	1.18	1.79	0.75	0.89	0.42	0.92
Max	2.90	3.17	2.40	2.89	2.23	2.49

Table 3.5.: Reading speed (syllable/s).

justification for this situation may be that the global context of the scene provided by the hybrid mode permits an easier and faster line following. This aspect also has a contribution for reading faster. In this case, there is no clear improvement tendency in relation to the scotoma size.

According to the ratio of speed with hybrid mode to that with linear mode in the overall results of route following, the minimum value of 1.1 shows that the hybrid mode permits the user to follow routes faster than the linear mode in the worst case; and in the best case it will improve the user speed up to 2.6 times. In Table 3.7 route following speed improvement is shown under the unit meters per second.

The gaze tracking permitted a natural eye movement for performing the tasks and a precise location to place the simulated scotoma and magnification transformation.

Qualitative feedback of volunteers shows that the global context of the scene (no-hidden information) supported by the hybrid mode provides an efficient spatial orientation.

3.7.5. Discussion

It is important to notice that without the assistance of an eye tracker, the scotoma simulation would have been unfeasible. Moreover, in the case of a real patient with a head-mounted magnification system, an eye tracker would permit a nat-

3. Head-Mounted Hybrid Magnification System

	Scotoma 0.5°	Scotoma 1.3°	Scotoma 2.1°
Median	1.3	1.2	1.3
Min	1.0	1.0	1.0
Max	2.0	1.8	2.3

Table 3.6.: Ratios of line return (hybrid mode over linear mode).

	Scotoma 0.5°	
	Linear	Hybrid
Median	0.0180	0.0246
Min	0.0079	0.0110
Max	0.0384	0.0543

Table 3.7.: Route following speed (m/s).

ural eye movement (for changing the focus of interest) along with a magnification centered in the preferred retinal locus of the patient, instead of a forced head movement with a static fixed magnification.

For more advanced states of AMD, larger scotoma sizes are presented. In the case of normal sighted subjects, adaptation to such scotoma sizes (e.g. 10°) would have consumed much more time, taking into account that for real patients the progression of the disease and hence visual adaptation can vary from months to years. In these experiments, the scotoma sizes were selected in order to examine the effects of the system in relation to the size increase, but seeking an easy visual adaptation for the normal sighted subject.

One of the main advantages of the hybrid magnification system is that, as a mediated-reality device, it can be enhanced with several computational techniques and used in different application domains where magnifying the working area while keeping a global information of the scene is of great benefit, e.g., focusing military targets at the distance, magnifying a vehicle registration plate during a police chase, identifying moving targets on the airspace, among others. Under this conception, a different application field was explored to evaluate the current magnification system and to analyze its efficiency scope. Such research is presented in the following section.

3.8. Sight-based Magnification System for Surgical Applications

In the medical domain, AR technology has been used to assist surgical procedures by visualizing medical image data registered with real anatomy [9, 12, 10]. Moreover, medical virtual tools have been developed, such as the concept of a virtual mirror for improving navigation within a medical augmented reality system [104, 64].

Magnification of the operating field provides considerable advantages for performing general microsurgical procedures in various disciplines of the medical field, such as neurosurgery, plastic surgery and orthopedics. The most common magnification equipment in the operating room (OR) are the operating microscope and binocular surgical loupes (magnifying glasses). The operating microscope has been an important element in the OR for magnifying the physician's view to visualize micro structures (i.e. small blood vessels and nerves) in order to assist interventions that cannot be done with a normal (20/20 visual acuity) human's vision.

Medical AR systems based on the use of surgical microscopes have been developed and tested during the last decade. Birkfellner et al. [11] introduced an adapted commercial head-mounted operating microscope for stereoscopic augmented reality visualization (Varioscope AR) with different assessments for various zoom factors and working distances of the head-mounted display (HMD). The work developed by King et al. [79] presents an integrated AR approach for overlaying preoperative images into the binocular optics of a surgical microscope in brain surgery. Further on, Aschke et al. [5] proposed a stereoscopic image augmentation system using the optics of the operating microscope for enhancing intraoperative planning. In a more recent work, Garcia et al. [45] have developed an augmented reality system to align preoperative tomographic images into a surgical microscope with a rigidly mounted mini-tracking system used to track the movements of surgical tools and the patient.

Despite the high quality of real optics in microscope-based augmented reality systems, there are some disadvantages related to these devices. For instance, surgeons have to maintain a fixed ergonomic position during the whole intervention. This is not the case for a head-mounted microscope, nevertheless, due to the continuous magnified view aligned to the eyes' sight, the surgeon is not able to vi-

sualize other areas inside the operating room with normal vision. Therefore, the surgeon is not able to perform simple tasks such as grabbing medical instruments without the help of an assistant, following their own hand movement while using a medical tool outside the device optical scope during the surgical procedure, or interacting visually with medical partners or external equipment in the OR.

In addition, the surgeon's peripheral vision is significantly reduced due to the constrained field of view from the optical eyepieces. Furthermore, the linear magnification provided causes the need to deal with hidden visual information occluded below the magnified space, restricting the observer to perceive complete information concerning surrounding areas near the operating field. Moreover, there is the need to handle an abrupt step from the magnified space to the non-magnified one during the visual perception of the operating field.

In order to overcome the above limitations of microscopes, to enhance skills of surgeons, and to analyze the performance of the hybrid magnification approach in a specific purpose task, a stereoscopic head-mounted magnification system with sight-based activation is proposed. The hybrid magnification approach for AMD patients is implemented in the system to provide no-hidden information, global context of the scene and a smooth transition between magnified and non-magnified visual information. The magnified view of the system will be activated when the line of sight of the head-mounted display is oriented towards the operating field of interest. Any other position will display a non-magnified view. This automatic dual-view functionality permits a hands-free control, similar to the one inherited in the use of medical loupes.

In addition, the system's digital interface is suitable for displaying the captured video of the operation procedure to an external monitor for medical assistants in the room to see or even store it for a later review.

3.8.1. Hardware Setup

The system integrates the head-mounted display system used in the hybrid magnification system setup explained in section 3.2.1 (see Figure 3.14). In addition, a pointer tool is used for determining a 3D point within a specified working area where the magnification will take place.

A video see-through device is being used due to the following advantages: full control for merging enhanced and real scene images, real scene images can be delayed to reduce relative lag (such a delay is small enough not to perturb hand-

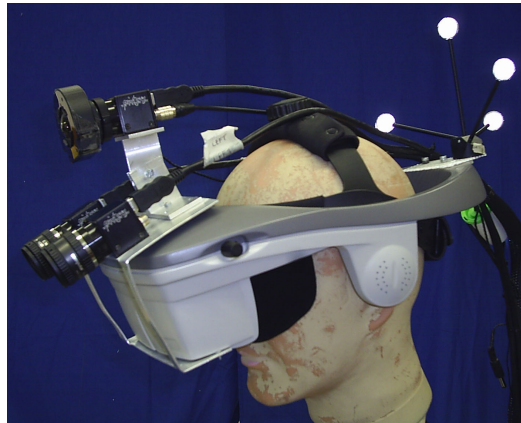


Figure 3.14.: Sight-based magnification head-mounted system.

eye coordination), and only camera-to-display transformations have to be known in contrast to eye-to-display transformation for an optical see-through system. In addition, a head-mounted display avoids difficulty with hand-eye coordination presented by an external monitor display.

The system uses two synchronized infrared based tracking systems in order to have a high-precision tracking (Figure 3.15). Both tracking devices are passive optical trackers, therefore the devices to be tracked (HMD and pointer) use a unique arrangement of retroreflective markers so that unambiguous identification is feasible [119].

The inside-out (internal) tracking system, termed RAMP, has been developed by Siemens Corporate Research (SCR) for real-time augmentation in medical procedures [132, 133, 134, 156]. It consists of a single infrared camera, mounted on the HMD, equipped with light-emitting diodes to generate an infrared flash for tracking a reference frame (a static set of retroreflective markers constituting an arc) in order to provide the HMD pose with a high rotational accuracy. RAMP is suitable for tasks within an arm's distance.

The inside-out tracking system needs about eight markers [157] for an accurate, reliable and robust tracking; therefore, fiducial markers of an object are likely to be occluded. In order to avoid this issue, an external tracking device was used.

The outside-in (external) tracking system, from A.R.T. GmbH (Weilheim, Germany), consist of a set of four infrared cameras attached to the ceiling that covers a working area of approximated 2.5 m^3 . The target's tracking accuracy provided by the system is around 0.35 mm . Since this is not a single, but multiple camera

3. Head-Mounted Hybrid Magnification System

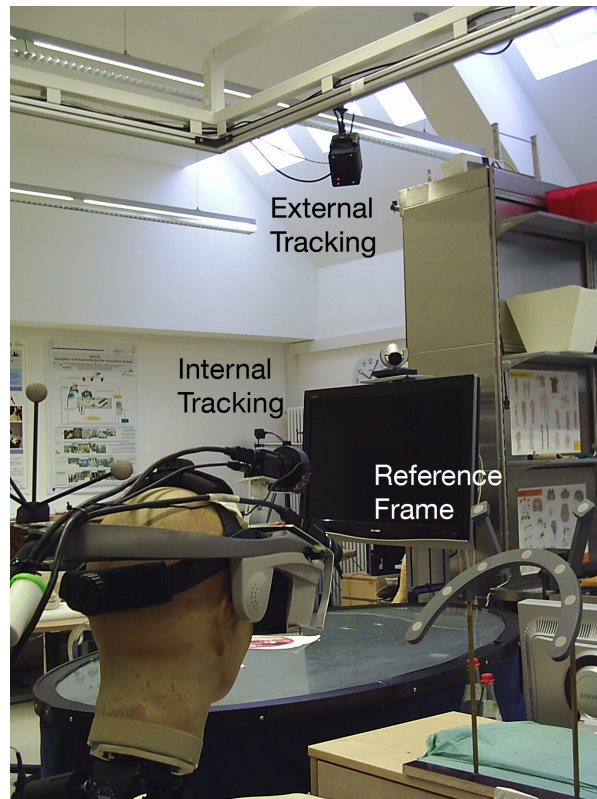


Figure 3.15.: Tracking system setup.

system, it requires an arrangement with a minimum of four fiducial markers for obtaining the six degrees of freedom (DOF) position of the target. This system is used for tracking the pointer tool's tip, the reference frame and the HMD pose in case that the reference frame target is out of scope of the RAMP system's infrared camera.

The main PC for computing the magnification approach and integrating the tracking data is a workstation with an Intel Core 2 Quad Q9550 processor at 2.83 GHz with 3.25 GB RAM and Nvidia GeForce GTX 280 graphics card (see table 3.2). The main PC workstation runs an instance of the AR software framework CAMPAR (for details see section 3.2.2), which combines all dynamic input data, i.e. tracking and video streams. On the same workstation an instance of the RAMP inside-out tracking software is executed that relays its results on the loopback device to the CAMPAR instance. For the developed methods and experiments presented in this chapter the GPU presented in table 3.2 was used. On a second

computer an instance of DTrack, ART's software for the outside-in tracking system is executed. The pose values from the outside-in tracking system are broadcasted via TCP/IP to CAMPAR on the main workstation. Figure 3.16 depicts an overview of all involved components and their connections within our setup.

3.8.2. Magnification Sight-based Activation

The magnification approach implemented on the HMD for this work was the hybrid magnification approach explained in section 3.4 (see Figure 3.8). For the research presented in this chapter, a CAMPAR output device plugin combining the techniques presented in section 3.4 was developed.

The system provides an intuitive control to activate and deactivate the magnified view by means of tracking the HMD's sight. When the user focuses on the operating field the magnification will be turned on. Focusing outside this area of interest will turn it off. This provides the surgeon with the freedom to perform other tasks with normal vision, such as grabbing surgical instruments, monitoring medical devices with information concerning patient or procedure status, or interacting visually with medical partners.

In order to establish when the user is focusing on the operative field, a vector of sight and its distance from the working area are determined as follows. For this work, transformations of all tracked objects have to be known with respect to the external tracking (ART) coordinate system (see Figure 3.16).

First, the position of the pointer's tip is saved to define location of operating field. Such position is directly given by the external tracking system. Next, the distance d between the saved location and left camera of the HMD is calculated. Then, the angle α between the camera's sight vector s and the normalized distance vector \hat{d} is computed based on the dot product of two vectors:

$$\alpha = \cos^{-1}(\hat{d} \cdot s) \quad (3.3)$$

If $d < 50$ cm and the angle $\alpha < 15^\circ$ (≈ 0.27 rad), then the magnification is activated. The previous conditional values for distance and angle were determined experimentally. Figure 3.17 provides an illustration of the magnification activation criteria.

The HMD camera location and orientation were obtained from the translation vector and rotation matrix contained in the following transformation:

$${}^{ext}T_{cam} = {}^{ext}T_{ref} * ({}^{ramp}T_{ref})^{-1} * ({}^{cam}T_{ramp})^{-1} \quad (3.4)$$

3. Head-Mounted Hybrid Magnification System

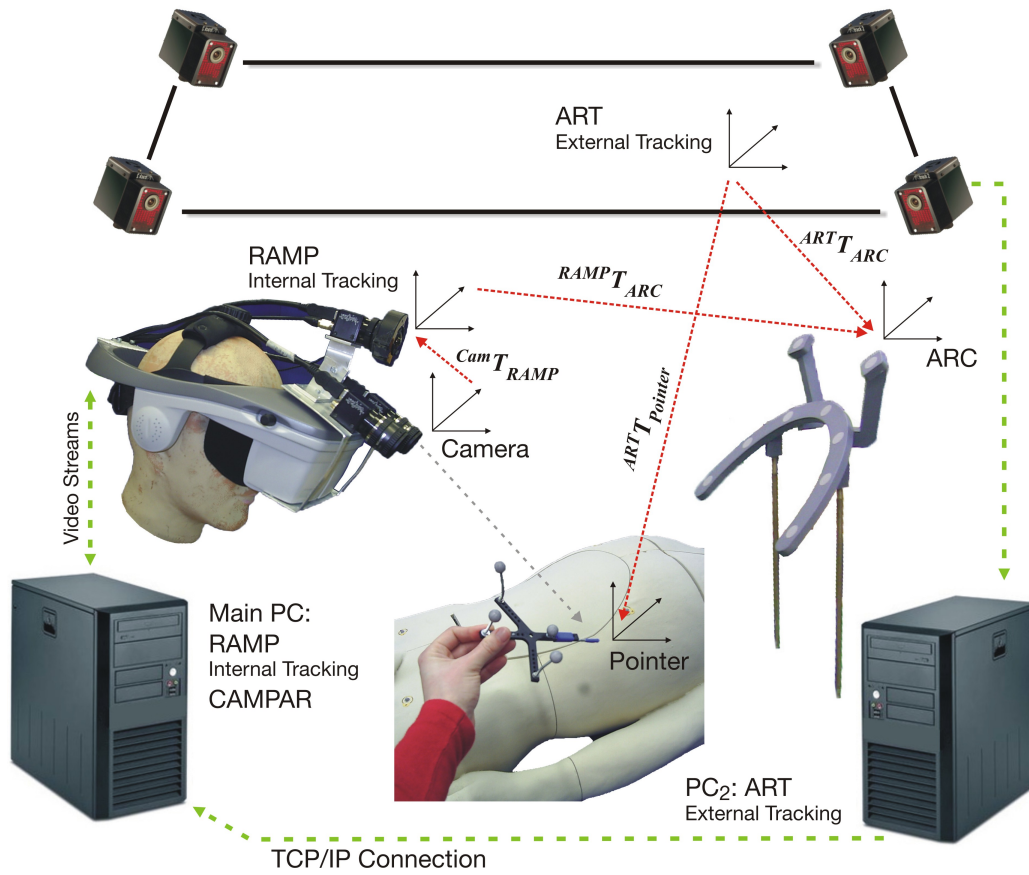


Figure 3.16.: Setup for AR system. All transformations are depicted by annotated red arrows.

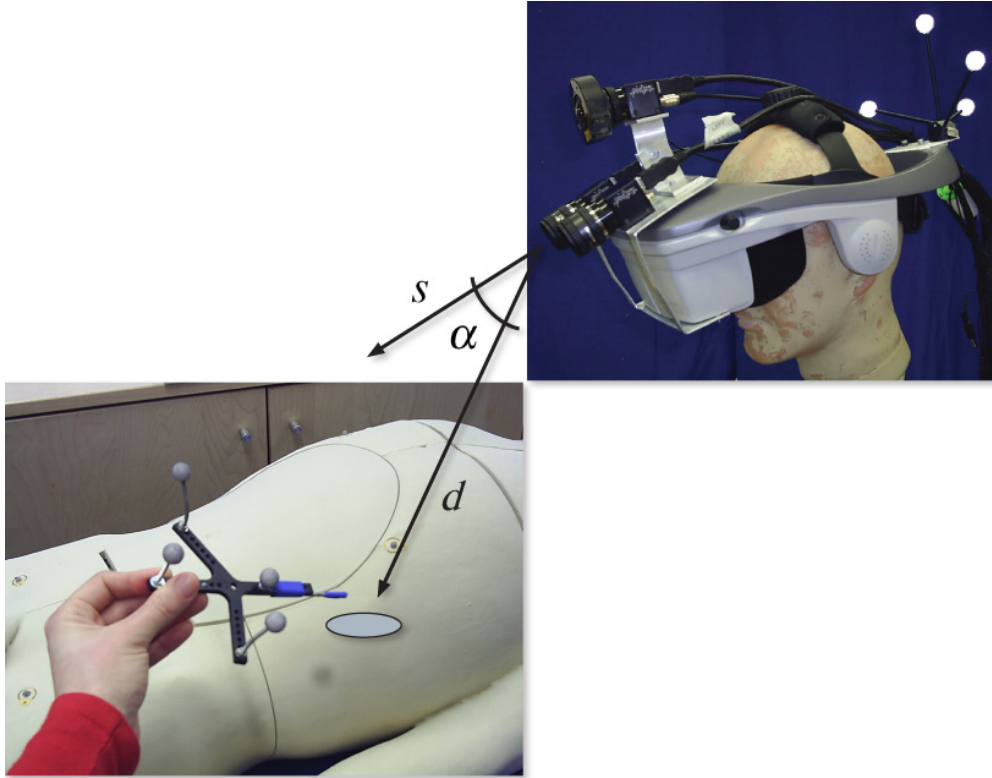


Figure 3.17.: Illustration of the magnification sight-based activation.

where ${}^{ext}T_{cam}$ denotes the transformation from the external tracking coordinate system to the HMD's left camera coordinate system, ${}^{ext}T_{ref}$ is the transformation from the external tracking coordinate system to the reference frame (ARC) coordinate system, ${}^{ramp}T_{ref}$ is the transformation from the RAMP coordinate system to the reference frame coordinate system and ${}^{cam}T_{ramp}$ is the transformation from the left camera coordinate system to the RAMP coordinate system. The latter transformation will be maintained constant because the camera is fixed rigidly to the HMD the same as the RAMP coordinate system.

3.8.3. Experiments

Five surgeons, experts on microsurgery, were volunteers for performing a suturing procedure assisted by the system (Figure 3.18). The experiment consisted on practicing two single knots on a suturing module for testing two different magnification modes ($2\times$ magnification factor): hybrid magnification and linear mag-

	Overall Trials	
	Linear mode	Hybrid mode
AVG	161.40	157.40
SD	24.17	43.31

Table 3.8.: Suturing task completion time.

nification (similar to the one presented on common magnifying devices). In Figure 3.19 it is possible to visualize the different magnification modes from the point of view of the HMD user.

The suturing tools comprised a needle with suture material, needle holder, forceps and scissors (Figure 3.20).

First, the artificial wound location is determined, by means of the tracked pointer, and saved in the system. Subsequently, the pointer is removed and the surgeon starts the suturing with a randomly selected mode. This process is repeated with the remaining magnification mode on a second suturing module. The procedure was recorded to evaluate the task completion time.

After every experiment, the volunteers filled out a multiple choice questionnaire in order to acquire qualitative feedback.

3.8.4. Results

In this section, the results of the measured data during the experiments are presented in qualitative and quantitative forms.

The results of experiments with five surgeons performing suturing procedures with two different magnification modes are presented in Table 3.8. The average (AVG) and standard deviation (SD) regarding duration of task accomplishment were measured in milliseconds (ms). The results show a small improvement in time using the hybrid magnification mode.

Due to the learning curve intrinsic in the experiments' repetition and adaptation to the AR system, it was expected that the time for performing the second suturing trial would be faster than the first trial. Because of this, it is considered relevant to analyze the set of experiments performed in the first trial (independently of the chosen mode) and the ones executed in the second trial.

Individual results corresponding to the task completion time of the first and second trial are presented in Table 3.9. For the first trial, three surgeons were

3.8. Sight-based Magnification System for Surgical Applications

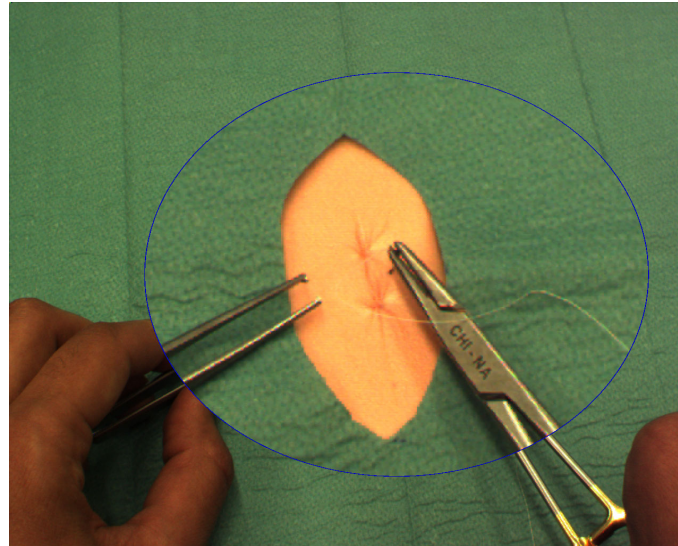


(a)

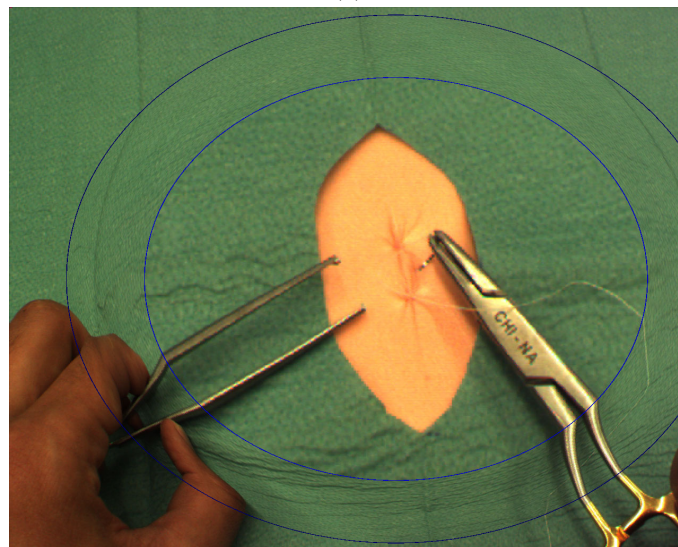


(b)

Figure 3.18.: Surgeons assisted by the magnification system.



(a)



(b)

Figure 3.19.: Magnification modes displayed into the HMD: (a) Linear, and (b) Hybrid.

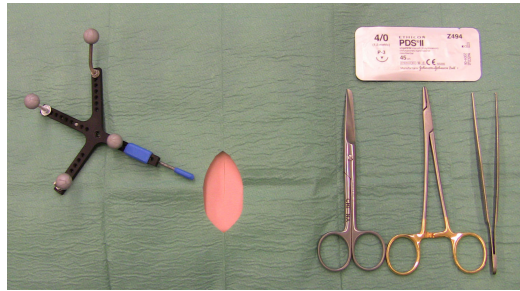


Figure 3.20.: Suturing module, pointer and surgical tools.

	First Trial		Second Trial	
	Linear mode	Hybrid mode	Linear mode	Hybrid mode
AVG	171.67	203.00	146.00	127.00
SD	26.31	9.90	12.73	15.39

Table 3.9.: First trial (linear mode: 3, hybrid mode: 2). Second trial (linear mode: 2, hybrid mode: 3).

evaluated initially with the linear mode and the remaining two participants with the hybrid one. In contrast, for the second trial two surgeons were evaluated with linear mode and the remaining three with the hybrid one.

It is very interesting to notice from these results that, during the first contact with the AR system (first trial), the surgeon performed the suturing procedure faster with the linear mode. This mode visualizes a magnification similar to the medical loupe, with which the surgeon is completely familiarized. On the other hand, after the user was adapted to the AR system (second trial), it took less time for suturing with the hybrid mode.

The multiple choice survey filled out by participants consisted of six questions with five optional answers: 1 = Strongly agree, 2 = Agree, 3 = Neither agree nor disagree, 4 = Disagree, and 5 = Strongly disagree. The results are the following:

1. "The system is useful for magnifying the operating field, even though the video quality is not as accurate as real optics of a medical loupe." (AVG 3.00, SD 0.89).
2. "The system is enough for performing the suturing procedure, even though the video quality is not as accurate as real optics of a medical loupe." (AVG 3.40, SD 0.80).

3. Head-Mounted Hybrid Magnification System

3. "The magnification system provides no advantages for magnifying the operating field." (AVG 2.60, SD 1.20).
4. "The system's automatic activation based on visual sight orientation is useful for visualizing and interacting outside the operating field without any manual control." (AVG 1.80, SD 0.40).
5. "The system with only classical magnification (no additional magnified information) is more helpful." (AVG 3.40, SD 0.80).
6. "The additional magnified information is visually distorted; however, it is beneficial to have a global context of the operating scene." (AVG 2.80, SD 0.75).
7. "The system's magnification with additional magnified information does not permit the right performance of the surgical task." (AVG 3.40, SD 0.80).

Generally, the participants were undecided as to whether to approve the system as good enough for magnification since the video quality is not comparable to real optics. Nevertheless, they agree with the possible advantages of having an automatic control based on the visual sight orientation. Moreover, they think that having additional magnified information provided by the hybrid mode could be beneficial for the task, or at least (and not less important), that this extra feature does not disturb the right performance of the surgical task. Some additional comments on improvements for the system were the following: higher video resolution, autofocus, system's weight reduction, and a higher magnification factor.

The AR system computational time has a mean of 1.08 ms with a standard deviation of 0.19 ms per two frames (left and right display for stereo vision). This outcome is less than the time for the arrival of the next video frame (every 33.33 ms) provided by the camera rate (30 fps). Thus, the video image processing can be executed in real-time without the loss of any video frame.

3.8.5. Discussion

The magnification approach implemented combines desirable properties from linear, non-linear and constrained magnifications within a single transformation. Due to non-linear magnification, there is no-hidden visual information, while the continuity between magnified and non-magnified areas is preserved. Moreover, the global context is well presented since the linear and non-linear magnifications



Figure 3.21.: Surgeon with surgical loupe attached to the glasses.

are applied within a constrained domain defined based on the 3D target of interest.

As the surgeons are already used to linear magnification from optical devices, they need time and training to adapt to a different magnified view, like the one presented in our method.

Display technologies are constantly being improved in terms of video resolution, field of view and weight. Nowadays, these technologies are not at the level of performance of real optical systems. As a result, it was not expected to have a complete acceptance of the virtual magnification system in its current form. The survey shows that even if this technology is not ready to replace the old one, the surgeons did not reject it and even exposed a positive response towards additional advantages provided by this system; in particular, they widely approved the efficiency of the magnification activation based on sight orientation.

By wearing a surgical loupe (see Figure 3.21), the user can also switch between regular and magnified views by moving the eyes; however, the user will get a semi-obstructed and restricted view. In contrast, the head-mounted magnification system allows the user to automatically recover a complete field of view for focusing on another area in the operating room. Moreover, an augmented reality system based on a stereoscopic head-mounted display could provide additional features taking advantages of digital manipulation, such as contrast enhancement, segmentation and remote assistance, which optical devices are not capable of.

Comparison of the system video resolution with real optics was not intended, but to provide the user with a magnification device that could support advantages of an augmented reality system offering exciting opportunities in the near future.

Metamorphopsia Modeling System

MACULAR disorders such as age-related macular degeneration, idiopathic epiretinal membrane (ERM), and macular holes have been found to cause metamorphopsia, a symptom described as the perception of distortion of objects. Patients with metamorphopsia visualize a straight line as an irregular or curved line. It is known that one of the main causes of metamorphopsia in individuals with macular diseases is the displacement of photoreceptors in the sensory retina [4]. Nevertheless, this disorder is not completely well understood.

4.1. Related Work

The use of Amsler charts is a common clinical approach for detecting metamorphopsia [2]. An Amsler grid is a printed square grid (10×10 cm) containing equally spaced parallel horizontal and vertical lines (see Figure 4.1). The Amsler chart should be placed at about the same distance of a reading material from the eyes of the patient (e.g., 30 cm), one eye should focus the dot in the center of the grid and the other eye should be covered. Any irregularity visually perceived in this grid (e.g., wavy or blurred lines, missing or dark areas) could be the sign of a vision problem resulting from damage to the macula.

Variants of the Amsler grid have been elaborated to examine central vision, but the original chart seems to perform better [96]. Although it is a standard method

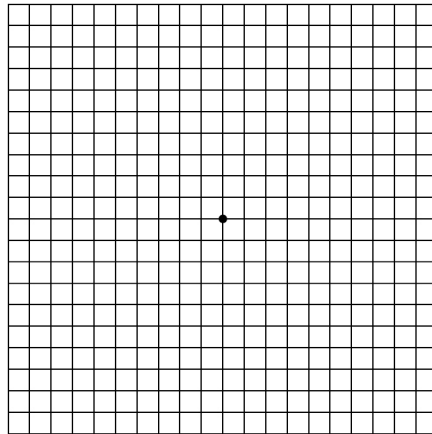


Figure 4.1.: The Amsler grid.

for diagnosing and measuring metamorphopsia, the test with an Amsler grid, in itself, yields no readily quantifiable data.

Some methods have been proposed for measuring the severity of metamorphopsia. Shinoda et al. presented a method for quantification of metamorphopsia to study distorted vision in patients with epiretinal membrane [141]. A modified Amsler chart (a grid of black lines on a white background measuring 12×12 cm with grid squares of 2×2 cm) was prepared. The patients were asked to trace on the chart any of the grid lines seen as irregular or curved. The length of all lines drawn by the patients was used to score the degree of metamorphopsia. An example is shown in Figure 4.2. Although this method seems to be simple to perform, it could be a very complex task for older patients since they would have to draw what they perceive with low visual acuity (peripheral vision) while fixating the center of the chart. Accuracy of drawings may diminish the more distant they are located from the center of vision, and so the final measurement.

Matsumoto et al. developed an interesting method for quantifying metamorphopsia in patients with ERM by the use of M-CHARTS™ [99]. The M-CHARTS had 19 dotted lines with dot intervals of between 0.2° (fine) and 2.0° (coarse) visual angles (Figure 4.3). As the displayed dot intervals were changed from fine to coarse, a decrease of the line distortion is perceived by the patient. The minimum visual angle of the dotted lines needed to cause the metamorphopsia to disappear was taken as the measurement to score the disorder.

The Preferential Hyperacuity Perimetry [89] (PreView PHP, Carl Zeiss Meditec,

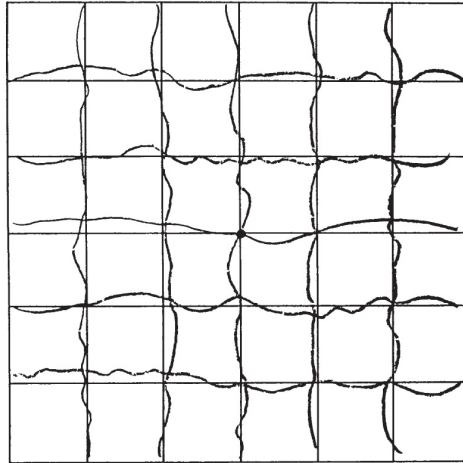


Figure 4.2.: Example of a chart drawn by a patient used to quantify metamorphopsia by Shinoda et al. [141].

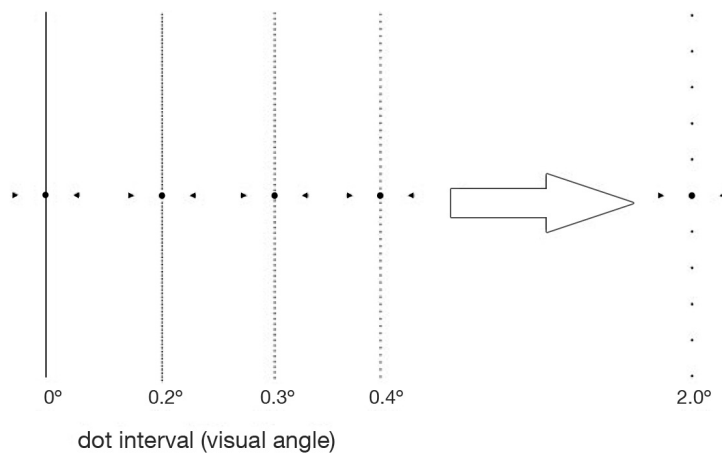


Figure 4.3.: Method of detecting metamorphopsia using M-CHARTS proposed by Matsumoto et al. [99].

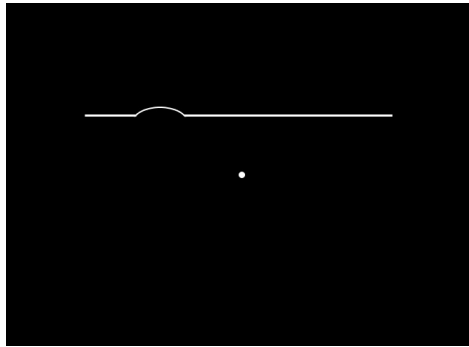


Figure 4.4.: Example of a stimulus used in the PHP. The subject should fixate the central dot during the test.

Dublin, CA) is a psychophysical test suitable for identifying and quantifying the area in the visual field affected by metamorphopsia and to follow the progression of deterioration. The PHP is based on visual *hyperacuity* (also known as Vernier acuity), that is the ability to recognize the relative spatial localization of two or more stimuli (i.e., the ability to discern a subtle misalignment of an object) [49]. The test consists of scanning the macula with a succession of stimuli, each stimulus is a dotted line with an artificially generated distortion flashed in an order that may appear random to the observer (Figure 4.4). The examinee is asked to touch the touch-sensitive screen at the location of any perceived abnormalities. If the stimulus is projected on a retinal lesion, a pathological distortion may be perceived instead of the artificial distortion. By varying the degree of artificial distortions, the amplitude of the pathology in the area of interest can be quantified. During the course of the examination, artificial distortions, imitating distortions similar to those seen by patients with neovascular AMD, are presented. These artificial distortions serve as control stimuli to quantify the extent of any presumably pathologic distortions originating from retinal lesions using preferential looking analysis [56].

Trevino [149] and Crossland [26] show different methods for macular assessment, but the main problem in these methods is the difficulty to reliably assess due to the lack of knowledge of the ground truth of the patient's vision, some defects may not be covered by the grid lines. In [42], a dynamic Amsler grid created in computer graphics was developed to overcome these deficiencies. Nevertheless, all these methods do not provide a model which projects the way patients

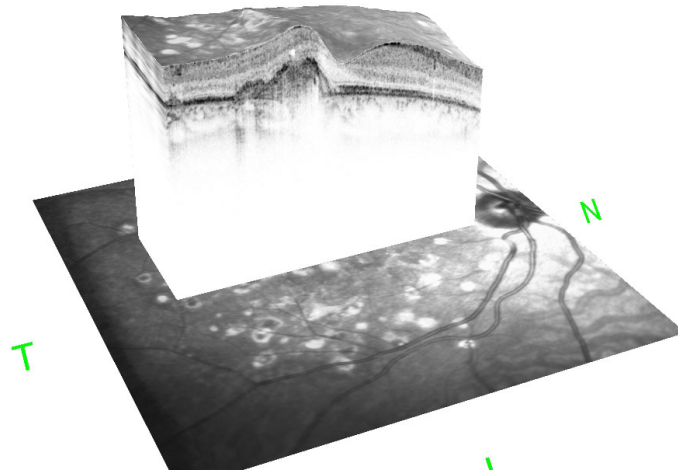


Figure 4.5.: Cross-sectional view of a retinal volume from optical coherence tomography images of a patient with metamorphopsia.

perceive their distorted world in detailed, this is, their visual deformation model.

4.2. Objective

As a first step in this research, a deformable Amsler grid based system is proposed to obtain an inverted deformation model, termed correction model of metamorphopsia. By having a deformation model it could be possible to localize the macular areas causing deformations in optical coherence tomography (OCT) images of the patient retina (Figure 4.5) and analyze them to see if it is viable to find any macular pattern related to the deformation's shape. Moreover, a correction model could be applied to images of AR display devices (e.g., a head-mounted display) and therefore, a correcting system for patients with distorted vision could be achieved.

4.3. Methods and Materials

The hardware used for modeling metamorphopsia is a portable workstation with a 15.4" monitor (1680×1050 pixels of resolution), an external mouse, and a chin rest (see Figure 4.6).

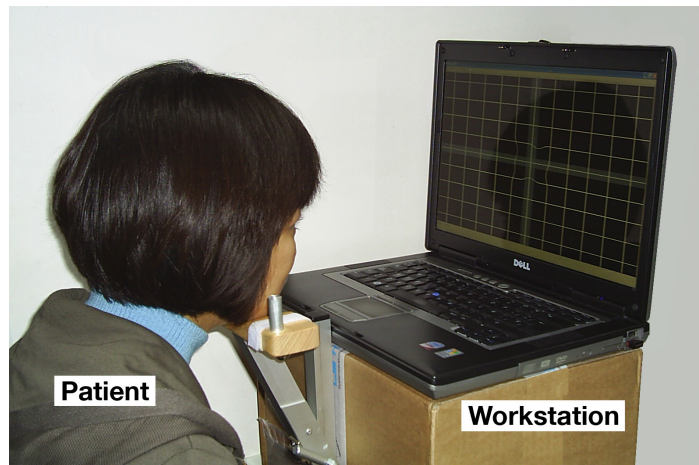


Figure 4.6.: Metamorphopsia modeling system.

In order to acquire the metamorphopsia correction model of a patient, the following steps are executed. First, the interactively deformable Amsler grid is displayed to the patient in a computer monitor at a fixed distance. The affected eye fixates the grid center and the remaining eye is covered. The patient will describe location and direction of the perceived distorted lines on the grid to an examiner. Assisted by a mouse and a keyboard, the examiner will deform one by one the corresponding lines in the opposite direction described until the patient perceive all the distorted lines straight again. At this point, the deformation will be considered corrected.

It is also possible that the correction procedure is performed by the patient. In that case, the patient will need an extra short time for learning how to interact with the system. For practical purposes, in the set of experiments carried out for this research only the examiner was in charge of interacting with the system.

Once the metamorphopsia model is acquired, it is aligned with the corresponding OCT images of the patient macula for further analysis. This procedure was performed on seven patients with macular disorders.

4.3.1. Deformable Amsler Grid

In order to create a deformable Amsler grid, a free form deformation (FFD) model [139], based on B-splines, was chosen. This is a feasible tool for modeling deformable objects. Basically, the idea of FFD's is to deform an object (i.e., Amsler

grid) by manipulating an underlying mesh of control points. The resulting deformation gives the model of metamorphopsia of the patient and produces a smooth and C^2 continuous transformation. To define a spline-based FFD, the domain of the image is denoted as $\Omega = \{(x, y) | 0 \leq x < X, 0 \leq y < Y\}$. Let Φ denote a $n_x \times n_y$ mesh of control points $\Theta_{i,j}$ with uniform spacing δ . Then, the FFD is defined as the 2D tensor product of the 1D cubic B-splines functions and the displacement of the control points:

$$T(x, y) = \sum_{m=0}^3 \sum_{n=0}^3 B_m(u) B_n(v) \Theta_{i+m, j+n} \quad (4.1)$$

where,

$$i = \lfloor x/n_x \rfloor - 1 \quad (4.2)$$

$$j = \lfloor y/n_y \rfloor - 1 \quad (4.3)$$

$$u = x/n_x - \lfloor x/n_x \rfloor \quad (4.4)$$

$$v = y/n_y - \lfloor y/n_y \rfloor \quad (4.5)$$

and where B_m presents the m -th basis function of the B-spline:

$$B_0(u) = (1 - u)^3/6 \quad (4.6)$$

$$B_1(u) = (3u^3 - 6u^2 + 4)/6 \quad (4.7)$$

$$B_2(u) = (-3u^3 + 3u^2 + 3u + 1)/6 \quad (4.8)$$

$$B_3(u) = u^3/6 \quad (4.9)$$

In contrast to thin-plate splines [13], B-splines are locally controlled. The resulting transformation from changing the control point $\Theta_{i,j}$ will only affect the local neighborhood of that control point. The degree of non-rigid deformation which can be modeled depends on the resolution of the mesh of control points Φ .

4.3.2. Localizing Metamorphopsia in OCT Images

Optical coherence tomography (OCT) is a noninvasive, non-contact medical imaging technology which uses reflected light (typically near-infrared light) to produce cross-sectional and three-dimensional (3D) images of biological tissue. In ophthalmology, OCT can be used to obtain detailed images of the retinal surface, in which the anatomic layers within the retina can be differentiated and retinal thickness can be measured.

4. Metamorphopsia Modeling System

	SPECTRALIS® SD-OCT
A-scans/second	40,000
Axial resolution (in tissue)	3.9 microns (digital)
Transverse resolution (in tissue)	14 microns
Scan depth	1.9 mm

Table 4.1.: SPECTRALIS SD-OCT specifications.

OCT has advantages over other medical imaging modalities such as magnetic resonance imaging (MRI) or ultrasound due to the much higher resolution it provides (better than 10 μm).

The correction model obtained can be used as a model to describe metamorphopsia for medical diagnosis by locating the affected areas in macular OCT and fundus images with the assistance of the system already developed.

For this work, acquisition of OCT images were done with SPECTRALIS® (Heidelberg Engineering, Inc.), a system using spectral-domain optical coherence tomography (SD-OCT). An early version of this technology, time-domain OCT (TD-OCT), uses a moving reference mirror for measuring the time it takes for light to be reflected. The newer Spectral (or Fourier)-domain OCT (SD-OCT) uses a significantly faster, non-mechanical technology. The SPECTRALIS® SD-OCT simultaneously measures multiple wavelengths of reflected light across a spectrum. The SPECTRALIS system is 100 times faster than TD-OCT and acquires 40,000 A-scans per second. For the SPECTRALIS SD-OCT specifications details see table 4.1.

SPECTRALIS also integrates infrared fundus imaging using long wavelengths of laser light to capture fundus images in fine detail even without dilation. The lower level of light is better tolerated by elderly patients who may experience discomfort with flash photography.

Furthermore, the SPECTRALIS system is combined with TruTrack™ technology, from the same developing company, to actively track the eye during imaging. SPECTRALIS utilizes two separate beams of light to capture two images simultaneously. One beam is designed to constantly image and track the fundus. It also acts as a reference, guiding the second beam of light to precisely position the cross-sectional OCT scan. As a result, the system provides precise follow-up scanning and measurement reproducibility of 1 micron [163]. It also ensures point-to-point correlation between fundus and OCT images without post-processing of the data.

For registering the OCT images and the patients' correction model obtained

from the experiments, the projected image (in mm) on top of the retina produced by the grid at the distance of 30 cm is generated. This is based on the fact that the visual plane of the subject is parallel to the grid and fixating its center (as done in the experiments). Thus, it is possible to approximately align the grid on top of the retina (fundus image) and therefore place the OCT images in the position where they were scanned, see Figures 4.7 and 4.8. This alignment of information could help for a better understanding of metamorphopsia and could create a set of valuable multi-modal data for evaluating the possibility of development of novel quantitative and/or qualitative analysis of visual distortion based on OCT images.

In order to calculate the object length R (e.g. grid width) projected in the retina, the following equation is computed:

$$R = \tan V * n \quad (4.10)$$

where V is the visual angle of the object in the visual field (which can be obtained from equation 3.2 in Chapter 3), and n is the distance from the nodal points in the eye (located immediately behind the back surface of the lens) to the retina, about 17 mm. For visual angles smaller than about 10 degrees, this simpler formula provides very close approximations:

$$\tan V = S/D \quad (4.11)$$

where S is the object length in the real world and D is the distance from the eye to the object location (i.e., monitor distance).

4.4. Results

Five patients with metamorphopsia could reliably fulfill the task, while the rest had problems for fixating the grid center. The correction procedure was stopped until the patient perceived a small or no distortion in the lines at all.

Fixed at a distance of 30 cm from the patient, the system provides a correction model of distorted vision in a range of 57.33° horizontal and 33.92° vertical visual angles. The grid lines are placed every 5.63° horizontal and 3.82° vertical visual angles. The resolution of the mesh of control points on the grid for modeling is 35×19 points. The resolution of the grid used was 1662×929 pixels. The deformable grid produced smooth deformations since it is based on cubic B-splines.

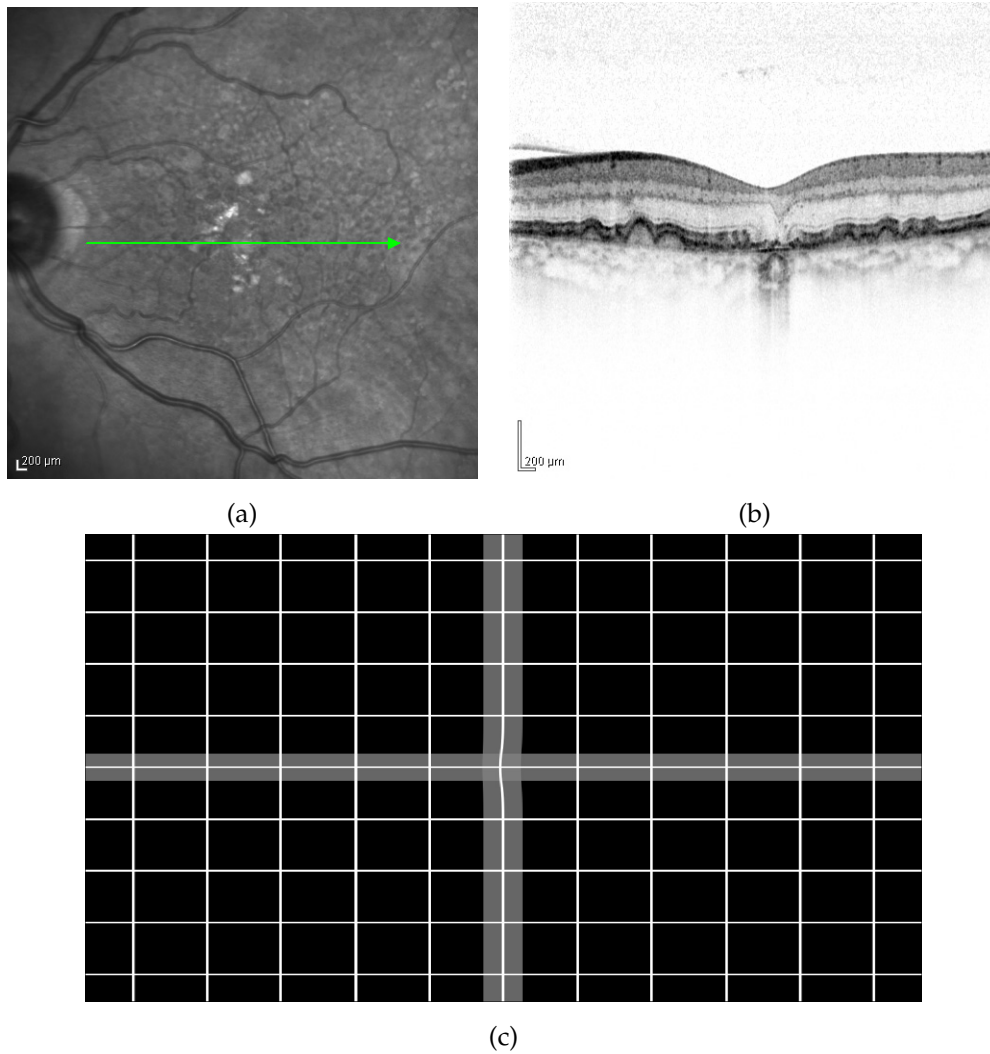


Figure 4.7.: Imaging components for alignment: (a) Fundus image, (b) OCT image, and (c) Metamorphopsia model grid.

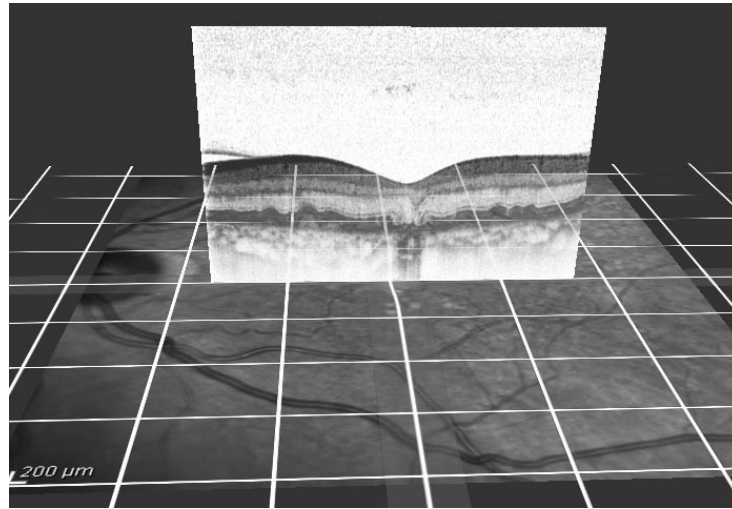


Figure 4.8.: Alignment of a macular OCT image and deformable Amsler grid on top of a fundus image.

	Real World lenght (cm)	Retinal lenght (mm)	Visual Angle (degrees)
Width	32.80	26.51	57.33
Height	18.30	11.43	33.92
Horizontal spacing	2.95	1.68	5.63
Vertical spacing	2.00	1.13	3.82

Table 4.2.: Deformable grid specifications.

The perceived distorted vision was modeled and the affected area was localized in macular OCT and fundus images (see Figure 4.9). The pathology matched the location of the distortion as graded by an experienced ophthalmologist.

In addition, the system can provide a measurement of the deformation seen in the grid (i.e., the average displacement of pixels) in order to have an estimation of the size of the affected area in the macula (in mm) according to the patient visual perception; which helps to evaluate the progression of the disease. The resolution of the mesh of control points in the grid can be increased to model more difficult metamorphopsia cases.

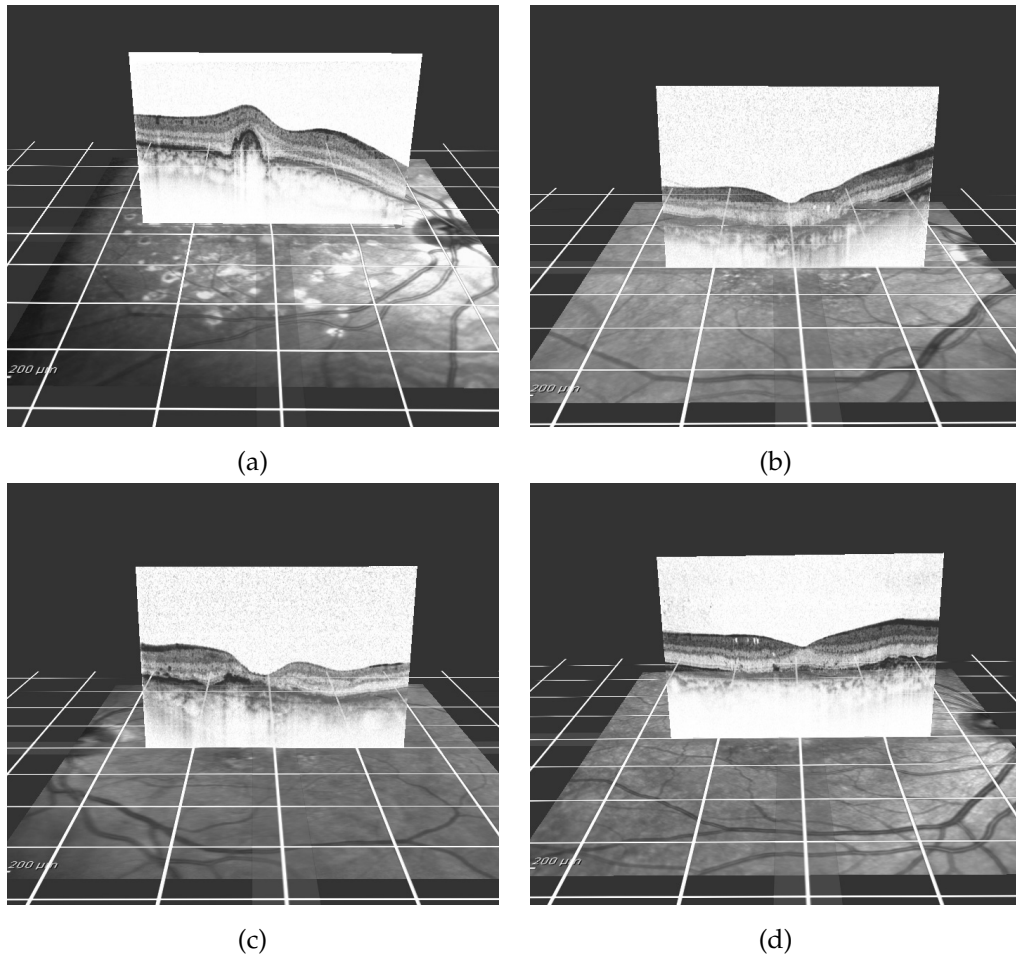


Figure 4.9.: Alignment examples of macular OCT images and deformable Amsler grid of four different patients: (a)–(d).

4.5. Discussion

The efficiency of the metamorphopsia modeling system cannot be measured by experimenting directly on patients with metamorphopsia considering that there is no possibility of comparing the patient current deformation with the deformation model obtained. Only a qualitative feedback from the patient can be afforded.

In order to overcome this problem and to have the possibility of evaluating the metamorphopsia modeling system with quantitative results, an innovative assessment approach is presented next.

4.6. Eye-Tracking based Metamorphopsia Simulation System

4.6.1. Motivation

A deformable Amsler grid based system with an eye tracker device is proposed to simulate distorted vision in healthy eyes in order to analyze reliability of the proposed metamorphopsia modeling system for acquiring a correction model, which can be applied to a head-mounted display device to compensate distorted vision of patients with metamorphopsia.

4.6.2. Method and Materials

The method consists of simulation of distorted vision for the human eye; acquisition of the correction model of the simulated visual distortion; and finally the analysis of the obtained results.

The hardware used includes a 17" external monitor (1680×1050 pixels of resolution), an eye tracker device with binocular tracking of 0.5 degrees of accuracy at 60 Hz data rate, and a workstation with Intel Core Duo CPU at 2.40 GHz, 2GB of RAM (see Figure 4.10). The deformable Amsler grid presented previously in this chapter is adopted.

4.6.3. Simulation of Distorted Vision

In order to simulate metamorphopsia on a normal sighted person, an image deformation is generated and placed on a specific location of the grid (Figure 4.11). Considering the grid center as the visual center (visual angle 0°), the eye tracker

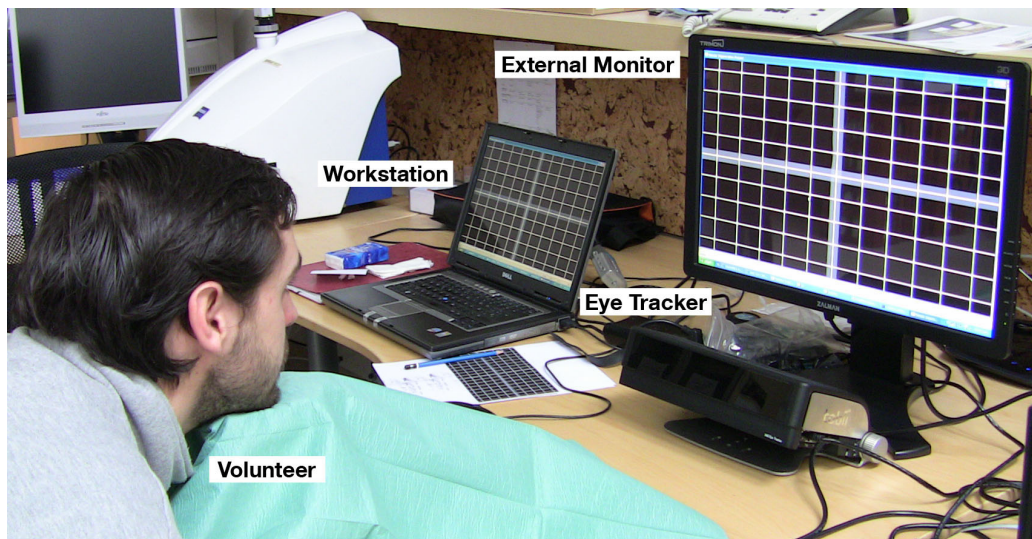


Figure 4.10.: Metamorphopsia simulation and modeling system.

follows the gaze so that the deformation is displayed all the time in the same selected location of the subject's visual field. As a result, it is possible to recreate the visual imperfection caused by the displacement of photoreceptors in the human eye.

In the same manner as with real metamorphopsia patients, to digitally correct distorted vision it is necessary to deform the grid section, located in the affected retinal field, in the opposite direction of the real perceived deformity. Therefore, to correct the simulated distortion an interaction with the mouse on the monitor moves the grid lines in the opposite trend of the perceived distortion until the person sees no deformation in the lines. This procedure will provide the metamorphopsia correction model.

4.6.4. Experiments

In order to evaluate whether the grid resolution can affect the discernment of distortions or not, a squared and a non-squared grid are tested. The dimension for every grid is 46.9×26.2 cm. Eight points on both grids are selected for locating a pre-generated distortion (Figure 4.12). Every location corresponds to a specific retinal area of the visual field (the grid center corresponds to visual angle 0°). The magnitude of deformation on every point of the grid is randomly defined covering a visual angle range of 0.18° to 1° . A group of volunteers is selected to participate

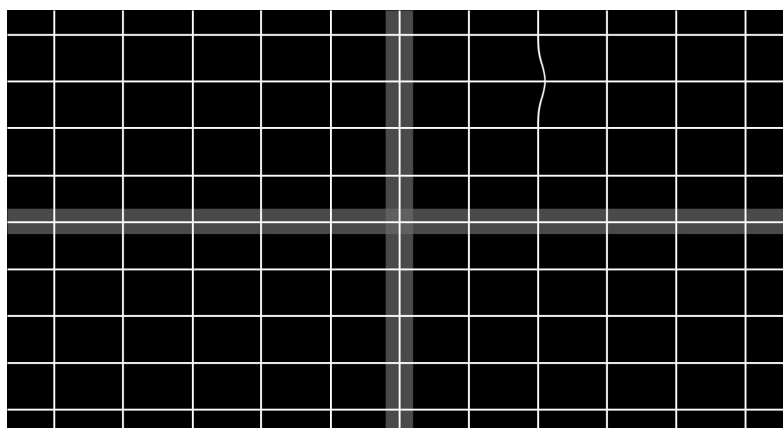
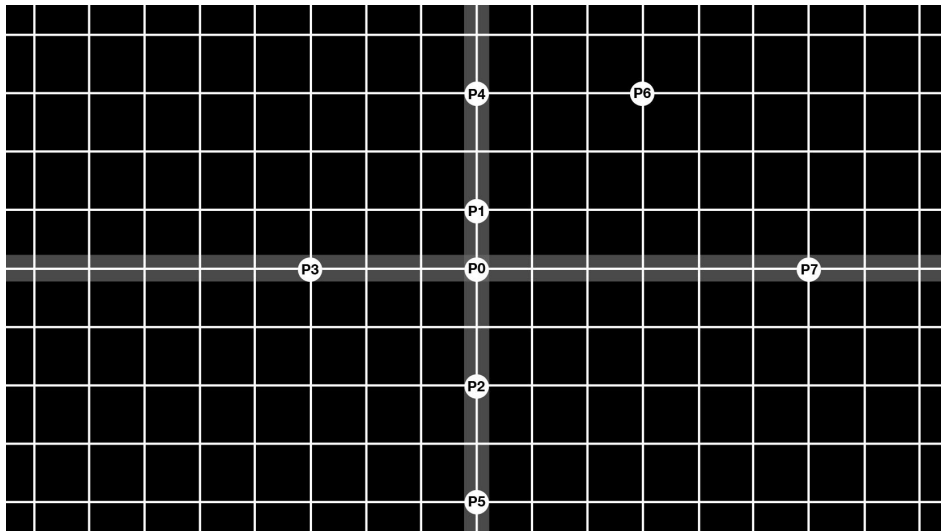


Figure 4.11.: Deformation example on a non-squared grid.

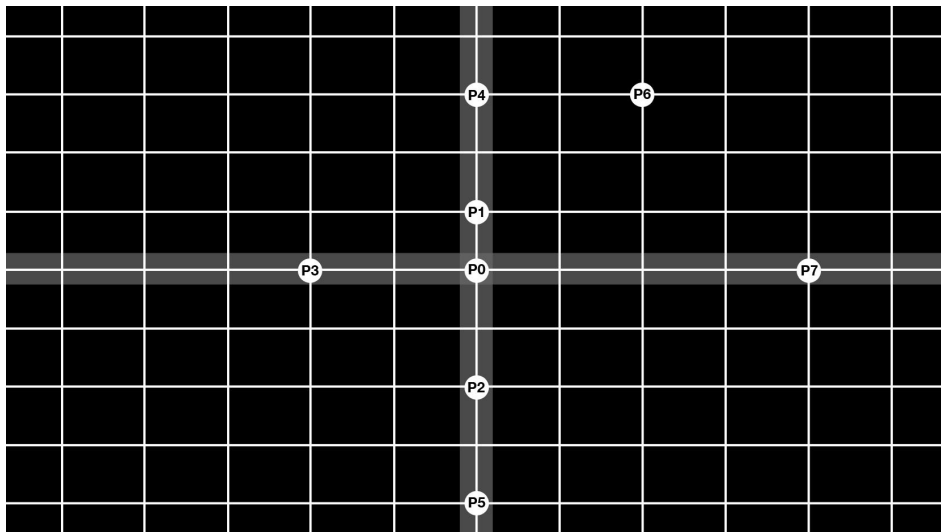
in the experiments. The criteria for inclusion is best corrected visual acuity equal to 20/20.

The experiment is as follows (Figure 4.13): the volunteer is located in front of the external monitor at a distance of 80 cm. One eye is covered and the other one is fixating the center of the displayed grid during the whole experiment. One of the eight predefined distortions is simulated on the screen. The examiner performs a *blind correction*; this is, without seeing the projected distortion to the volunteer (to recreate the real situation with a patient where the examiner cannot see what the patient perceives). During this simulated environment, the examiner obtains from the subject a description of the perceived distortion (location and shape orientation). Once the description is provided, the examiner stops the simulated distortion. The grid will become regular again (i.e., with straight lines) and the examiner will now see the screen to interact with the grid in order to acquire the correction model for that specific distortion; this is, to deform the grid, in the provided location and in the opposite given orientation. After this step, the examiner does not look at the screen anymore and turns on the simulated distortion on the grid recomputed with the examiner's modification. At this time, the simulated distortion may be reduced (or disappear completely) and the grid line affected by the simulated distortion may seem straighter (or completely straight). The blind correction procedure will be performed until the person cannot perceive any distortion. The procedure is done with the squared and non-squared grid (the first one being tested is randomly chosen for each volunteer).

Once the experiment is finished, the correction rate related to the original sim-



(a)



(b)

Figure 4.12.: Evaluated locations in: (a) Squared grid, and (b) Non-squared grid.

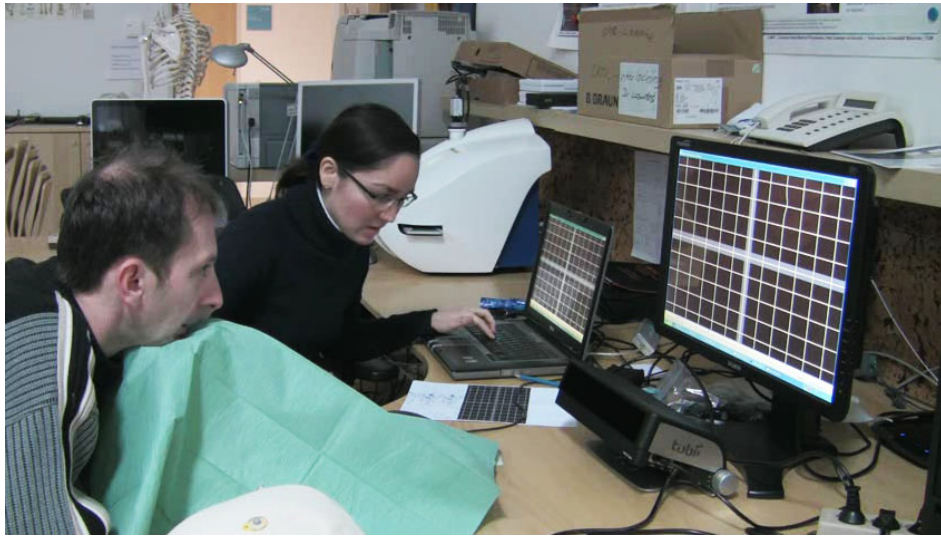


Figure 4.13.: Volunteer and examiner performing an experiment.

ulated deformation is analyzed. The correction percentage will be measured by calculating which rate of the magnitude of the displacement vector of the control point for simulating the distortion was reduced after the correction procedure. If the magnitude of the displacement vector after correction is 0, a 100% of correction will be measured.

The eye tracker avoids the natural instinct of trying to fixate not the grid center, but the simulated distortion projected out of the central vision. Therefore, the eye tracker moves the simulated distortion to its corresponding location in the visual field according to the gaze movement, thus the distortion shifts its location and the person cannot focus it with the central vision.

The visual angle V corresponding to each one of the eight points in the grid can be obtained by the equation 3.2, presented in Chapter 3.

4.6.5. Results

The system provides a model of distorted vision in a range of 32.67° horizontal and 18.60° vertical visual angles. The non-squared grid has a horizontal line spacing of 2.97° and a vertical line spacing of 2.08° in visual angles. In the case of the squared grid, the lines have an approximately equal spacing of 1.98° horizontal and 2.08° vertical. The resolution of the mesh of control points on the grid for modeling transformations is 35×19 points.

4. Metamorphopsia Modeling System

	Squared Grid	Non-Squared Grid
AVG	75.75	75.78
SD	10.12	07.36

Table 4.3.: Total correction rate (percent) on squared and non-squared grids.

In total, 17 normal subjects (17 eyes) could reliably fulfill the task. The average (AVG) and standard deviation (SD) of the correction rate obtained are presented in Table 4.3. The Table 4.4 shows the visual angle (in degrees) corresponding to each selected location for evaluation on the grid with its correction rate. These results are plotted in a graph for easy visualization and analysis (see Figure 4.14). According to the results, the average correction rates do not show any significant difference when using a squared or a non-squared grid.

To go deeper in the studies, it is relevant to analyze the minimum recognizable visual angles for every selected location; this is obtained based on the final magnitude of the displacement vector of the control point for simulating the distortion after the correction procedure. Table 4.5 presents the results. In Figure 4.15, it is shown that with a non-squared grid it is possible to distinguish smaller deformations in the middle peripheral vision (p2 to p5). For locations near the visual center (p0 and p1) and far away from it (p6 and p7) a squared grid has better results.

As it could be expected, there is an incremental trend relating the minimum recognizable deformation and its location in the visual field, this means that the farther away the deformation is from the visual center the less a subject can recognize it. However, for these locations, a subject can still guide the examiner to perform a reasonable correction as seen in the results of Figure 4.15.

An eye tracker device plays a very important role for simulating and modeling of metamorphopsia for a healthy eye, not only because it reproduces the feeling of having a real distortion moving with the gaze, but also for preventing the person from looking directly at the distortion during the experiment to describe it, instead of fixing the center of the grid. On the other hand, an eye tracker could provide feedback of whether the real patient is fixating the grid center or not, increasing the accuracy of correction and localization of the affected areas in the macula for further analysis. Therefore, tracking accuracy of a single eye is an essential parameter for success in modeling and correcting distorted vision.

The final correction model acquired can be implemented in a head-mounted display based augmented reality system. Thus, it will be possible to compensate

Location	Visual Angle	Squared Grid		Non-Squared Grid	
		AVG	SD	AVG	SD
p0	0.00	90.63	07.58	80.23	12.97
p1	2.08	81.91	14.26	81.13	08.69
p2	4.15	57.23	31.57	72.85	23.47
p3	5.94	74.07	22.64	73.49	23.50
p4	6.22	70.36	17.44	76.05	16.29
p5	8.29	79.16	12.89	81.49	11.31
p6	8.60	79.71	19.07	66.61	26.47
p7	11.85	72.90	25.15	74.38	12.02

Table 4.4.: Correction rate (percent) for each evaluated location.

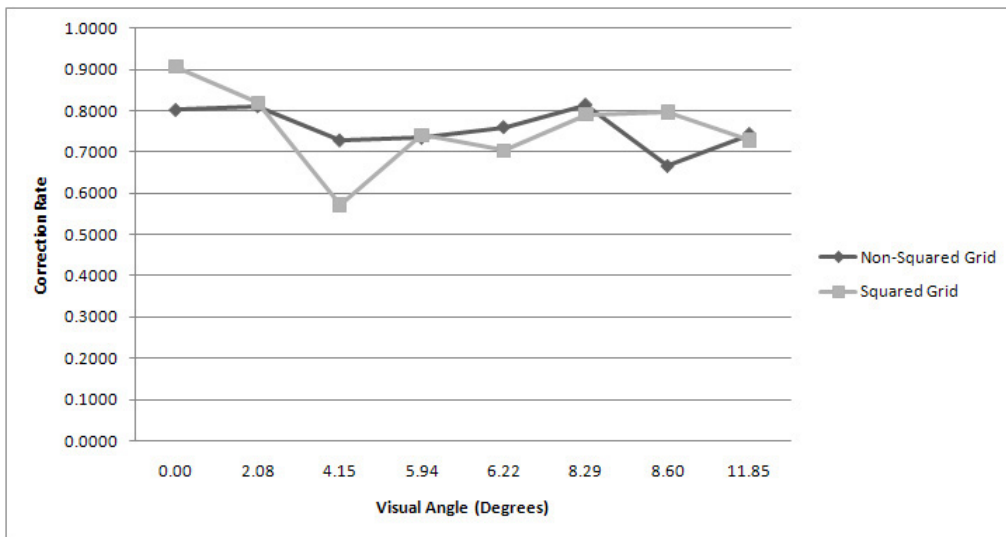


Figure 4.14.: Correction rate.

4. Metamorphopsia Modeling System

Location	Visual Angle	Squared Grid		Non-Squared Grid	
		AVG	SD	AVG	SD
p0	0.00	0.0364	0.0303	0.1290	0.1147
p1	2.08	0.0871	0.0621	0.0986	0.0722
p2	4.15	0.1259	0.0804	0.1163	0.1120
p3	5.94	0.1518	0.1224	0.1192	0.0993
p4	6.22	0.1662	0.1032	0.1328	0.0922
p5	8.29	0.1643	0.1170	0.0918	0.0852
p6	8.60	0.1204	0.1346	0.1336	0.0860
p7	11.85	0.1593	0.1182	0.1705	0.0908

Table 4.5.: Minimum recognizable visual angles (in degrees) for each evaluated location.

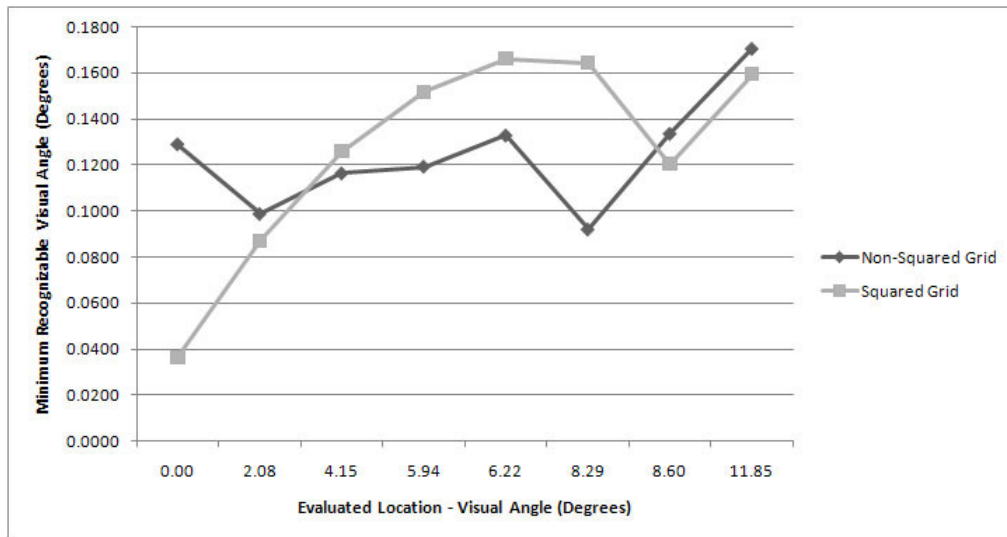


Figure 4.15.: Minimum recognizable visual angles.

distorted vision in real patients.

4.6.6. Discussion

The implementation of the metamorphopsia correction model obtained with the proposed modeling system into a head-mounted device can only be completely functional with the support of an eye-tracking system since the correction should always be aligned with the affected area. An eye tracker is able to follow the gaze and can provide the required location for correction.

Lamentably, the same disadvantage of eye-tracking technology exposed in the head-mounted hybrid magnification system (Chapter 3) is attributed in this context, i.e., the calibration procedure embedded in the current eye trackers inside an HMD is not still adequate for users with fixation problems.

Moreover, in order to get an efficient head-mounted system as an enhancement device for patients with metamorphopsia it is necessary that the eye-tracking accuracy is extremely precise since the human eye can recognize distortions from 0.0303° in the central vision to 0.1705° in the periphery (Table 4.5). Current eye-tracking systems mounted into an HMD (e.g., Arrington Research, Inc.) sustain an accuracy of approximately $0.25^\circ - 1.0^\circ$.

Another issue affecting the accuracy of eye-tracking systems is the use of glasses for correcting vision. Generally, older people need glasses for daily life use. Frequently, systems using infrared video as tracking method are misled by the light refraction effect caused by the glasses.

In addition to the previous points, the overall system should process the correction in real time, so there is no image delay in the visualization.

The general approach presented in this chapter comprises an innovative solution thought for the time when all the hardware technology is suitable for acquiring an efficient vision enhancement system for patients with maculopathies.

Part III.

Final Conclusions

CHAPTER 5

Conclusions

THE present chapter summarizes the major contributions and findings derived from the research conducted in this thesis. Finally, it is concluded by exposing a set of remaining challenges, future directions and ideas worth investigating.

5.1. Summary

Age-related macular degeneration is the most common cause of visual impairment in the western hemisphere, affecting older adults through the loss of central vision along with distorted visual perception. Considering the rapid increase of incidence of older people's population, this study is focused on enhancing vision of people with age-related macular degeneration via advanced imaging methods implemented on a head-mounted display. The potential solutions proposed in this dissertation are summarized in the following paragraphs.

Head-Mounted Hybrid Magnification System. In this vanguard application a hybrid magnification approach integrated with a two-camera system fixed on a head-mounted display as a vision enhancement device for AMD patients was successfully developed. The system works in real-time due to the integration of GPU-accelerated algorithms. The system preliminary experiments exhibited positive feedback from AMD patients.

A more extensive evaluation of the application efficiency was achieved through the profitable development of an eye-tracking based AMD simulation system, de-

monstrating that the hybrid magnification approach improves the reading speed 1.2 times and the spatial orientation within complex environments 1.5 times in contrast to a linear magnification approach.

Additionally, a comprehensive evaluation of the application feasibility was performed by means of a sight-based magnification system for surgical applications. The results showed that the system sustained stereo vision, undistorted central zooming, continuity between magnified and non-magnified areas, prevents occlusions, and provided a global context of the operating scene. Moreover, the sight-based magnification control supplied surgeons with a novel functionality for switching between normal and magnified views with an intuitive movement.

Metamorphopsia Modeling System. In this novel application a deformable Am-ler grid based system which provides a simple and useful method for modeling distorted vision in patients with metamorphopsia is presented. The grid based on cubic B-splines provided smooth transformations suitable to correct visual deformations. Alignment of the model with macular OCT images can be used to identify macular features, which could help in the development of an automatic method to model metamorphopsia.

The application efficiency was quantitatively evaluated via a system for simulating and modeling metamorphopsia. The feasible correction rate for distorted vision by using a deformable non-squared grid and the guidance of the patient qualitative feedback was 75.78%. The use of an eye tracker increases the reliability of the results. Implementation of the correction model on an AR display device could improve the vision of patients with metamorphopsia.

Essentially, all the novel solutions proposed in this work are visionary applications with higher potential in terms of functionality than optical devices. As advances in hardware will provide the scientific community with more portable, practical and efficient head-mounted displays, and more accurate eye trackers, these innovative solutions pave the path towards integration of augmented reality into low vision rehabilitation.

5.2. Future Work

It is relevant to suggest that the acquisition of the distorted vision model for patients with metamorphopsia should be included as part of the standard clinical measures of visual function when the symptom is prevalent. In this way, a larger

amount of medical data could be collected to analyze macular patterns related to the deformation patterns. Even today, such macular features are not completely identified in ophthalmology since they are not beneficial for developing medical treatments for this disorder. Such patterns may be the target for developing new segmentation and classification algorithms to consolidate an automatic modeling method which could be incorporated into an AR display device to compensate distorted visual perception.

In the case of enhancing peripheral vision, an HMD with a panoramic field of view (as wide as the human visual field) and high resolution would be ideal. Although head-mounted display technology has limitations at present, technological progress would enable such devices to have a significant impact on the rehabilitation of low vision patients in the future.

On the other hand, one of the main problems related to the integration of an eye tracker into a head-mounted system for patients with maculopathies is the calibration process embedded in the gaze-tracking initialization method. This procedure normally requires localization of the cornea center (as a reference of central focus point) through a mechanism which involves fixation of points visualized on the corresponding monitor. Patients with central vision loss may perform this procedure using a new retinal focus point (preferred retinal locus), which is not considered in the calibration process.

Eye-tracking calibration algorithms specially designed for subjects with central field loss should be developed. For example, the "wagon wheel" pattern, introduced in the Macular Mapping Test (MMTest) of MacKeben et al. [92], could be useful for fixating the corresponding points in the eye-tracking calibration process. Figure 5.1 shows an example of the mentioned pattern. The pattern was created to help gaze stabilization in the assessment of parafoveal function in macular disorders. The MMTest consists of a computer-based procedure that displays briefly single letters as recognition stimuli on a computer monitor to measure parafoveal function. Since patients with central vision loss cannot fixate a target, the pattern provides subjects a sense where the center of the circular area (i.e., target) is located. In the case of the calibration procedure of eye trackers, each point (i.e., target to fixate) could be surrounded by a wagon wheel pattern.

Once the eye-tracking technologies overcome the current limitations of patients with maculopathies (i.e., central fixation basically) and head-mounted displays become more suitable for daily life, we will have the possibility of developing an eye-tracking based head-mounted vision enhancement system, which will ex-

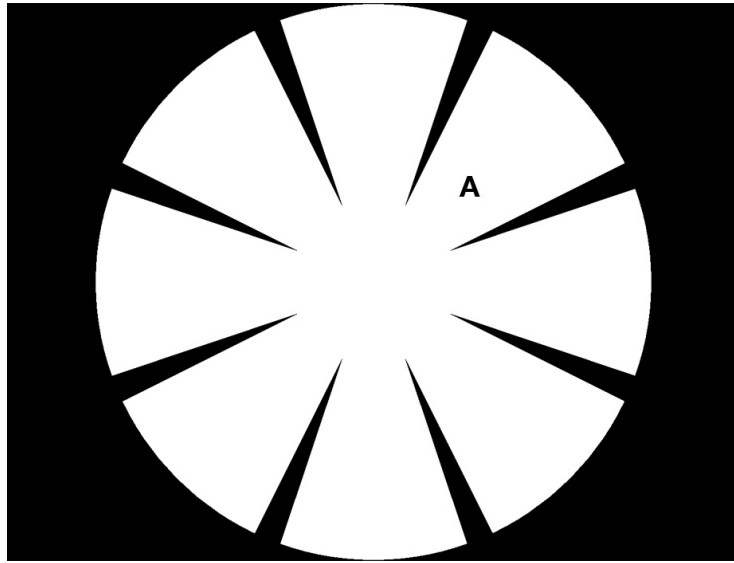


Figure 5.1.: Wagon wheel pattern used in the Macular Mapping Test [92].

pand the functionality of peripheral vision via the hybrid magnification in the preferred retinal locus of a patient, and also compensate distorted vision in the affected macular areas. This revolutionary system will improve vision of patients with age-related macular degeneration, along with their quality of life.

Appendix

APPENDIX A

Eye Tracking

A.1. Introduction

Eye movements are fundamental to the operation of the visual system. The human eye monitors a visual field of about 200° , but receives detailed information from the fovea of only 2° [87]. The fovea is moved at speeds of up to 500° a second, during which its sensitivity drops to near blindness levels [98, 145]. During the 200–300 milliseconds it is at rest, however, over 30,000 densely packed photoreceptors in the fovea provide high acuity color vision.

The fastest movements produced by the human body are called **saccades**, which are voluntary eye movements to place the retinal images of objects of interest onto the fovea within tens of milliseconds [86]. The word saccade appears to have been created by the French ophthalmologist Émile Javal, who observed the eye movements during reading using a mirror on one side of a page [73]. Saccades are quick, simultaneous movements of both eyes in the same direction [19]. Saccades to an unexpected stimulus normally take about 200–300 milliseconds (ms) to initiate.

Eye fixations are defined as a spatially stable gaze lasting for approximately 200–300 milliseconds, during which visual attention is directed to a specific area of the visual display. Fixations represent the instances in which information acquisition and processing is able to occur [126].

Eye tracking is a technique which allows to determine eye movement and eye-fixation patterns of a person. An **eye tracker** is a device for measuring eye posi-

tions and eye movement. Typical application domains for eye trackers are: psychology and vision research, as well as neuroscience and psychiatry, ergonomics, cognitive linguistics, advertising and product design.

A.2. Technological Basics of Eye Tracking

There are a number of ways for determining the motion of the eyes, nevertheless existing eye tracking methods can be classified principally into two categories [68]: two-dimensional (2D) tracking and three-dimensional (3D) tracking. In 2D tracking methods, only the relative line of sight with respect to the user's head is measured, disregarding the 3D position of the eye. The main disadvantage of 2D tracking methods is that they require the head of the users to be absolutely stationary relative to the monitoring device to achieve a good accuracy. In 3D tracking methods, the 3D position of the eye is determined, and thus the complete 3D representation of the line of sight with respect to a fixed reference is provided. Such methods tolerate head movements to some extent and are less restrictive to users.

The 2D tracking techniques can be classified in non-imaging and imaging-based methods.

A.2.1. Non-imaging Eye Tracking Approaches

The non-imaging approaches include the following:

The **scleral search coils**, consists of applying a coil of wire, embedded in a contact lens, to the eye. Movements of this coil in a magnetic field, generated by a set of field coils, induces an electric current in the eye coil proportional to its position in the field. This current, suitably amplified and filtered, provides, strictly speaking, an eye in space position signal (see Figure A.1). The major advantage of such a method is the excellent spatial and temporal resolution [24]. Nevertheless, the coil can affect the eye by decreasing visual acuity, increasing intraocular pressure, and damaging the corneal and conjunctival surface [103, 166]. In addition, the thin wire connecting the coil with the measuring device is not comfortable for the subject.

The **electrooculography** (EOG) consists of measuring electric potential differences between locations on different sides of the eye with sensors attached at the skin around the eyes (see Figure A.2). The method is sensitive to electro-magnetic interferences, but works well as the technology is advanced. The major advan-

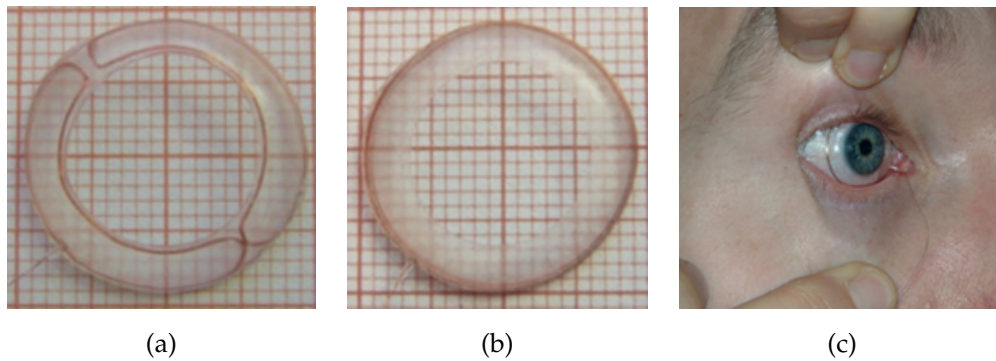


Figure A.1.: Scleral search coils: Coils embedded in contact lenses. (*Image source: www.chronos-vision.de/scleral-search-coils*).



Figure A.2.: Electro-oculography: Skin electrodes placed around the eyes to collect electrical potential variations. (*Image source: www.metrovision.fr*).

tage of the method is its ability to detect the movements even when the eye is closed (e.g. while sleeping). In [105] several studies were made of the accuracy and precision of the EOG in tracking the eye gaze.

The previous two methods explained present mechanical devices that must have caused participants great discomfort due to their size and invasiveness, and therefore these are not optimal for interaction by gaze.

A.2.2. Imaging-based Eye Tracking Approaches

The most widespread methods are the imaging-based tracking approaches. These methods estimate the direction of gaze from the video image delivered by a camera focusing on one or both eyes. Most modern eye-trackers use near-infrared (NIR) light reflected by the eye to take the advantage of the spectral properties of

the eye under this illumination. The typical features that may be tracked include the limbus, pupil, and reflection images formed by the cornea and the eye lens.

In the **limbus tracking**, the limbus is the boundary between the white sclera and the dark iris of the eye. Since the sclera is (normally) white and the iris is darker, this boundary can easily be optically detected and tracked. The limbus tracking detects the iris boundary using the high contrast of the white of the eye and the dark iris. This method is precise for horizontal tracking, but inaccurate for vertical eye movement as the upper and lower part of the iris is covered by the eyelids [66].

The **pupil tracking** technique is similar to limbus tracking, only here the smaller boundary between the pupil and the iris is used instead. Pupil tracking is more reliable than limbus tracking because: (1) the pupil is far less covered by the eyelids than the limbus, and thus enables vertical tracking; and (2) the border of the pupil is often sharper than that of the limbus and thus yields a higher resolution. The disadvantage is that the difference in contrast is lower between the pupil and iris than between the iris and sclera, making the border detection more difficult.

There are two methods of illumination to detect the pupil, depending on the configurations of the infrared (IR) illuminator: the dark and the bright pupil method. In the **dark pupil method**, IR light is emitted into the eye from an off-axis position relative to the optical axis of the imaging device, creating a dark-pupil effect, where the pupil becomes a concavity of IR light and looks darker than the iris and other eye features. In the **bright pupil method**, a bright-pupil effect is observed with an on-axis IR illuminator, where the pupil looks brighter than the iris. This effect is well known as "red eye" in photography, and it is due to the retro-reflective property of the retina [151].

The **corneal reflection tracking**, also known as glint tracking, is less sensitive to eye movement than pupil tracking. A corneal reflection image, also known as a *glint image* or *first Purkinje image*, is formed by the reflection of the cornea (see Figure A.3).

Combinations of techniques have been explored for eye movement tracking. For example, the **pupil center corneal reflection** method is probably the most effective and the most commonly used one. The method is based on the idea that the direction of a person's gaze is directly related to the relative positions of the pupil and the corneal reflection. The pupil center corneal reflection tracking detects the vector difference between the pupil center and the first Purkinje image.

Many eye trackers (e.g. Tobii Eye Tracking Research) use pupil center corneal

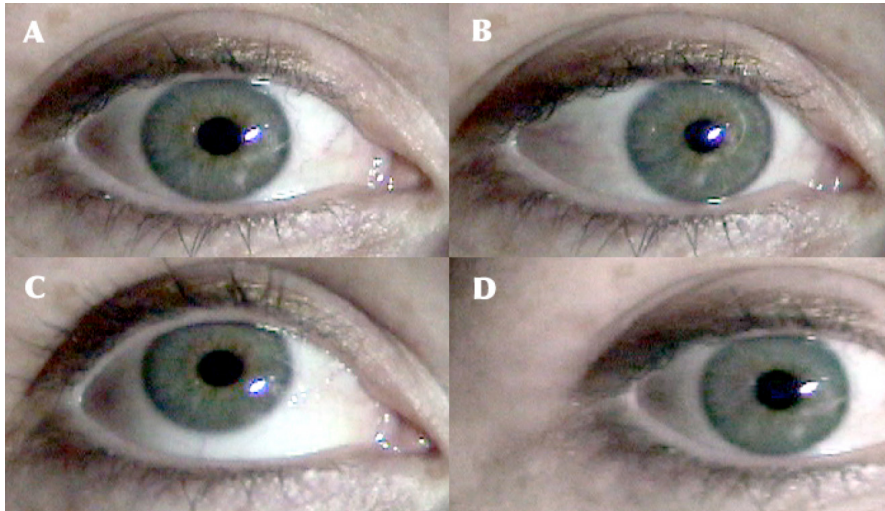


Figure A.3.: The corneal reflections produced by different eye-head positions. The corneal reflection appears as a bright white dot, just to the right of the pupil (A). The relative positions of the pupil and the corneal reflection change when the eye rotates around its horizontal (B) and vertical (C) axes. This relationship does not change, however, when the head moves and the eye is stable (D). (*Image source: Adaptation from Richardson and Sivey (2004) [128]*).

reflection tracking to estimate the direction of gaze. As the cornea has a nearly perfect sphere shape, a glint stays in the same position for any direction of gaze while the pupil moves. As the radius of the cornea differs from person to person this simple eye tracking method needs a calibration for each person. Calibration normally involves participants looking at an image (e.g., a dot or a fixation cross) in a known location. The eye tracking system compares the true location of the image to where it detects the participant's gaze on the screen, and applies a suitable correction for future fixations.

Most of the 2D tracking methods can be extended to 3D tracking, nevertheless, 3D tracking systems typically require multiple eye features or other facial features and multiple cameras to estimate the center of eye rotation, or require other mechanisms to determine the eye location [68]. The 3D tracking systems are usually remote-mounted, and the field of view (FOV) of the tracking cameras has to be sufficiently large to allow users to move their heads freely in a limited area. However, large FOV cameras provide limited resolution of the eye features for gaze

A. Eye Tracking

tracking. As a plausible solution, several researchers propose systems that use the combination of a wide and narrow FOV cameras [85, 109, 110].

APPENDIX B

Glossary and Acronyms

Glossary

A-scan. The A-scan technique uses a single transducer to scan along a line in the body.

Fundus. Fundus of the eye is the interior surface of the eye, including the retina, optic disc, macula and fovea.

Lipoprotein. Lipoprotein is a molecule made of proteins and lipids, and it is the principal mean by which lipids (fats) are transported in the blood.

Ophthalmology. Ophthalmology is the branch of medicine which deals with the anatomy, physiology and diseases of the eye.

Optometry. Optometry is a health care profession concerned with eyes and related structures, as well as vision, visual systems, and vision information processing in humans.

Triglyceride. Triglyceride is a type of fat in the bloodstream and fat tissue. It is the main constituent of vegetable oil and animal fats.

Acronyms

1D one-dimensional

2D two-dimensional

3D three-dimensional

AMD Age-related Macular Degeneration

AOA American Optometric Association

AR Augmented Reality

AREDS Age-Related Eye Disease Study

ATDV Apoio Tecnológico aos Deficientes Visuais – Technological Support for Visual Impairments

AVG Average

CCTV Closed-Circuit Television

CGI Computer-Generated Image

cm centimeter

CNV Choroidal Neovascularization

CPU Central Processing Unit

DOF Degrees of Freedom

EOG Electrooculography

ERM Epiretinal Membrane

FFD Free Form Deformation

FOV Field of View

fps frames per second

g gram

GB Gigabyte

GHz Gigahertz

GLSL OpenGL Shading Language

GPGPU General Purpose GPU

GPU Graphics Processing Unit

HDL High-Density Lipoprotein

HMD Head-Mounted Display

Hz Hertz

ICD International Statistical Classification of Diseases

IR Infrared

LVES Low Vision Enhancement System

LVIS Low Vision Imaging System

mm millimeter

MMTest Macular Mapping Test

MRI Magnetic Resonance Imaging

ms millisecond

NIR Near-infrared

OCT Optical Coherence Tomography

OpenGL Open Graphics Library

OR Operating Room

PC Personal Computer

PDT Photodynamic Therapy

PHP Preferential Hyperacuity Perimetry

PRL Preferred Retinal Locus

B. Glossary and Acronyms

PVA Personal Visual Assistant

px pixel

rad radian

RAM Random-Access Memory

RAMP Reality Augmentation for Medical Procedures

RPE Retinal Pigment Epithelium

SD Standard Deviation

TwAE Twinkle After-Effect

VEGF Vascular Endothelial Growth Factor

VOR Vestibulo-Ocular Reflex

VR-QOL Vision-Related Quality of Life

WHO World Health Organization

wpm words per minute

Bibliography

- [1] M. A. Ali and M. A. Klyne. *Vision in vertebrates*. Plenum Press, New York and London, 1985.
- [2] Marc Amsler. Earliest symptoms of diseases of the macula. *British Journal of Ophthalmology*, 37:521–537, 1953.
- [3] S. Anstis. A chart demonstrating variation in acuity with retinal position. *Vision Research*, 14:589–592, 1974.
- [4] E. Arimura, C. Matsumoto, S. Okuyama, S. Takada, S. Hashimoto, and Y. Shimomura. Retinal contraction and metamorphopsia scores in eyes with idiopathic epiretinal membranes. *Investigative Ophthalmology & Visual Science*, 46(8):2961–2966, 2005.
- [5] M. Aschke, C. R. Wirtz, J. Raczekowsky, H. Wörn, and S. Kunze. Augmented reality in operating microscopes for neurosurgical interventions. In *Proceedings of the 1st International IEEE EMBS Conference on Neural Engineering*, pages 652–655, 2003.
- [6] J. J. Assink, C. C. Klaver, J. J. Houwing-Duistermaat, R. C. Wolfs, C. M. van Duijn, A. Hofman, and P. T. de Jong. Heterogeneity of the genetic risk in age-related macular disease: a population-based familial risk study. *Ophthalmology*, 112:482–7, 2005.

- [7] American Optometric Association. Definition of vision rehabilitation, June 2004.
- [8] E. Aulhorn and G. Köst. Rauschfeldkampimetric: eine perimetrische Untersuchungsweise. *Klin Monatsbl Augenheilkd*, 192:284–288, 1988.
- [9] M. Bajura, H. Fuchs, and R. Ohbuchi. Merging virtual objects with the real world: seeing ultrasound imagery within the patient. In *Proceedings of the 19th annual conference on Computer graphics and interactive techniques*, ACM Press, pages 203–210, 1992.
- [10] C. Bichlmeier, F. Wimmer, S. M. Heining, and N. Navab. Contextual Anatomic Mimesis: Hybrid In-Situ Visualization Method for Improving Multi-Sensory Depth Perception in Medical Augmented Reality. In *Proceedings of the 6th International Symposium on Mixed and Augmented Reality (ISMAR)*, pages 129–138, November 2007.
- [11] W. Birkfellner, M. Figl, K. Huber, F. Watzinger, F. Wanschitz, J. Hummel, R. Hanel, W. Greimel, P. Homolka, R. Ewers, and H. Bergmann. A head-mounted operating binocular for augmented reality visualization in medicine – design and initial evaluation. *IEEE Transaction on Medical Imaging*, 21:991–997, August 2002.
- [12] M. Blackwell, C. Nikou, A. M. D. Gioia, and T. Kanade. An image overlay system for medical data visualization. In *Proceedings of the 1998 Medical Imaging Computing and Computer Assisted Intervention Conference (MICCAI)*, 1998.
- [13] F. L. Bookstein. Principal wraps: Thin-plate splines and the decompositions of deformations. *IEEE Trans. Pattern Anal. Machine Intell.*, 11:567–585, 1989.
- [14] A. Bowers, G. Luo, N. Rensing, and E. Peli. Evaluation of a prototype mini-fied augmented-view device for patients with impaired night vision. *Ophthalmic and Physiological Optics*, 24:296–312, 2004.
- [15] N. M. Bressler. Early detection and treatment of neovascular age-related macular degeneration. *The Journal of the American Board of Family Practice*, 15(2):142–152, 2002.

- [16] Lionel Bretillon, Niyazi Acar, Alain Bron, and Catherine Creuzot-Garcher. New insight into the genetics of age-related macular degeneration in connection with lipid metabolism. *Expert Review of Ophthalmology*, 5(1):15–18, 2010.
- [17] D. Brewster. *Letters on Natural Magic, Addressed to Sir Walter Scott*. John Murray London, 1832.
- [18] C. Carabellese, I. Appollonio, R. Rozzini, A. Bianchetti, G. B. Frisoni, and L. Frattola. Sensory impairment and quality of life in a community elderly population. *Journal of the American Geriatric Society*, 41:401–407, 1993.
- [19] B. Cassin and S. Solomon. *Dictionary of Eye Terminology*. Gainesville, Florida: Triad Publishing Company, 1990.
- [20] U. Chakravarthy, C. Augood, G. C. Bentham, P. T. de Jong, M. Rahu, J. Seland, G. Soubrane, L. Tomazzoli, F. Topouzis, J. R. Vingerling, J. Vioque, I. S. Young, and A. E. Fletcher. Cigarette smoking and age-related macular degeneration in the EUREYE study. *Ophthalmology*, 114(6):1157–63, 2007. Epub 2007 Mar 6.
- [21] U. Chakravarthy, T. Y. Wong, A. Fletcher, E. Piauult, C. Evans, G. Zlateva, R. Buggage, A. Pleil, and P. Mitchell. Clinical risk factors for age-related macular degeneration: A systematic review and meta-analysis. *BMC Ophthalmol*, 10(31), 2010.
- [22] E. W. Chong, T. Y. Wong, A. J. Kreis, J. A. Simpson, and R. H. Guymer. Dietary antioxidants and primary prevention of age related macular degeneration: systematic review and meta-analysis. *BMJ*, 335:755, 2007.
- [23] R. G. Cole. Consideration in low vision prescribing. *Probl Optom*, 3:416–32, 1991.
- [24] H. Collewijn, F. van der Mark, and T. C. Jansen. Precise recording of human eye movements. *Vision Research*, 14:447–50, 1975.
- [25] P. P. Connell, P. A. Keane, E. C. O’Neill, R. W. Altaie, E. Loane, K. Neelam, J. M. Nolan, and S. Beatty. Risk factors for age-related maculopathy. *J Ophthalmol*, 2009:360764, 2009. Epub 2009 Sep 6.

- [26] M. Crossland and G. Rubin. The Amsler chart: absence of evidence is not evidence of absence. *British Journal of Ophthalmology*, 91(3):391–393, 2007.
- [27] M. D. Crossland and P. J. Bex. Spatial alignment over retinal scotomas. *Invest Ophthalmol Vis Sci*, 50(3):1464–1469, 2009.
- [28] M. D. Crossland, S. C. Dakin, and P. J. Bex. Illusory stimuli can be used to identify retinal blind spots. *PLoS ONE*, 2:e1060, 2007.
- [29] A. M. Damiano, N. M. Bressler, H. A. Strong, L. A. Pilson, C. F. Snyder, and E. Y. Adler. The health-related quality-of-life impact of late-stage age-related macular degeneration. *Investigative Ophthalmology and Visual Science*, 39:S602, 1998.
- [30] P. T. de Jong. Age-related macular degeneration. *The New England Journal of Medicine*, 355(14):1474–1485, 2006.
- [31] P. de Weerd, R. Desimone, and L. Ungerleider. Perceptual filling-in: a parametric study. *Vision Research*, 38(4):2721–273, 1998.
- [32] D. D. Dilks, J. T. Serences, B. J. Rosenau, S. Yantis, and M. McCloskey. Human adult cortical reorganization and consequent visual distortion. *J Neurosci*, 27:9585–9594, 2007.
- [33] J. R. Evans, A. E. Fletcher, and R. P. Wormald. 28,000 cases of age related macular degeneration causing visual loss in people aged 75 years and above in the United Kingdom may be attributable to smoking. *Br J Ophthalmol*, 89:550–3, 2005.
- [34] M. R. Everingham, B. T. Thomas, and T. Troscianko. Head-mounted mobility aid for low vision using scene classification techniques. *International Journal of Virtual Reality*, 3(4):1–10, 1998.
- [35] M. R. Everingham, B. T. Thomas, and T. Troscianko. Wearable mobility aid for low vision using scene classification in a markov random field model framework. *International Journal of Human-Computer Interaction*, 15(2):231–244, 2003.
- [36] P. Farago, L. Barros, G. Cunha, L. Landau, and R. M. Costa. ATDV: An image transforming system. In V. S. Sunderam, G. D. van Albada, P. M. Slood, and

-
- J. J. Dongarra, editors, *Fifth International Conference on Computational Science (ICCS 2005) – LNCS*, volume 3514, pages 727–734, 2005.
- [37] F. L. Ferris, S. L. Fine, and L. Hyman. Age-related macular degeneration and blindness due to neovascular maculopathy. *Arch Ophthalmol*, 102(11):1640–2, 1984.
- [38] Andrew M. Fine, Michael J. Elman, Jane E. Ebert, Paula A. Prestia, JoAnn S. Starr, and Stuart L. Fine. Earliest symptoms caused by neovascular membranes in the macula. *Archives of Ophthalmology*, 104:513–4, 1986.
- [39] A. Fletcher, G. Bentham, M. Agnew, I. Young, C. Augood, U. Chakravarthy, P. T. de Jong, M. Rahu, J. Seland, G. Soubrane, L. Tomazzoli, F. Topouzis, J. R. Vingerling, and J. Vioque. Sunlight exposure, antioxidants, and age-related macular degeneration. *Archives of Ophthalmology*, 126(10):1396–403, 2008.
- [40] S. Fraser-Bell, J. Wu, R. Klein, S. P. Azen, C. Hooper, A. W. P. Foong, R. Varma, and the Los Angeles Latino Eye Study Group. Cardiovascular risk factors and age-related macular degeneration: The Los Angeles Latino Eye Study. *Am J Ophthalmol*, 145(2):308–316, 2008.
- [41] D. S. Friedman, J. Katz N. M. Bressler, and B. Rahmani J. M. Tielsch. Racial differences in the prevalence of age-related macular degeneration: the Baltimore Eye Survey. *Ophthalmology*, 106(6):1049–55, 1999.
- [42] L. Frisén. The Amsler grid in modern clothes. *British Journal of Ophthalmology*, 93:714–716, 2009.
- [43] S. Fukuda, F. Okamoto, M. Yuasa, T. Kunikata, Y. Okamoto, T. Hiraoka, and T. Oshika. Vision-related quality of life and visual function in patients undergoing vitrectomy, gas tamponade and cataract surgery for macular hole. *Br J Ophthalmol*, 93:1595–1599, 2009.
- [44] Maria-Andreea Gamulescu, Viola Radeck, Bruno Lustinger, Bianca Fink, and Horst Helbig. Bevacizumab versus ranibizumab in the treatment of exudative age-related macular degeneration. *International Ophthalmology*, 30(3):261–266, 2010.
- [45] J. Garcia, M. Caversaccio, I. Pappas, J. Kowal, U. Rohrer, G. Martin, C. Baur, L. P. Nolte, and M. A. Gonzalez. Design and clinical evaluation of an image-

- guided surgical microscope with an integrated tracking system. *IJCARS* 2007, 1:253–264, February 2007.
- [46] Karl R. Gegenfurtner and Daniel C. Kiper. Color vision. *Annual Review of Neuroscience*, 26:181–206, 2003.
- [47] H. J. Gerrits and G. J. Timmerman. The filling-in process in patients with retinal scotomata. *Vision Research*, 9:439–442, 1996.
- [48] H. Goldmann. Ein selbstregistrierendes projektionskugelperimeter. *Ophthalmologica*, 109:71–79, 1945.
- [49] M. Goldstein, A. Loewenstein, A. Barak, A. Pollack, A. Bukelman, H. Katz, A. Springer, A. P. Schachat, N. M. Bressler, S. B. Bressler, M. J. Cooney, Y. Alster, O. Rafaeli, and R. Malach. Results of a multicenter clinical trial to evaluate the preferential hyperacuity perimeter for detection of age-related macular degeneration. *Retina*, 25(3):296–303, 2005.
- [50] R. C. Gonzalez and R. E. Woods. *Digital Image Processing*. Addison-Wesley Pub, 2nd edition, 1992.
- [51] G. L. Goodrich and J. Kirby. A comparison of patient reading performance and preference: optical devices, handheld CCTV (Innoventions MagniCam) or stand-mounted CCTV (Optelec Clearview or TSI Genie). *Optometry*, 72(8):519–28, 2001.
- [52] E. S. Gragoudas, A. P. Adamis, E. T. Jr. Cunningham, M. Feinsod, and D. R. Guyer. VEGF Inhibition Study in Ocular Neovascularization Clinical Trial Group. Pegaptanib for neovascular age-related macular degeneration. *New Engl J Med*, 351:2805–16, 2004.
- [53] Eye Disease Case-Control Study Group. Risk factors for neovascular age-related macular degeneration. *Arch Ophthalmol*, 110(12):1701–8, 1992.
- [54] Macular Photocoagulation Study Group. Subfoveal neovascular lesions in age-related macular degeneration. Guidelines for evaluation and treatment in the Macular Photocoagulation Study. *Arch Ophthalmol*, 109(6):1242–57, 1991.
- [55] Macular Photocoagulation Study Group. Risk factors for choroidal neovascularization in the second eye of patients with juxtafoveal or subfoveal

- choroidal neovascularization secondary to age-related macular degeneration. *Arch Ophthalmol*, 115(6):741–7, 1997.
- [56] Preferential Hyperacuity Perimetry Research Group. Preferential hyperacuity perimeter (PreView PHP) for detecting choroidal neovascularization study. *Ophthalmology*, 112(10):1758–1765, 2005.
- [57] Submacular Surgery Trials (SST) Research Group. Surgery for hemorrhagic choroidal neovascular lesions of age-related macular degeneration: ophthalmic findings. SST report no. 13. *Ophthalmology*, 111:1993–2006, 2004.
- [58] R. Haber, M. S. Shephard, J. F. Abel, R. H. Gallagher, and D. P. Greenberg. A general two-dimensional, graphical finite element preprocessor utilizing discrete transfinite mappings. *International Journal for Numerical Methods in Engineering*, 17(7):1015–1044, 1981.
- [59] A. Hall. Effective management of low vision patients. *Journal of Vision Rehabilitation*, 1(3):15–24, 1987.
- [60] R. Harper, L. Culham, and C. Dickinson. Head-mounted video magnification devices for low vision rehabilitation: a comparison with existing technology. *Br J Ophthalmol*, 83:495–500, 1999.
- [61] David O. Harrington and Michael V. Drake. *The Visual Fields: Text and Atlas of Clinical Perimetry*. C.V. Mosby Co., sixth edition, 1990.
- [62] M. Harris and D. Luebke. GPGPU: General-purpose computation on graphics hardware. In *International Conference on Computer Graphics and Interactive Techniques: ACM SIGGRAPH 2005 Courses: Los Angeles, California, Association for Computing Machinery, Inc*, pages 10036–5701, New York, USA, 2005.
- [63] C. A. Hazel, K. L. Petre, R. A. Armstrong, M. T. Benson, and N. A. Frost. Visual function and subjective quality of life compared in subjects with acquired macular disease. *Investigative Ophthalmology and Visual Science*, 41:1309–1315, 2000.
- [64] Sandro-Michael Heining, Christoph Bichlmeier, Ekkehard Euler, and Nassir Navab. Smart device: Virtually extended surgical drill. In *Proceedings of the 8th Computer Assisted Orthopedic Surgery (CAOS 2008)*, Hong Kong, China, June 2008.

- [65] P. Henkind, R. I. Hansen, and J. Szalay. Ocular circulation. In Records RE, editor, *Physiology of the human eye and visual system*, pages 98–155. New York: Harper & Row, 1979.
- [66] C. W. Hess, R. Muri, and O. Meienberg. Recording of horizontal saccadic eye movements: methodological comparison between electro-oculography and infrared reflection oculography. *Neuro-Ophthalmology*, 6:264–272, 1986.
- [67] R. E. Hogg and U. Chakravarthy. Visual function and dysfunction in early and late age-related maculopathy. *Prog Retin Eye Res*, 25:249–76, 2006.
- [68] Hong Hua, Prasanna Krishnaswamy, and Jannick P. Rolland. Video-based eyetracking methods and algorithms in head-mounted displays. *Optics Express*, 14(10):4328–4350, 2006.
- [69] David H. Hubel. *Eye, Brain, and Vision*. W. H. Freeman, second edition, 1995.
- [70] S. Hung and J. M. Seddon. The relationship between nutritional factors and age-related macular degeneration. In A. Bendich and R. J. Deckelbaum, editors, *Preventive nutrition: the comprehensive guide for health professionals*, Totowa, NJ, 1997. Humana Press Inc.
- [71] L. Hyman. Epidemiology of AMD. In G. R. Hampton and P. T. Nelsen, editors, *Age-related macular degeneration: principles and practice*, New York, 1992. Raven Press.
- [72] R. Q. Ivers, R. G. Cumming, P. Mitchell, and K. Attebo. Visual impairment and falls in older adults: the Blue Mountains Eye Study. *Journal of the American Geriatrics Society*, 46:58–64, 1998.
- [73] É. Javal. Essai sur la physiologie de la lecture. *Annales d’oculistique*, 80:61–73, 1878.
- [74] J. S. Karlsson. Self-reports of psychological distress in connection with various degrees of vision impairment. *Journal of Vision Impairment & Blindness*, 92:483–490, 1998.
- [75] J. Katz, J. M. Tielsch, and H. A. Quigley. Automated perimetry detects visual field loss before manual Goldmann perimetry. *Ophthalmology*, 102(3):21–26, 1995.

- [76] I. Kaur, Y. Ghanekar, and S. Chakrabarti. Understanding the genetics of age-related macular degeneration: Some insights into the disease pathogenesis. *Int J Hum Genet*, 8(1-2):161–169, 2008.
- [77] T. Alan Keahey and Edward L. Robertson. Techniques for non-linear magnification transformations. In *IEEE Visualization*, pages 38–45, 1996.
- [78] J. L. Keltner and C. A. Johnson. Automated and manual perimetry - a six year overview: special emphasis on neuro-ophthalmic problems. *Ophthalmology*, 91:68–85, 1984.
- [79] A. P. King, P. J. Edwards, C. R. Maurer, D. A. de Cunha, R. P. Gaston, M. Clarkson, D. L. G. Hill, D. J. Hawkes, M. R. Fenlon, A. J. Strong, T. C. S. Cox, and M. J. Gleeson. Stereo augmented reality in the surgical microscope. *Presence: Teleoperators and Virtual Environments*, 9:360–368, 2000.
- [80] C. C. Klaver, R. C. Wolf, J. J. Assink, C. M. van DuJin, A. Hofman, and P. T. de Jong. Genetic risk of age-related maculopathy. Population-based familial aggregation study. *Arch Ophthalmol*, 116(12):1646–1651, 1998.
- [81] R. Klein, B. E. Klein, M. D. Knudtson, S. M. Meuer, M. Swift, and R. E. Gangnon. Fifteen-year cumulative incidence of age-related macular degeneration: the Beaver Dam Eye Study. *Ophthalmology*, 114(2):253–62, 2007.
- [82] R. Klein, B. E. Klein, M. D. Knudtson, T. Y. Wong, M. F. Cotch, K. Liu, G. Burke, M. F. Saad, and D. J. Jr. Jacobs. Prevalence of age-related macular degeneration in 4 racial/ethnic groups in the multi-ethnic study of atherosclerosis. *Ophthalmology*, 113(3):373–80, 2006.
- [83] R. Klein, B. E. Klein, S. C. Tomany, S. M. Meuer, and G. H. Huang. Ten-year incidence and progression of age-related maculopathy: The Beaver Dam eye study. *Ophthalmology*, 109(10):1767–79, 2002.
- [84] Dieter Koller, Gudrun Klinker, Eric Rose, David Breen, Ross Whitaker, and Mihran Tuceryan. Real-time vision-based camera tracking for augmented reality applications. In *VRST-97*, pages 87–94, September 1997.
- [85] Y. Kondou and Y. Ebisawa. Easy eye-gaze calibration using a moving visual target in the head-free remote eye-gaze detection system. In *IEEE Conference on Virtual Environments, Human-Computer Interfaces and Measurement Systems, 2008. VECIMS 2008*, pages 145–150, 2008.

- [86] R. J. Krauzlis. The control of voluntary eye movements: new perspectives. *The Neuroscientist*, 11(2):124–37, 2005.
- [87] D. M. Levi, S. A. Klein, and A. P. Aitsebaomo. Vernier acuity, crowding and cortical magnification. *Vision Research*, 25(7):963–977, 1985.
- [88] Yan Li, John E. Crews, Laurie D. Elam-Evans, Amy Z. Fan, Xinzhi Zhang, Amanda F. Elliott, and Lina Balluz. Visual impairment and health-related quality of life among elderly adults with age-related eye diseases. *Quality of Life Research*, 20(6):845–852, 2010.
- [89] A. Loewenstein, R. Malach, M. Goldstein, I. Leibovitch, A. Barak, E. Baruch, Y. Alster, O. Rafaeli, I. Avni, and Y. Yassur. Replacing the Amsler grid: a new method for monitoring patients with age-related macular degeneration. *Ophthalmology*, 110:966–970, 2003.
- [90] D. S. Loshin and R. D. Juday. The programmable remapper: clinical applications for patients with field defects. *Optometry and Vision Science*, 66(6):389–95, 1989.
- [91] G. Luo, N. Rensing, E. Weststrate, and E. Peli. Registration of an on-axis see-through head-mounted display and camera system. *Optical Engineering*, 44(2):024002, 2005.
- [92] M. MacKeben, A. Colenbrander, and A. Gofen. Use your PC to quickly map remaining vision after foveal vision loss. *Perimetry Update 1998/1999*, pages 307–316, 1999.
- [93] S. Mann. Mediated reality. TR 260, M.I.T. Media Lab Perceptual Computing Section, Cambridge, Massachusetts, 1994.
- [94] Steve Mann. Wearable, tetherless computer-mediated reality: WearCam as a wearable face-recognizer, and other applications for the disabled. TR 361, M.I.T. Media Lab Perceptual Computing Section; Also appears in **AAAI Fall Symposium on Developing Assistive Technology for People with Disabilities**, 9-11 November 1996, MIT; <http://wearcam.org/vmp.htm>, Cambridge, Massachusetts, February 2 1996.
- [95] S. N. Markowitz. Principles of modern low vision rehabilitation. *Can J Ophthalmol*, 41:289–312, 2006.

- [96] M. F. Marmor. A brief history of macular grids: from Thomas Reid to Edvard Munch and Marc Amsler. *Survey of Ophthalmology*, 44(4):343–353, 2000.
- [97] R. W. Massof and D. L. Rickman. Obstacles encountered in the development of the low vision enhancement system. *Optometry and Vision Science*, 69(1):32–41, 1992.
- [98] E. Matin. Saccadic suppression: A review and an analysis. *Psychological Bulletin*, 81(12):899–917, 1974.
- [99] C. Matsumoto, E. Arimura, S. Okuyama, S. Takada, S. Hashimoto, and Y. Shimomura. Quantification of metamorphopsia in patients with epiretinal membranes. *Investigative Ophthalmology & Visual Science*, 44(9):4012–4016, 2003.
- [100] M. E. McClure, P. M. Hart, A. J. Jackson, M. Stevenson, and U. Chakravarthy. Macular degeneration: do conventional measurements of impaired visual function equate with visual disability? *British Journal of Ophthalmology*, 84:244–50, 2000.
- [101] E. Midena. Microperimetry. *Arch Soc Esp Oftalmol*, 81:183–186, 2006.
- [102] E. Midena, P. P. Radin, E. Pilotto, A. Ghirlando, E. Convento, and M. Varano. Fixation pattern and macular sensitivity in eyes with subfoveal choroidal neovascularization secondary to age-related macular degeneration. A microperimetry study. *Semin Ophthalmol*, 19:55–61, 2004.
- [103] P. J. Murphy, A. L. Duncan, A. J. Glennie, and P. C. Knox. The effect of scleral search coil lens wear on the eye. *British Journal of Ophthalmology*, 85:332–335, 2001.
- [104] Nassir Navab, Marco Feuerstein, and Christoph Bichlmeier. Laparoscopic virtual mirror - new interaction paradigm for monitor based augmented reality. In *Virtual Reality*, pages 43–50, USA, March 2007.
- [105] A. W. North. Accuracy and precision of electrooculographic recording. *Invest Ophthalmol*, 4:343–348, 1965.
- [106] F. Okamoto, Y. Okamoto, S. Fukuda, T. Hiraoka, and T. Oshika. Vision-related quality of life and visual function after vitrectomy for various vitreoretinal disorders. *Invest Ophthalmol Vis Sci*, 51(2):744–751, 2010.

- [107] World Health Organization. *International Statistical Classification of Diseases, Injuries, and Causes of Death, Tenth Revision*. Geneva, 1993.
- [108] J. Owens, D. Luebke, N. Govindaraju, M. Harris, J. Kruger, A. Lefohn, and T. Purcell. A survey of general-purpose computation on graphics hardware. *Computer Graphics Forum*, 26:80–113, 2007.
- [109] K. R. Park. Gaze detection by wide and narrow view stereo camera. *Lecture Notes in Computer Science (CIARP'2004)*, 3287:140–147, 2004.
- [110] K. R. Park. A real-time gaze position estimation method based on a 3-D eye model. *IEEE Transactions on Systems, Man, and Cybernetics, Part B: Cybernetics*, 37(1):199–212, 2007.
- [111] Verteporfin Roundtable Participants. Guidelines for using verteporfin (Vissudyne) in photodynamic therapy to treat choroidal neovascularization due to age-related macular degeneration and other causes: update. *Retina*, 25:119–34, 2005.
- [112] E. Peli. Head-mounted display as a low vision aid. In *Virtual Reality Conference Proceedings*, California State University Northridge, 1994.
- [113] E. Peli. Simple 1-D image enhancement for head-mounted low vision aid. *Visual Impairment Research*, 1(1):3–10, 1999.
- [114] E. Peli. Augmented vision for central scotoma and peripheral field loss. In C. Stuenkel, A. Arditi, A. Horowitz, M. A. Lang, B. Rosenthal, and K. Seidman, editors, *Vision Rehabilitation: Assessment, Intervention and Outcomes*, pages 70–74, Lisse, The Netherlands, 2000. Swets & Zeitlinger.
- [115] E. Peli. Vision multiplexing: an engineering approach to vision rehabilitation device development. *Optometry and Vision Science*, 78(5):304–315, 2001.
- [116] E. Peli, R. B. Goldstein, G. M. Young, C. L. Trempe, and S. M. Buzne. Image enhancement for the visually impaired: Simulations and experimental results. *Investigative Ophthalmology and Visual Science*, 32(8):2337–2350, 1991.
- [117] E. Peli, G. Luo, A. Bowers, and N. Rensing. Applications of augmented-vision head-mounted systems in vision rehabilitation. *J Soc Inf Disp*, 15(12):1037–1045, 2007.

- [118] E. Peli, G. Luo, A. Bowers, and N. Rensing. Development and evaluation of vision multiplexing devices for vision impairment. *International Journal on Artificial Intelligence Tools*, 18(3):365–378, 2009.
- [119] Terry Peters and Kevin Cleary. *Image-Guided Interventions*. Springer Science, 2008.
- [120] D. J. Pieramici and S. B. Bressler. Age-related macular degeneration and risk factors for the development of choroidal neovascularization in the fellow eye. *Curr Opin Ophthalmol*, 9:38–46, 1998.
- [121] S. L. Pineles, N. J. Volpe, E. Miller-Ellis, S. L. Galetta, P. S. Sankar, K. S. Shindler, and M. G. Maguire. Automated combined kinetic and static perimetry: an alternative to standard perimetry in patients with neurophthalmic disease and glaucoma. *Arch Ophthalmol*, 124(3):363–369, 2006.
- [122] D. J. Plummer, S. P. Azen, and W. R. Freeman. Scanning laser entoptic perimetry for the screening of macular and peripheral retinal disease. *Arch Ophthalmol*, 118:1205–10, 2000.
- [123] S. L. Polyak. *The Retina*. University of Chicago Press, 1941.
- [124] V. S. Ramachandran and R. L. Gregory. Perceptual filling in of artificially induced scotomas in human vision. *Nature*, 350:699–702, 1991.
- [125] R. S. Ramrattan, R. C. Wolfs, S. Panda-Jonas, J. B. Jonas, D. Bakker, H. A. Pols, A. Hofman, and P. T. de Jong. Prevalence and causes of visual field loss in the elderly and associations with impairment in daily functioning: the Rotterdam Study. *Arch Ophthalmol*, 119(12):1788–1794, 2001.
- [126] K. Rayner. Eye movements in reading and information processing: 20 years of research. *Psychological Bulletin*, 124:372–422, 1998.
- [127] Serge Resnikoff, Donatella Pascolini, Daniel Etya'ale, Ivo Kocur, Ramachandra Pararajasegaram, Gopal P. Pokharel, and Silvio P. Mariotti. Global data on visual impairment in the year 2002. *Bulletin of the World Health Organization*, 82:844–851, 2004.
- [128] D. C. Richardson and M. J. Spivey. Eye-tracking: Characteristics and methods. In G. Wnek and G. Bowlin, editors, *Encyclopedia of biomaterials and biomedical engineering*, pages 568–572, New York: Dekker, 2004.

- [129] L. Ringering and P. Amaral. The role of psychosocial factors in adaptation to visual impairment and rehabilitation outcomes for adults and older adults. In B. Silverstone, M. A. Lang, B. P. Rosenthal, and E. F. Faye, editors, *The Lighthouse handbook on vision impairment and vision rehabilitation*, pages 1029–48, New York, 2000. Oxford University Press.
- [130] R. W. Rodieck and R. K. Brening. Retinal ganglion cells: properties, types, genera, pathways and trans-species comparisons. *Brain Behav Evol*, 23(3–4):121–64, 1983.
- [131] Randi J. Rost. *OpenGL Shading Language*. Addison-Wesley Professional, second edition, 2006.
- [132] F. Sauer, A. Khamene, B. Bascle, and G. J. Rubino. A head-mounted display system for augmented reality image guidance: Towards clinical evaluation for iMRI-guided neurosurgery. In *Proceedings of the 4th International Conference on Medical Image Computing and Computer-Assisted Intervention, MICCAI '01*, pages 707–716, London, UK, UK, 2001. Springer-Verlag.
- [133] F. Sauer, A. Khamene, and S. Vogt. An augmented reality navigation system with a single-camera tracker: System design and needle biopsy phantom trial. In *Medical Image Computing and Computer Assisted Intervention (MICCAI)*, 2002.
- [134] F. Sauer, F. Wenzel, S. Vogt, Y. Tao, Y. Genc, and A. Bani-Hashemi. Augmented workspace: designing an AR testbed. In *Proceedings IEEE and ACM International Symposium on Augmented Reality*, pages 47–53, 2000.
- [135] R. A. Schuchard. Preferred retinal loci and macular scotoma characteristics in patients with age-related macular degeneration. *Can J Ophthalmol*, 40(3):303–12, 2005.
- [136] R. A. Schuchard, D. C. Fletcher, and J. H. Maino. A scanning laser ophthalmoscope (SLO) low vision rehabilitation system. *Clin Eye Vis Care*, 6:101–7, 1994.
- [137] Ronald A. Schuchard, Saad Naseer, and Kristina de Castro. Characteristics of AMD patients with low vision receiving visual rehabilitation. *Journal of Rehabilitation Research and Development*, 36(4):294–302, 1999.

- [138] J. M. Seddon, W. C. Willett, F. E. Speizer, and S. E. Hankinson. A prospective study of cigarette smoking and age-related macular degeneration in women. *JAMA*, 276(14):1141–6, 1996.
- [139] T. W. Sederberg and S. R. Parry. Free-form deformation of solid geometric models. In *Proceedings of SIGGRAPH '86, Computer Graphics*, 20, 4, pages 151–160, August 1986.
- [140] J. Sergent. An investigation into perceptual completion in blind areas of the visual field. *Brain*, 111(2):347–373, 1988.
- [141] Kei Shinoda, Susumu Ishida, Shinichi Kawashima, Tadayuki Matsuzaki, Kyoko Yamada, and Hiroshi Katsura. A new method for quantification of metamorphopsia in patients with epiretinal membrane. *Jpn J Ophthalmol*, 44:424–427, 2000.
- [142] T. Sielhorst, M. Feuerstein, J. Traub, O. Kutter, and N. Navab. Campar: A software framework guaranteeing quality for medical augmented reality. *International Journal of Computer Assisted Radiology and Surgery*, 1:29–30, 2006.
- [143] W. Smith, J. Assink, R. Klein, P. Mitchell, C. C. Klaver, B. E. Klein, A. Hofman, S. Jensen, J. J. Wang, and P. T. de Jong. Risk factors for age-related macular degeneration: Pooled findings from three continents. *Ophthalmology*, 108(4):697–704, 2001.
- [144] A. Thakkinstian, P. Han, M. McEvoy, W. Smith, J. Hoh, K. Magnusson, K. Zhang, and J. Attia. Systematic review and meta-analysis of the association between complement factor H Y402H polymorphisms and age-related macular degeneration. *Hum Mol Genet*, 15(18):2784–90, 2006. Epub 2006.
- [145] A. Thiele, P. Henning, M. Kubischik, and K. P. Hoffmann. Neural mechanisms of saccadic suppression. *Science*, 295(5564):2460–2462, 2002.
- [146] J. Thornton, R. Edwards, P. Mitchell, R. A. Harrison, I. Buchan, and S. P. Kelly. Smoking and age-related macular degeneration: a review of association. *Eye*, 19(9):935–44, 2005.
- [147] A. Y. Ting, T. K. Lee, and I. M. MacDonald. Genetics of age-related macular degeneration. *Curr Opin Ophthalmol*, 20(5):369–76, 2009.

- [148] S. Trauzettel-Klosinski and R. P. Tornow. Fixation behavior and reading ability in macular scotoma. *Neuro Ophthalmol*, 16:241–253, 1997.
- [149] R. Trevino. Recent progress in macular function self-assessment. *Ophthalmic and Physiological Optics*, 28(3):183–192, 2008.
- [150] J. D. Trobe, P. C. Acosta, J. J. Shuster, and J. P. Krischer. An evaluation of the accuracy of community-based perimetry. *Am J Ophthalmol*, 90:654–660, 1980.
- [151] J. van de Kraats and D. van Norren. Directional and nondirectional spectral reflection from the human fovea. *J Biomed Optics*, 13:024010, 2008.
- [152] R. van Leeuwen, C. C. Klaver, J. R. Vingerling, A. Hofman, and P. T. de Jong. The risk and natural course of age-related maculopathy: follow-up at 6 1/2 years in the Rotterdam study. [erratum appears in Arch Ophthalmol. 2003 Jul;121(7):955. *Archives of Ophthalmology*, 121(4):519–26, 2003.
- [153] F. Vargas-Martin and E. Peli. Augmented view for tunnel vision: device testing by patients in real environments. In *Digest of Technical Papers, Society for Information Display International Symposium*, pages 602–605, San Jose, CA, 2001.
- [154] J. R. Vingerling, I. Dielemans, J. C. Witteman, A. Hofman, D. E. Grobbee, and P. T. de Jong. Macular degeneration and early menopause: a case-control study. *BMJ*, 310:1570–1, 1995.
- [155] J. R. Vingerling, C. C. Klaver, A. Hofman, and P. T. de Jong. Epidemiology of age-related maculopathy. *Epidemiol Rev*, 17:347–60, 1995.
- [156] S. Vogt, A. Khamene, and F. Sauer. Reality augmentation for medical procedures: System architecture, single camera marker tracking, and system evaluation. *International Journal of Computer Vision*, 70:179–190, 2006.
- [157] S. Vogt, A. Khamene, F. Sauer, and H. Niemann. Single camera tracking of marker clusters: Multiparameter cluster optimization and experimental verification. In *IEEE and ACM International Symposium on Mixed and Augmented Reality*, pages 127–136, 2002.
- [158] H. W. Wahl and F. Oswald. The person-environment perspective of vision impairment. In *B. Silverstone, M.A. Lang, B.P. Rosenthal, E.F. Faye (Eds.). The*

- Lighthouse handbook on vision impairment and vision rehabilitation*, pages 1069–1088, New York, 2000. Oxford University Press.
- [159] A. W. Walsh, L. E. Magargal, F. Wright, and L. A. Donoso. The early natural history of subfoveal neovascular membranes in eyes with age-related macular degeneration. *Ann Ophthalmol*, 21:348–50, 1989.
- [160] S. K. West, G. S. Rubin, A. T. Broman, B. Muñoz, K. Bandeen-Roche, and K. Turano. How does visual impairment affect performance on tasks of everyday life? *Archives of Ophthalmology*, 120(6):774–80, 2002.
- [161] R. A. Williams, B. L. Brody, R. G. Thomas, R. M. Kaplan, and S. I. Brown. The psychosocial impact of macular degeneration. *Archives of Ophthalmology*, 116:514–20, 1998.
- [162] W. Wittich, O. Overbury, M. A. Kapusta, D. H. Watanabe, and J. Faubert. Macular hole: perceptual filling-in across central scotomas. *Vision Research*, 46:4064–4070, 2006.
- [163] U. E. Wolf-Schnurrbusch, L. Ceklic, C. K. Brinkmann, M. E. Iliev, M. Frey, S. P. Rothenbuehler, V. Enzmann, and S. Wolf. Macular thickness measurements in healthy eyes using six different optical coherence tomography instruments. *Invest Ophthalmol Vis Sci*, 50(7):3432–3137, 2009.
- [164] Eugene Wolff. *Eugene Wolff's Anatomy of the eye and orbit: Including the central connexions, development, and comparative anatomy of the visual apparatus*. W. B. Saunders Company, 7th edition, 1976.
- [165] Santiago Ramon y Cajal. *Histologie du systeme nerveux de l'homme et des vertebres*. A. Maloine, Paris, 1909.
- [166] J. E. Zacher, E. L. Irving, R. S. Allison, and M. E. Callander. Effects of scleral search coil wear on visual function and acuity. *Invest Ophthalmol Vis Sci*, 39(3):S767, 1998.
- [167] D. Zur and S. Ullman. Filling-in of retinal scotomas. *Vision Research*, 43:971–982, 2003.